(4)

TECHNICAL REPORT BRL-TR-2975

BRL

1938 – Serving the Army for Fifty Years – 1988

DERIVATION OF A GODUNOV ONE DIMENSIONAL FLUID DYNAMICS CODE

HUBERT W. MEYER, JR.

DECEMBER 1988

U.S. ARMY LABORATORY COMMAND

BALLISTIC RESEARCH LABORATORY
ABERDEEN PROVING GROUND, MARYLAND

DESTRUCTION NOTICE

Destroy this report when it is no longer needed. DO NOT return it to the originator.

Additional copies of this report may be obtained from the National Technical Information Service, U.S. Department of Commerce, Springfield, VA 22161.

The findings of this report are not to be construed as an official Department of the Army position, unless so designated by other authorized documents.

The use of trade names or manufacturers' names in this report does not constitute indorsement of any commercial product.

SECURITY CLASSIFICATION OF THIS PAGE

REPORT DOCUMENTATION PAGE

Form Approved OMB No. 0704-0188

1a. REPORT SECURITY CLASSIFICATION: UNCLASSIFIED	1b. RESTRICTIVE MARKINGS
2a. SECURITY CLASSIFICATION AUTHORITY	3. DISTRIBUTION/AVAILABILITY OF REPORT: Approved for Public Release; Distribution Unlimited
2b. DECLASSIFICATION/DOWNGRADING SCHEDULE	
4. PERFORMING ORGANIZATION REPORT NUMBER(S): BRL-TR-2975	5. MONITORING ORGANIZATION REPORT NUMBER(S)
6a. NAME OF PERFORMING ORGANIZATION: Ballistic Research Laboratory; 6b. OFFICE SYMBOL (If applicable): SLCBR-TB-AA	7a. NAME OF MONITORING ORGANIZATION
6c. ADDRESS (City, State, and ZIP Code): Aberdeen Proving Ground, MD 21005-5066	7b. ADDRESS (City, State, and ZIP Code)
8a. NAME OF FUNDING/SPONSORING ORGANIZATION; 8b. OFFICE SYMBOL (If applicable)	9. PROCUREMENT INSTRUMENT IDENTIFICATION NUMBER
8c. ADDRESS (City, State, and ZIP Code)	10. SOURCE OF FUNDING NUMBERS: PROGRAM ELEMENT NO. / PROJECT NO. / TASK NO. / WORK UNIT ACCESSION NO.

11. TITLE (Include Security Classification)
Derivation of a Godunov One Dimensional Fluid Dynamics Code

12. PERSONAL AUTHOR(S)
Meyer, Hubert W., Jr.

13a. TYPE OF REPORT	13b. TIME COVERED FROM ____ TO ____	14. DATE OF REPORT (Year, Month, Day)	15. PAGE COUNT

16. SUPPLEMENTARY NOTATION

17. COSATI CODES			18. SUBJECT TERMS (Continue on reverse if necessary and identify by block number)
FIELD	GROUP	SUB-GROUP	

19. ABSTRACT (Continue on reverse if necessary and identify by block number)

This report details the development of a one dimensional code using the Godunov method, which is the first part of a larger effort to develop an axisymmetric fluid dynamics code. The ultimate objective of this effort is the development of an axisymmetric code to study the hypersonic flow field associated with a shaped charge jet, in order to study how and to what extent perturbations of the jet are caused by interactions of the flow field with various target geometries.

The report contains detailed derivations of the equations involved in the one dimensional Godunov method, and the incorporation of these equations into a computer program. Many of these basic relationships are applicable to the axisymmetric code. A shock tube experiment was conducted to test the predictions of the program. The program accurately predicted all aspects of the shock tube flow, being within 2% of experimental values for pressure, 6% of experimental values for velocity, and 1% of theoretical values for density.

20. DISTRIBUTION/AVAILABILITY OF ABSTRACT	21. ABSTRACT SECURITY CLASSIFICATION	
☒ UNCLASSIFIED/UNLIMITED ☐ SAME AS RPT. ☐ DTIC USERS	UNCLASSIFIED	
22a. NAME OF RESPONSIBLE INDIVIDUAL: HUBERT W. MEYER, JR.	22b. TELEPHONE (Include Area Code): 301-278-6019	22c. OFFICE SYMBOL: SLCBR-TB-AA

DD Form 1473, JUN 86 — Previous editions are obsolete. — SECURITY CLASSIFICATION OF THIS PAGE

TABLE OF CONTENTS

LIST OF FIGURES

LIST OF TABLES

LIST OF SYMBOLS

General

$\vec{\omega}$ any vector function of time and position
σ scalar element of surface area
$\hat{n}$ unit vector normal to σ; unit vector normal to boundary
V volume
S surface of control volume
t time
τ length of time step

Flowfield

$\vec{V}$ fluid velocity
u component of fluid velocity in positive x direction
ρ fluid density
p fluid pressure
e fluid specific internal energy
ϵ fluid specific total energy
∞ subscript to denote a property of the free stream fluid
γ ratio of specific heats; = 1.4 (perfect air)

Grid

h width of cell (in x direction)
x axial position
i cell index number
m boundary index number
M total number of cells
S area of cell boundary

Riemann Problem

U x component of fluid velocity at the boundary
R fluid density at the boundary
P fluid pressure at the boundary
E specific internal energy of the fluid at the boundary
p_0 pressure on the contact discontinuity
u_0 velocity on the contact discontinuity
a mass velocity of both waves in the linear Riemann problem, or mass velocity of negative running wave in nonlinear Riemann prob
b mass velocity of positive running wave in nonlinear Riemann prob
ρ_2 density between positive running wave and contact discontinuity
ρ_3 density between negative running wave and contact discontinuity
w velocity of the wave relative to the fluid ahead
W absolute velocity of the wave

ACKNOWLEDGEMENT

The author wishes to acknowledge the participation of Dr. James Danberg in all phases of this project, and Monte Coleman in debugging the program. Also, the author acknowledges the assistance of Brian Bertrand and George Coulter in conducting the shock tube experiment, and Andy Mark and Klaus Opalka in running the Beam-Warming code for comparison. Thanks to you all for your help.

INTRODUCTION

Background

The ultimate objective of this effort is to study the hypersonic flow field associated with a shaped charge jet. Of concern will be how and to what extent perturbations of the jet are caused by interactions of the flow field with various target geometries. This report details the first part of the effort to develop an axisymmetric fluid dynamics code: the derivation of applicable equations and the development of a one dimensional code. Many basic relationships applicable to both codes are derived here.

Considerable research has been conducted in the fields of jet formation and jet penetration, but little effort has been devoted to studying the aerodynamic forces that influence the jet. At typical jet velocities of greater than Mach 20, an extremely strong flow field is developed which may cause severe perturbations in the jet. For example, an extremely strong bow shock wave is formed. As the jet flies through the hole in a guidance package, or through the hole in a skirting plate made by the leading portion of the jet, the bow shock is reflected back to impinge on a trailing portion of the jet, applying potentially disruptive forces. Another potentially disruptive force results from the strong wake behind a jet particle. The subsequent particles must fly through this turbulence. The situation may be even more severe for particles farther back in the jet.

The problem is studied by numerical solution of the equations of motion utilizing a method developed by S. K. Godunov, a Russian mathematician. This first order inviscid method is suitable to hypersonic flow regimes. It has been used by the Launch and Flight Division of the BRL to solve a geometrically similar problem of a projectile's flight through a muzzle brake. This problem, however, involved only one projectile at less than hypersonic velocities. The code will be validated by solving some problems with known solutions. Then a cylindrical hole of circular cross section will be studied. These calculations will be experimentally verified. Finally, more complex geometries may be numerically studied.

In the first phase of this study, reported here, the necessary equations are derived and a one-dimensional code is written for an inviscid, perfect gas. Theoretical and experimental verifications are carried out which show that the technique accurately predicts those flow phenomena critical to this study: shock and expansion wave formation, wave reflection, and wave/wave collisions.

The Godunov Technique

The one-dimensional scheme developed by Godunov is explained and expanded to two dimensions (and axi-symmetric) in a 1961 paper in the Russian Journal of Mathematics and Mathematical Physics (Ref 1). The principal advantage of the method lies in the physically realistic approach used to obtain the mathematical solution of the equations of fluid motion. That the solution technique can be so well expressed in physical terms is

fascinating, and a fine comment on the beauty with which mathematics expresses the physical laws of nature. In fact, Godunov (Ref 2) derives all the necessary equations (except the conservation equations) purely from mathematical considerations. As a final step, he indicates that his equations are the same as those that would result from consideration of a physical system. The physical system will be the basis of the equations derived here.

The physical system referred to above is the one dimensional fluid discontinuity, sometimes called the Riemann problem (after the German mathematician who was the first to attempt to calculate shock properties) or the shock tube analogy. To see how this Riemann problem helps in the solution of the equations of fluid motion, consider a one dimensional fluid, divided into finite cells and at initial time t_0 containing the pressure distribution as shown in figure 1a. Similar curves can be imagined for the other dependent variables, velocity (u), density (ρ), internal energy (e). The problem being addressed here is one of unsteady flow, so these quantities will be functions of time as well as functions of x.

Thus the gas is divided into one-dimensional regions of thickness Δx. Some appropriate average values for p, u, ρ, e are chosen for each layer (at say, $t = \tau$). These are denoted by $p_{m-1/2}$, $u_{m-1/2}$, etc. Consequently, the values in neighboring layers may not be the same, as seen in figure 1b. Because of the incremental nature of the assumed form of the pressure distribution, a pressure discontinuity exists at the boundary between cells. This is analogous to the classical shock tube problem, which considers the solution of the Riemann problem, as depicted in figure 1c. Of course in the present case the diaphragm is imaginary. It is imagined to rupture by unfreezing the time variable and permitting the discontinuities in pressure, density and velocity to seek equilibrium. The discontinuities at x_m are thus resolved into a shock wave, expansion wave and contact discontinuity (or some other combination), propagating from the cell boundary at x_m, or simply m, toward its neighbors at m-1 and m+1.

The conditions behind these waves are well known from shock tube theory, and can be computed from the known initial conditions on the two sides of the diaphragm. More importantly, the conditions behind the waves are constant. The essence of the Godunov technique is to utilize these constant conditions at the cell boundaries to compute the flux of properties into each cell during the time step. The conservation equations are used to compute new average properties in each cell and the entire process is repeated in the next time step. The integral form of the conservation equations must be used if the solution is to be valid for flow fields containing discontinuities (shock waves).

The equations which constitute the general solution of the Riemann (shock tube) problem are nonlinear. For weak (sonic) waves, the equations can be linearized. Figures 1a and 1b show that the magnitude of the discontinuities in each individual Riemann problem (which result from the approximation to the continuous distribution) are governed in part by the size of the increment Δx. Thus the resulting waves can be guaranteed to be

weak waves by selection of a sufficiently fine grid. The consequential linearized Riemann system is valid in all cases except the one in which a discontinuity in the flow field (e.g. bow shock wave, reflected wave, etc.) actually passes through one of the two cells.

To insure validity of the Riemann model when approximating continuous flow, the fluid properties at the point x_m must remain constant during the time step; they must not be disturbed by the waves propagating from the neighboring points x_{m-1} and x_{m+1}. That is, the properties at x_m must only result from the resolution of the discontinuity at x_m. The fact that the region between points x_m and x_{m+1} (or x_m and x_{m-1}) is complicated by the presence of additional waves emanating from x_{m+1} (or x_{m-1}) is of no consequence to the properties at x_m. The properties computed for point x_m will remain valid until the waves from the neighboring points arrive at x_m. Thus the time interval Δt must be less than the time required for the wave to traverse the distance Δx. If W is the wave speed relative to the fixed coordinate frame,

$$\Delta t < \frac{\Delta x}{W}$$

is the physically required relationship between the step sizes. Godunov also derives this criterion from a purely mathematical stability analysis, again demonstrating the harmony between physical and mathematical descriptions of nature.

General Approach to Solving the Fluid Dynamics Problem

The Godunov technique requires the solution of two fluid dynamics problems. The primary problem involves use of the conservation laws to update the properties in each cell based on the flux of each property across the cell boundaries. Since dicontinuities may exist in the flowfield, the integral form of the conservation equations must be used.

The secondary fluid dynamics problem to be solved is the Riemann problem at the cell boundaries. The fluid condition behind the waves constitutes the solution, and these conditions are used in the conservation laws (the primary problem) to determine fluxes and hence new average cell properties.

Figure 2 shows a schematic of the conditions in the Riemann problem. For simplicity, the subscript 4 denotes conditions in cell (m-1/2) and subscript 1 denotes conditions in cell (m+1/2). The negative running wave and positive running wave may also fall in the same quadrant (either one), but by definition the positive running wave has the more positive absolute (i.e. relative to the fixed cell boundary) velocity. The location of each

wave (left or right quadrant) will depend on the initial fluid velocities in the two cells, and the resultant wave velocity relative to the fluid.

From classical shock tube theory, the pressure and velocity of the gas on either side of the contact discontinuity are known to be equal and constant; hence the terminology p_0 and u_0 in the regions behind the waves, regions 2 and 3. Similarly, the density is known to be different on the two sides of the contact discontinuity, but to be constant in each of the regions 2 and 3. That is, the density is discontinuous across the contact discontinuity. p_1 , u_1 , ρ_1 , and p_4 , u_4 , ρ_4 are the known and constant conditions of the gas prior to the passing of the wave. Note that a compressive wave is characterized by a higher pressure behind the wave than in front ($p_0 > p_1$ or $p_0 > p_4$) while an expansion wave leaves a lower pressure behind ($p_0 < p_1$ or $p_0 < p_4$).

Since the integral equations must be used for discontinuties in the flow field, they will be used to derive the conditions behind the shock wave. The expansion wave is not a discontinuity in the flow, so the less awkward differential form of the equations of fluid motion will be used to derive the conditions behind the expansion wave.

Chapter 1

THE EQUATIONS OF INVISCID FLUID MOTION

The conservation equations (or equations of motion) are used three times in the following chapters: in Chapter 2 for the derivation of the finite difference equations that are used to compute the flux of properties into the cell during the time step; in Chapter 3 to derive the shock wave equations for the Riemann problem; and again in Chapter 3 to derive the expansion wave equations for the Riemann problem.

To derive these conservation laws using a Lagrangian approach is aesthetically more satisfying than using an Eulerian approach. In the Lagrangian approach, a particular element of fluid is studied as it flows. The control volume in this case is that which encloses the element of fluid under study. It can change size and shape as it moves along in the flow field, but unlike the Eulerian control volume, the mass within it is constant. For this reason the Lagrangian approach seems more naturally suited to the derivation of conservation laws.

Both the differential and the integral form of the conservation equations are derived in this chapter. To arrive at the differential form of the conservation equations, total derivatives of volume integrals are expressed in Eulerian terms (the differentiation is moved inside the integral) by use of the Reynold's Transport Theorem. This form is then used to generate the finite difference equations (which compute the flux of properties into each cell during the time step), and to derive the expansion wave equations for the Riemann problem. The derivation of the shock wave equations for the Riemann problem is facilitated by use of the integral form of the conservation equations. This form results directly from a Lagrangian derivation, as detailed in the latter portion of this chapter.

The Differential Equations of Motion

The Reynold's Transport Theorem is required for the derivation of the differential equations of motion. In deriving the Reynold's Transport Theorem, use is made of the Gauss Divergence Theorem. It relates a surface integral to a volume integral and is written (ref 3):

$$\int_S \hat{n}\cdot\vec{\omega}\,d\sigma = \int_V \vec{\nabla}\cdot\vec{\omega}\,d\tau$$

where $\vec{\omega}$ is any vector function of time and position, $d\sigma$ is a scalar element of surface area, $\hat{n}$ is a unit vector normal to $d\sigma$ and directed outward, and $d\tau$ is a scalar element of volume. Replacing $\hat{n}d\sigma$ with $d\vec{S}$ and $d\tau$ with dV (also a scalar), the Gauss Divergence Theorem is written

$$\int_S \vec{\omega}\cdot d\vec{S} = \int_V \vec{\nabla}\cdot\vec{\omega}\ dV \qquad (101)$$

For a scalar function of time and position (ω), the Gauss Divergence Theorem is (ref 3, eq. 9.124)

$$\int_S \omega \, d\vec{S} = \int_V \vec{\nabla}\omega \, dV \tag{102}$$

Reynold's Transport Theorem

In the Lagrangian approach (figure 3), the moving mass of fluid being studied is imagined to be enclosed by a moving control volume that may change size and shape, but always contains the same mass; i.e. no mass crosses its surface. An observer moving with this Lagrangian control volume can detect no change in a fluid property α with respect to any spatial coordinates, since to him the control volume and any mass within it are stationary. But the property α is changing as time passes, so in the Lagrangian sense, $\alpha = \alpha(t)$ only.

Of interest is the integral of the property α over the volume V:

$$I(t) = \int_{V(t)} \alpha(t) \, dV \tag{103}$$

Furthermore, the time rate of change of this integral is desired:

$$\frac{dI(t)}{dt} = \frac{d}{dt} \int_{V(t)} \alpha(t) \, dV \tag{104}$$

The fundamental theorem of the differential calculus is used to expand eq. 104 to the following form.

$$\frac{d}{dt} \int_{V(t)} \alpha(t) \, dV = \lim_{\Delta t \to 0} \frac{1}{\Delta t} \left[\int_{V(t+\Delta t)} \alpha(t+\Delta t) \, dV - \int_{V(t)} \alpha(t) \, dV \right] \tag{105}$$

The geometry of figure 3 is used to modify this expression to the following intermediate form of the Reynold's Transport Theorem.

$$\frac{d}{dt} \int_{V(t)} \alpha(t) \, dV = \int_{V(t)} \frac{\partial \alpha(t)}{\partial t} dV + \int_{S(t)} \alpha(t) \, [\vec{v} \cdot d\vec{S}] \tag{106}$$

Note that the time derivative of the quantity I(t) (eq. 103) at a certain time t has been expressed in terms of quantities evaluated at the same time. This has important implications for the explicit finite difference technique being derived.

The Gauss Divergence Theorem (eq. 101) converts the surface integral into a volume integral, and eq. 106 becomes the following.

$$\frac{d}{dt}\int_{V(t)} \alpha(t)\, dV = \int_{V(t)} \left[\frac{\partial \alpha}{\partial t} + \vec{\nabla}\cdot\alpha\vec{v} \right] dV \tag{107}$$

Equation 107 is the Reynold's Transport Theorem. It accomplishes two things. Mathematically, it moves the differentiation inside the integral. Physically, it relates Lagrangian terms on the left hand side to Eulerian terms on the right hand side.

Conservation of Mass

In a Lagrangian frame of reference, the mass within the control volume does not change. An element of mass within V is written ρdV. The total mass of fluid within V is

$$m = \int_{V(t)} \rho dV$$

Since the mass does not change with time, the time derivative of the integral must be zero.

$$\frac{dm}{dt} = \frac{d}{dt}\int_{V(t)} \rho dV = 0 \tag{111}$$

With the Reynold's Transport Theorem (eq. 107), eq. 111 becomes

$$\frac{d}{dt}\int_{V(t)} \rho(t)\, dV = \int_{V(t)} \left[\frac{\partial \rho}{\partial t} + \vec{\nabla}\cdot\rho\vec{v} \right] dV = 0$$

and since the volume is arbitrary (see also ref 4, pg 153), the only way for the integral to be zero for all control volumes V is if the integrand itself is zero at every point in V.

$$\frac{\partial \rho}{\partial t} + \vec{\nabla}\cdot\rho\vec{v} = 0 \tag{112}$$

Equation 112 is the general differential form of the continuity equation in the three dimensional case. For a one dimensional problem, it reduces to

$$\frac{\partial}{\partial t} + \frac{\partial}{\partial x}(\rho u) = 0 \tag{113}$$

Conservation of Momentum

The resultant force acting on the fluid within the control volume is equal to the time rate of change of momentum.

$$\Sigma F = \frac{dM}{dt} \tag{114}$$

Neglecting body forces (gravitational, electro-magnetic) and viscous shear forces (inviscid fluid), the only force acting on the fluid within V is due to the pressure acting on the surface of V.

$$\Sigma \vec{F} = \int_S p(-d\vec{S}) \tag{115}$$

Here the negative sign is required since $d\vec{S}$ is positive outward, but the resultant force is to be positive inward.

The fluid within the control volume V changes momentum due to changes in velocity resulting from its unsteady motion or its flowing around objects. The momentum of an element of this fluid is $(\rho dV)\vec{v}$. The momentum of the entire volume of fluid is

$$M = \int_V \rho\vec{v}\, dV$$

Substituting this and eq. 115 into eq. 114,

$$-\int_S p\, d\vec{S} = \frac{d}{dt}\int_V \rho\vec{v}\, dV$$

The surface integral may be converted to a volume integral by use of the scalar form of the Gauss Divergence Theorem, eq. 102.

$$-\int_V \vec{\nabla}p\, dV = \frac{d}{dt}\int_V \rho\vec{v}\, dV \tag{116}$$

The integral on the right hand side of eq. 116 can be converted to Eulerian terms by the Reynold's Transport Theorem (eq. 107). Since $\alpha(t)$ in eq. 107 is a scalar, the quantity $\rho\vec{v}$ in eq. 116 must first be written in scalar form. That is, the vector momentum equation will have to be rewritten in its three equivalent scalar components first. For the present work, only the x-momentum equation is of interest. Thus eq. 116 becomes

$$- \int_V \frac{\partial p}{\partial x} dV = \frac{d}{dt} \int_V \rho u \, dV$$

With the Reynold's Transport Theorem (eq. 107), this becomes

$$\int_V \left[\frac{\partial}{\partial t}(\rho u) + \bar{\nabla} \cdot \rho u \vec{v} + \frac{\partial p}{\partial x} \right] dV = 0$$

Since V is arbitrary,

$$\left[\frac{\partial}{\partial t}(\rho u) + \bar{\nabla} \cdot \rho u \vec{v} + \frac{\partial p}{\partial x} \right] = 0 \tag{117}$$

Equation 117 is the general differential form of the x-momentum equation. Note that it is a scalar equation. For a one dimensional problem, it reduces to

$$\frac{\partial}{\partial t} (\rho u) + \frac{\partial}{\partial x} (\rho u^2) = - \frac{\partial p}{\partial x} \tag{118}$$

This can be expanded to the following form.

$$\frac{u}{\rho} \left[\frac{\partial \rho}{\partial t} + \frac{\partial}{\partial x} (\rho u) \right] + \frac{\partial u}{\partial t} + u \frac{\partial u}{\partial x} = - \frac{1}{\rho} \frac{\partial p}{\partial x}$$

But the term in brackets is zero by the continuity equation (eq. 113). Thus the one dimensional momentum equation is:

$$\frac{\partial u}{\partial t} + u \frac{\partial u}{\partial x} = - \frac{1}{\rho} \frac{\partial p}{\partial x} \tag{119}$$

Conservation of Energy

The principle of conservation of energy states that the rate of change of energy of the fluid within the control volume V is equal to the rate at which heat is added plus the rate at which work is done on the fluid. The energy balance is written:

$$\begin{bmatrix}\text{rate at which heat}\\ \text{is added to fluid}\\ \text{within V}\end{bmatrix} + \begin{bmatrix}\text{rate at which work}\\ \text{is done on fluid}\\ \text{within V}\end{bmatrix} = \begin{bmatrix}\text{rate of change of}\\ \text{energy of fluid}\\ \text{within V}\end{bmatrix} \tag{120}$$

Heat conduction and radiation in the fluid will be neglected. This is permissible for the very short times being computed (milliseconds). Since no mass enters or leaves the Lagrangian control volume, no heat can be convected across S, the surface of V. Thus the first term in the energy balance is zero.

The work in the second term is done by forces; since body forces and shear stresses are being neglected, the only active force is due to the pressure on S, $p d\vec{S}$. The rate of work done by this force on a fluid moving at velocity v is $p d\vec{S} \cdot \vec{v}$. The total rate of work done by the pressure exerted on the fluid within V is

$$W = - \int_S p\vec{v} \cdot d\vec{S} \tag{121}$$

where the negative sign is required to make W positive for pressure acting inward, since p and $d\vec{S}$ are positive in opposite directions.

The specific energy of a mass of fluid is its specific internal energy e, plus its specific kinetic energy, $v^2/2$, where $v^2 = \vec{v} \cdot \vec{v}$, a scalar. All other forms of energy (potential, chemical, etc.) have been neglected.

Since the mass of an element of fluid within V is ρdV and its specific energy is $(e + v^2/2)$, the total energy of the fluid within V is

$$E = \int_V \rho [e + v^2/2] \, dV \tag{122}$$

Substitute eq's. 121 and 122 into eq. 120, recalling that the first term in eq. 120 is zero.

$$- \int_S p\vec{v} \cdot d\vec{S} = \frac{d}{dt} \int_V \rho [e + v^2/2] \, dV$$

The term on the left hand side is converted to a volume integral by the Gauss divergence Theorem (eq. 101).

$$- \int_V \vec{\nabla} \cdot p\vec{v} \, dV = \frac{d}{dt} \int_V \rho [e + v^2/2] \, dV$$

The term on the right hand side is simplified by the Reynold's Transport Theorem (eq. 107). After rearranging, the following equation results.

$$\int_V \left[\frac{\partial}{\partial t} \rho [e + v^2/2] + \vec{\nabla} \cdot \rho [e + v^2/2] \vec{v} + \vec{\nabla} \cdot p\vec{v} \right] dV = 0$$

Since V is arbitrary,

$$\left[\frac{\partial}{\partial t} \rho [e + v^2/2] + \vec{\nabla} \cdot \rho [e + v^2/2] \vec{v} + \vec{\nabla} \cdot p\vec{v} \right] = 0 \tag{123}$$

Equation 123 is the general differential form of the conservation of energy. For a one dimensional problem, it reduces to the following.

$$\frac{\partial}{\partial t}\rho[e + u^2/2] + \frac{\partial}{\partial x}\rho u[e + u^2/2 + \frac{p}{\rho}] = 0 \tag{124}$$

The Integral Equations of Motion

In the Lagrangian approach, we consider a certain body of fluid as it moves along in the flowfield. The integral equations are simplified by this approach since the mass of the fluid element under study does not change with time. As seen in figure 4, this fluid occupies a region of the x axis from $a_0(t)$ to $a_1(t)$, and contains a discontinuity (shock wave) at $x = \xi(t)$. Note that subscript 0 denotes conditions behind the shock wave, and subscript 1 denotes conditions ahead. This is consistent with figure 2.

Conservation of Mass

In this one dimensional analysis we consider a unit area in the direction of flow (i.e. perpendicular to the x axis). The mass of an element of this fluid is then

$$dm = \rho(x,t)\ [1dx]$$

and the total mass of this body of fluid is

$$m = \int_{a_0(t)}^{a_1(t)} \rho(x,t)\ dx$$

The mass of this fluid is constant; this is implicit in the Lagrangian approach. The principle of conservation of mass follows directly:

$$\frac{d}{dt}\int_{a_0(t)}^{a_1(t)} \rho(x,t)\ dx = 0 \tag{125}$$

Conservation of Momentum

The momentum of an element of the fluid is

$$dM = \rho(x,t)\ [1dx]\ u(x,t)$$

so the total momentum of the body of fluid is:

$$M = \int_{a_0(t)}^{a_1(t)} \rho(x,t)\ u(x,t)\ dx$$

The only forces acting on our one-dimensional fluid mass are the pressures at the ends, $1 \cdot p_0$ and $-1 \cdot p_1$, where 1 is the area of each end. Body and shear forces are neglected. Combining the fluid momentum, pressure forces, and Newton's Law yields the principle of conservation of momentum:

$$\frac{d}{dt} \int_{a_0(t)}^{a_1(t)} \rho(x,t)\ u(x,t)\ dx = p_0 - p_1 \tag{126}$$

Note that both velocity and pressure-force have been considered positive in the +x direction.

Conservation of Energy

If the body of fluid is not undergoing any chemical reactions and has no heat transferred in or out, we may assume it changes energy only because of the work done by the external forces, $1 \cdot p_0$ and $1 \cdot p_1$. The rate at which work is done (power) must be equal to the rate at which the energy of the body of fluid is increasing. This is the conservation of energy.

p_0 does positive work at the rate of $1 \cdot p_0 u_0$
p_1 does negative work at the rate of $1 \cdot p_1 u_1$

If $e(x,t)$ is the specific internal energy and $u(x,t)^2/2$ is the specific kinetic energy, and all other forms of energy are neglected (chemical, potential, etc.), then the total energy of an element of the fluid is

$$dE = [e(x,t) + u(x,t)^2/2]\ \rho(x,t)\ [1dx]$$

and the total energy of the entire fluid mass is

$$E = \int_{a_0(t)}^{a_1(t)} [e(x,t) + u(x,t)^2/2]\ \rho(x,t)\ [1dx]$$

Finally, the conservation of energy follows.

$$\frac{d}{dt} \int_{a_0(t)}^{a_1(t)} [e(x,t) + u(x,t)^2/2]\ \rho(x,t)\ dx = p_0 u_0 - p_1 u_1 \tag{127}$$

Chapter 2

THE FINITE DIFFERENCE EQUATIONS

The following differential equations of motion for one-dimensional inviscid fluid flow problems were derived previously.

$$\frac{\partial}{\partial t}[\rho] + \frac{\partial}{\partial x}[\rho u] = 0 \tag{113}$$

$$\frac{\partial}{\partial t}[\rho u] + \frac{\partial}{\partial x}[p+\rho u^2] = 0 \tag{118}$$

$$\frac{\partial}{\partial t}\left[\rho(e + \frac{u^2}{2})\right] + \frac{\partial}{\partial x}\left[\rho u(e + \frac{u^2}{2} + \frac{p}{\rho})\right] = 0 \tag{124}$$

These equations are valid at any point in the flow field (and at any time) provided the flow variables are changing continuously at that point (and time). If points (times) exist in the flowfield at which the flow variables are changing discontinuously, the differential equations of motion must be integrated over some arbitrary but finite area containing the discontinuity. In this way the discontinuity is made mathematically continuous.

For example, consider the pressure discontinuity in space (i.e. shock wave) shown in figure 5. The derivative $\frac{dp}{dx}$ is clearly infinite at x=b, owing to the pressure discontinuity at that point. This difficulty would made an equation like eq. 118 meaningless. However, if the derivative is integrated over some finite interval containing the discontinuity, the result is well behaved. The discontinuity can be written mathematically with the help of the Heavyside step function (ref 3).

$$H(x-b) = \begin{cases} 1 & x > b \\ 0 & x < b \end{cases}$$

Thus the pressure function pictured in figure 5 is written as follows.

$$p(x) = p_1 + [p_2 - p_1]\, H(x-b)$$

The derivative of this discontinuous function is of concern. The derivative is integrated over a region containing the discontinuity, say x=a to x=c.

$$\int_a^c \frac{dp}{dx}\,dx = \int_a^c \frac{d}{dx}\left[p_1+(p_2-p_1)H(x-b)\right]dx$$

$$= (p_2-p_1)\int_a^c H'(x-b)\,dx$$

Notice that p_1 and p_2 are constant in the region of integration. Since the integral of a derivative of a function is simply that function, the integral above is simply the Heavyside function evaluated at x=c minus the function at x=a (1 and 0 respectively, by definition). The original integral is rewritten, showing that the discontinuity has been mathematically avoided:

$$\int_a^c \frac{dp}{dx}\,dx = (p_2-p_1)$$

Since discontinuities in the flow field can exist in either time or space, the differential equations of motion must be integrated twice. Consider an arbitrary flow variable $\phi(x,t)$ (density, momentum, or energy) as shown in figure 6. Notice in the figure that the letters f and F are used to indicate the value of the fluid property ϕ on the boundaries of the cell. These will be discussed in greater detail below. The derivatives of the property ϕ are integrated over the x-t region shown in figure 6.

$$\int_{t_n}^{t_{n+1}}\int_{x_m}^{x_{m+1}} \frac{\partial\phi}{\partial x}\,dx\,dt = \int_{t_n}^{t_{n+1}}\left[\int_{x_m}^{x_{m+1}} \frac{\partial\phi}{\partial x}\,dx\right]dt$$

$$= \int_{t_n}^{t_{n+1}}\left[\phi(x_{m+1},t) - \phi(x_m,t)\right]dt \qquad (201)$$

Here $\phi(x_m,t)$ is the instantaneous value of ϕ at the point x_m, so $\phi(x_m,t)$ is a function of time only. It is now assumed to be constant over the time step (from t_n to t_{n+1}), although it may vary from one time step to the next. A similar assumption is made about $\phi(x_{m+1},t)$. Denote these values by F_m and F_{m+1}. These two values are defined by the following expressions.

$$F_m = \frac{1}{\tau}\int_{t_n}^{t_{n+1}} \phi(x_m,t)\,dt \qquad (202)$$

$$F_{m+1} = \frac{1}{\tau}\int_{t_n}^{t_{n+1}} \phi(x_{m+1},t)\,dt \qquad (203)$$

That is F is a time averaged value (over a single time step) taken along the beginning or ending cell boundary. Henceforth, all upper case variable names (R for density, U for velocity, E for energy) will represent such time averaged values. They are also the fluid properties behind the waves that are imagined to emanate from the cell boundaries due to the discontinuities in fluid properties that exist there. They are found by solving the Riemann problem at the boundary, which is detailed in chapter 3. Substitution of eqs. 202 and 203 into eq. 201 yields the desired result.

$$\int_{t_n}^{t_{n+1}} \int_{x_m}^{x_{m+1}} \frac{\partial \phi}{\partial x} \, dx \, dt = \tau \left[F_{m+1} - F_m \right] \tag{204}$$

The time derivative of ϕ is integrated in an analogous manner.

$$\int_{x_m}^{x_{m+1}} \int_{t_n}^{t_{n+1}} \frac{\partial \phi}{\partial t} \, dt \, dx = \int_{x_m}^{x_{m+1}} \left[\int_{t_n}^{t_{n+1}} \frac{\partial \phi}{\partial t} \, dt \right] dx$$

$$= \int_{x_m}^{x_{m+1}} \left[\phi(x, t_{n+1}) - \phi(x_n, t) \right] dt \tag{205}$$

Here $\phi(x,t_n)$ represents the value of ϕ at any point at the time t_n; that is $\phi(x,t_n)$ is a function of x only. It is now assumed to be constant over the space step (the 1-D analogy of the 2-D computational cell) x_m to x_{m+1}, although ϕ may vary from one position (space step) to the next. A similar assumption is made about $\phi(x,t_{n+1})$. These average values are denoted by $f_{m+1/2}$ and $f^{m+1/2}$ (see figure 6). In this notation, the m+1/2 denotes the average value over the x interval from m (i.e. x_m) to m+1 (i.e. x_{m+1}), the superscript denotes an average taken at the end of the time step, t_{n+1}, and the subscript denotes an average taken at the beginning of the time step, t_n. The average value of a property may be written in the following manner.

$$f^{m+1/2} = \frac{1}{h} \int_{x_m}^{x_{m+1}} \phi(x, t_{n+1}) \, dx \tag{206}$$

$$f_{m+1/2} = \frac{1}{h} \int_{x_m}^{x_{m+1}} \phi(x, t_n) \, dx \tag{207}$$

Thus f is a space averaged value (over a single space step) taken at either the beginning or end of the time step. Henceforth, lower case variable names (ρ for density, u for velocity, and e for energy) will be used to denote the fluid properties that exist within the cell. They have been assumed to be constant within the cell. Notice that the spatial averaging procedure forces any discontinuities in the flow field to be displaced to the border of a computational cell. Substitution of eq. 206 and eq. 207 into eq. 205 yields the desired result.

$$\int_{x_m}^{x_{m+1}} \int_{t_n}^{t_{n+1}} \frac{\partial \phi}{\partial t} \, dt \, dx = h \left[f^{m+1/2} - f_{m+1/2} \right] \tag{208}$$

Conservation of Mass

As previously noted, the differential equations of motion must be integrated over time and over space in order to be valid for flow fields containing shock waves. Equations 204 and 208 provide tools for performing numerical integrations of these equations. Begin by integrating eq. 113.

$$\int_{t_n}^{t_{n+1}} \int_{x_m}^{x_{m+1}} \left[\frac{\partial}{\partial t} [\rho] + \frac{\partial}{\partial x} [\rho u] \right] dx \, dt = 0$$

$$\int_{x_m}^{x_{m+1}} \int_{t_n}^{t_{n+1}} \frac{\partial}{\partial t} [\rho] \, dt \, dx + \int_{t_n}^{t_{n+1}} \int_{x_m}^{x_{m+1}} \frac{\partial}{\partial x} [\rho u] \, dx \, dt = 0$$

Note that reversing the order of integration for well behaved (constant) functions presents no mathematical difficulty. With the help of eqs. 204 and 208, eq 113 is reduced to the finite difference form.

$$\rho^{m+1/2} = \rho_{m+1/2} - \frac{\tau}{h} \left[[RU]_{m+1} - [RU]_m \right] \tag{209}$$

This relates the density in the space step (x_m to x_{m+1}) at time (t_{n+1}) to known values in the space step from the previous time step (t_n).

Conservation of Momentum

Integrating eq. 118 leads to the following.

$$\int_{t_n}^{t_{n+1}} \int_{x_m}^{x_{m+1}} \left[\frac{\partial}{\partial t} [\rho u] + \frac{\partial}{\partial x} [p + \rho u^2] \right] dx \, dt = 0$$

$$\int_{x_m}^{x_{m+1}} \int_{t_n}^{t_{n+1}} \frac{\partial}{\partial t} [\rho u] \, dt \, dx + \int_{t_n}^{t_{n+1}} \int_{x_m}^{x_{m+1}} \frac{\partial}{\partial x} [p+\rho u^2] \, dx \, dt = 0$$

Again eqs. 204 and 208 are used to reduce this to the finite difference form.

$$[\rho u]^{m+1/2} = [\rho u]_{m+1/2} - \frac{\tau}{h} \left[[P+RU^2]_{m+1} - [P+RU^2]_m \right] \tag{210}$$

Equation 210 relates the momentum in the space step at time (t_{n+1}) to known values in the space step from the previous time step (t_n).

Conservation of Energy

To obtain the finite difference form of the Conservation of Energy equation, begin by integrating eq. 124.

$$\int_{t_n}^{t_{n+1}} \int_{x_m}^{x_{m+1}} \left[\frac{\partial}{\partial t} [\rho(e+\frac{u^2}{2})] + \frac{\partial}{\partial x} [\rho u(e+\frac{u^2}{2}+\frac{p}{\rho})] \right] dx \, dt = 0$$

$$\int_{x_m}^{x_{m+1}} \int_{t_n}^{t_{n+1}} \frac{\partial}{\partial t}[\rho(e+\frac{u^2}{2})] \, dt \, dx + \int_{t_n}^{t_{n+1}} \int_{x_m}^{x_{m+1}} \frac{\partial}{\partial x}[\rho u(e+\frac{u^2}{2}+\frac{p}{\rho})] \, dx \, dt = 0$$

Again, eqs. 204 and 208 are used, with the following result.

$$[\rho(e+\frac{u^2}{2})]^{m+1/2} = [\rho(e+\frac{u^2}{2})]_{m+1/2} - \frac{\tau}{h}\left[[RU(E+\frac{U^2}{2}+\frac{P}{R})]_{m+1} - [RU(E+\frac{U^2}{2}+\frac{P}{R})]_m \right] \tag{211}$$

Equation 211 relates the energy in the space step at time (t_{n+1}) to known values in the space step from the previous time step (t_n).

Equations 209, 210, and 211 form the basis of the finite difference technique utilized. Recall from figure 6 that the lower case letters indicate space averages at a particular instant, and the upper case letters indicate time averages at a particular location.

The same results can be obtained more formally (but less physically) by use of the two-dimensional Green's Theorem, which relates a surface integral to a contour integral.

Chapter 3

COMPUTATION OF THE RIEMANN PROBLEM

The essence of Godunov's method lies in the technique used to estimate the assumedly constant properties on the cell boundaries, as depicted by upper case letters (e.g. F in figure 6). Each boundary is considered as a Riemann Problem (or shock tube analogy) as discussed in the Introduction above. The equations describing the constant (in time) fluid properties behind the waves resulting from the resolution of the discontinuities at the cell boundaries will now be derived. The two types of waves that may result (expansion and compression, or shock) will be considered separately.

Shock Wave Equations

Recall that each computational cell is assigned an average value for each property, and this average value is considered constant throughout the cell. The difference in value from one cell to the next results in a discontinuity at the common cell boundary. If the resolution of the discontinuity (the rupturing of the diaphragm in the shock tube analogy) results in a shock wave, its properties may be computed using the integral equations of motion, equations 125, 126, and 127, as shown below. (ref 5 and ref 6).

Note that the three integral equations of motion involve integrals of the following form.

$$I(t) = \int_{a_0(t)}^{a_1(t)} f(x,t)\ dx \tag{301}$$

where $f(x,t)$ represents ρ, ρu, or $\rho(e+u^2/2)$, and is discontinuous at $x = \xi$, as shown in figure 7. Note also that the subscript 1 denotes conditions ahead of the discontinuity, while subscript 0 denotes those behind. The conservation laws require evaluation of the derivative of eq. 301.

$$\frac{d}{dt}I(t) = \frac{d}{dt}\int_{a_0(t)}^{a_1(t)} f(x,t)\ dx \tag{302}$$

Since $f(x,t)$ is discontinuous at $x = \xi$, the integral is split as follows.

$$\frac{d}{dt}I(t) = \frac{d}{dt}\left\{ \lim_{\epsilon \to 0} \left[\int_{a_0(t)}^{\xi(t)-\epsilon} f(x,t)\ dx + \bar{f}(x,t)[(\xi+\epsilon)-(\xi-\epsilon)] + \int_{\xi(t)+\epsilon}^{a_1(t)} f(x,t)\ dx \right] \right\}$$

where $\bar{f}(x,t)$ is (by the mean value theorem) some value between the minimum value of $f(x,t)$ (f_1) and the maximum value (f_0) in the interval $[\xi \pm \epsilon]$. That is, $\bar{f}(x,t)$ is finite. Since the term in the large curly brackets above is a limit of the sum of three well behaved functions, the order of the operations may be reversed and the sum of three limits may be substituted.

$$\frac{d}{dt}I(t) = \frac{d}{dt}\left\{ \lim_{\epsilon \to 0}\left[\int_{a_0(t)}^{\xi(t)-\epsilon} f(x,t)\ dx \right] + \lim_{\epsilon \to 0}\left[2\epsilon \bar{f}(x,t) \right] + \lim_{\epsilon \to 0}\left[\int_{\xi(t)+\epsilon}^{a_1(t)} f(x,t)\ dx \right] \right\}$$

Since $\bar{f}(x,t)$ is finite, the second limit term is zero. Furthermore,

$$\lim_{\epsilon \to 0}\left[\int_{a_0(t)}^{\xi(t)-\epsilon} f(x,t)\ dx \right] = \int_{a_0(t)}^{\xi(t)} f(x,t)\ dx$$

$$\lim_{\epsilon \to 0}\left[\int_{\xi(t)+\epsilon}^{a_1(t)} f(x,t)\ dx \right] = \int_{\xi(t)}^{a_1(t)} f(x,t)\ dx$$

So eq. 302 may be written:

$$\frac{d}{dt}I(t) = \frac{d}{dt}\int_{a_0(t)}^{\xi(t)} f(x,t)\ dx + \frac{d}{dt}\int_{\xi(t)}^{a_1(t)} f(x,t)\ dx \qquad (303)$$

Leibnitz' rule (ref 3) states that if

$$J(t) = \int_{a_0(t)}^{a_1(t)} f(x,t)\ dx$$

then

$$\frac{d}{dt}J(t) = \frac{d}{dt}\int_{a_0(t)}^{a_1(t)} f(x,t)\ dx$$

$$= \int_{a_0(t)}^{a_1(t)} \frac{\partial f(x,t)}{\partial t}\ dx + f(a_1,t)\frac{da_1}{dt} - f(a_0,t)\frac{da_0}{dt}$$

With this, eq. 303 becomes

$$\frac{d}{dt}I(t) = \int_{a_0(t)}^{\xi(t)} \frac{\partial f(x,t)}{\partial t}\, dx + f_0(\xi,t)\frac{d\xi}{dt} - f(a_0,t)\frac{da_0}{dt}$$

$$+ \int_{\xi(t)}^{a_1(t)} \frac{\partial f(x,t)}{\partial t}\, dx + f(a_1,t)\frac{da_1}{dt} - f_1(\xi,t)\frac{d\xi}{dt}$$

where $f_0(\xi(t),t)$ and $f_1(\xi(t),t)$, or more simply f_0 and f_1, are shown in figure 7. Also,

$$\frac{da_0}{dt} = u_0 \quad ; \quad \frac{da_1}{dt} = u_1 \quad ; \quad \frac{d\xi}{dt} = W$$

Note that W is the wave velocity, measured relative to the fixed frame of reference (the x axis), and make the following substitutions.

$$\frac{d}{dt}I(t) = \int_{a_0(t)}^{\xi(t)} \frac{\partial f(x,t)}{\partial t}\, dx + \int_{\xi(t)}^{a_1(t)} \frac{\partial f(x,t)}{\partial t}\, dx$$

$$+ f_0 W - f(a_0(t),t)u + f(a_1(t),t)u_1 - f_1 W$$

Now shrink the interval so that it contains only the discontinuity. That is, let $a_0 \to \xi$ and $a_1 \to \xi$. Note the following limits:

$$\lim_{a_0 \to \xi} \int_{a_0(t)}^{\xi(t)} \frac{\partial f(x,t)}{\partial t}\, dx = 0$$

$$\lim_{a_1 \to \xi} \int_{\xi(t)}^{a_1(t)} \frac{\partial f(x,t)}{\partial t}\, dx = 0$$

$$\lim_{a_0 \to \xi} \left[f(a_0(t),t) \right] = f_0$$

$$\lim_{a_1 \to \xi} \left[f(a_1(t),t) \right] = f_1$$

With these substitutions, the integral equation is reduced to an algebraic equation.

$$\frac{d}{dt}I(x,t) = 0 + 0 + f_0W - f_0u_0 + f_1u_1 - f_1W$$

$$\frac{d}{dt}I(x,t) = f_1(u_1-W) - f_0(u_0-W)$$

Combine this with eq. 302 to obtain the following result.

$$\frac{d}{dt}\int_{a_0(t)}^{a_1(t)} f(x,t)\,dx = f_1(u_1-W) - f_0(u_0-W) \tag{304}$$

Recall that subscript 1 denotes conditions on the leading edge of the shock wave, and 0 denotes those on the trailing edge. W is the velocity of the shock wave relative to the fixed frame. Equation 304 may be used to reduce the integral equations of motion (eq's. 125, 126, and 127) to algebraic equations relating the flow parameters across the discontinuity.

First combine eq's. 125 and 304 to obtain the continuity equation in algebraic form.

$$\rho_1(u_1-W) - \rho_0(u_0-W) = 0$$

Define

$$w = W - u_1 \tag{305}$$

as the velocity of the wave relative to the fluid into which the wave is propagating. With this substitution, the continuity equation becomes

$$\rho_1[u_1-(w+u_1)] - \rho_0[u_0-(w+u_1)] = 0$$

$$\rho_1 w\left[\frac{1}{\rho_1} - \frac{1}{\rho_0}\right] + \left[u_1 - u_0\right] = 0$$

$$\rho_1 w\left[\frac{1}{\rho}\right] + [u] = 0 \tag{306}$$

The square brackets in eq. 306 indicate the change in a discontinuous quantity across the shock wave. For the case of a positive running wave (W is positive), let the mass velocity of the wave (the mass of fluid swept over by the wave in a unit time per unit area [ref 7]) be denoted by b, where

$$b = \rho_1 w \tag{307}$$

so that eq. 306 becomes

$$b\left[\frac{1}{\rho}\right] + [u] = 0 \tag{308}$$

For the case of a negative running wave (W is negative), the mass velocity is denoted by a, as follows.

$$a = -\rho_1 w \tag{309}$$

Substituting into eq. 306 yields the conservation of mass for the negative running wave.

$$a \left[\frac{1}{\rho} \right] - [\, u \,] = 0 \tag{310}$$

Combining eq. 126 and eq. 304 yields the momentum equation in algebraic form.

$$\rho_1 u_1 (u_1 - W) - \rho_0 u_0 (u_0 - W) = p_0 - p_1$$

Substitute eq. 305.

$$\rho_1 u_1 [u_1 - (w + u_1)] - \rho_0 u_0 [u_0 - (w + u_1)] = (p_0 - p_1)$$

Rearrange:

$$-\rho_1 w(u_1 - u_0) + (p_1 - p_0) = -\rho_0 u_0 \left\{ \rho_1 w \left[\frac{1}{\rho_1} - \frac{1}{\rho_0} \right] + (u_1 - u_0) \right\}$$

The quantity in curly brackets is zero by the continuity equation (eq. 306).

$$\rho_1 w(u_1 - u_0) - (p_1 - p_0) = 0 \tag{311}$$

For a positive running wave, substitute eq. 307.

$$b(u_1 - u_0) - (p_1 - p_0) = 0$$

or with the bracket notation,

$$b[\, u \,] - [\, p \,] = 0 \tag{312}$$

For a negative running wave, substitute eq. 309.

$$-a(u_1 - u_0) - (p_1 - p_0) = 0$$

or with the bracket notation,

$$a[\, u \,] + [\, p \,] = 0 \tag{313}$$

Finally, combining eq. 127 and eq. 304 yields the energy equation in algebraic form.

$$\rho_1(e_1+\frac{u_1^2}{2})(u_1-W) - \rho_0(e_0+\frac{u_0^2}{2})(u_0-W) = (p_0u_0-p_1u_1)$$

For simplicity, let

$$\epsilon = e + \frac{u^2}{2}$$

and substitute eq. 305.

$$\rho_1\epsilon_1[u_1-(w+u_1)] - \rho_0\epsilon_0[u_0-(w+u_1)] = (p_0u_0-p_1u_1)$$

Rearrange:

$$\rho_1w(\epsilon_1-\epsilon_0) - (p_1u_1-p_0u_0) = \rho_0\epsilon_0 \left\{ \rho_1w \left[\frac{1}{\rho_1} - \frac{1}{\rho_0} \right] + (u_1-u_0) \right\}$$

Again the term in the curly brackets is zero by the continuity equation, eq. 306.

$$\rho_1w(\epsilon_1-\epsilon_0) - (p_1u_1-p_0u_0) = 0 \tag{314}$$

For a positive running wave, substitute eq. 307. With the square bracket notation, the energy equation is written

$$b\left[e + \frac{u^2}{2} \right] - [\, pu \,] = 0 \tag{315}$$

For a negative running wave, substitute eq. 307. With the square bracket notation, the energy equation is written

$$a\left[e + \frac{u^2}{2} \right] + [\, pu \,] = 0 \tag{316}$$

The shock wave equations are summarized in Table 1. The square brackets denote jump conditions across the wave, and now subscripts are as denoted in figure 2.

Positive Running Wave	Negative Running Wave
$b\left[\frac{1}{\rho}\right] + [u] = 0$	$a\left[\frac{1}{\rho}\right] - [u] = 0$
$b[u] - [p] = 0$	$a[u] + [p] = 0$
$b\left[e + \frac{u^2}{2}\right] - [pu] = 0$	$a\left[e + \frac{u^2}{2}\right] + [pu] = 0$
$b = \rho_4 w$	$a = -\rho_1 w$

Table 1. Equations relating flow parameters across a discontinuity.

The next task is to evaluate a and b. To do so, the positive running wave and the negative running wave must be considered separately. A negative running compression wave (figure 2) is characterized by $p_0 > p_4$. Equations 310 and 313 are combined to eliminate the velocity by solving Eq. 310 for [u] and substituting the result into eq. 313.

$$a[a(\frac{1}{\rho})] + [p] = 0$$

$$a = \left[\frac{p_4 - p_0}{\frac{1}{\rho_4} - \frac{1}{\rho_3}}\right]^{1/2} \tag{317}$$

For an ideal gas (see Appendix A),

$$\frac{1}{\rho_3} = \left[\frac{(\gamma-1)p_0 + (\gamma+1)p_4}{(\gamma+1)p_0 + (\gamma-1)p_4}\right]\frac{1}{\rho_4}$$

When this is substituted into eq. 317 and the terms rearranged, the result is the following equation for the mass velocity of the negative running compression wave.

$$a = \sqrt{\gamma p_4 \rho_4}\left\{1 - \frac{\gamma+1}{2\gamma}\left[1 - \frac{p_0}{p_4}\right]\right\}^{1/2} \tag{318}$$

The positive running compression wave (figure 2) is characterized by $p_0 > p_1$. The above steps are repeated, this time using equations 308 and 312. Equation 308 is solved for [u] and the result is substituted into eq. 312. When the actual pressures and densities from figure 2 are used in place of the bracket notation, the result is the following.

$$a = \left[\frac{p_1 - p_0}{\frac{1}{\rho_1} - \frac{1}{\rho_2}} \right]^{1/2} \tag{319}$$

For an ideal gas (see Appendix A),

$$\frac{1}{\rho_1} = \left[\frac{(\gamma-1)p_1 + (\gamma+1)p_0}{(\gamma+1)p_1 + (\gamma-1)p_0} \right] \frac{1}{\rho_2}$$

When this is substituted into eq. 319 and the terms rearranged, the result is the following equation for the mass velocity of the positive running compression wave.

$$b = \sqrt{\gamma p_1 \rho_1} \left\{ 1 - \frac{\gamma+1}{2\gamma} \left[1 - \frac{p_0}{p_1} \right] \right\}^{1/2} \tag{320}$$

Expansion Wave Equations

The differential equations of motion are valid across an expansion wave. To reiterate, these are:

$$\frac{\partial}{\partial t} (\rho) + \frac{\partial}{\partial x} (\rho u) = 0 \tag{113}$$

$$\frac{\partial u}{\partial t} + u \frac{\partial u}{\partial x} = - \frac{1}{\rho} \frac{\partial p}{\partial x} \tag{119}$$

$$\frac{\partial}{\partial t} \left[\rho \left(e + \frac{u^2}{2} \right) \right] + \frac{\partial}{\partial x} \left[\rho u \left(e + \frac{u^2}{2} + \frac{p}{\rho} \right) \right] = 0 \tag{124}$$

Equation 124 will not be used in this form. It will be replaced by the isentropic gas law,

$$\frac{p}{\rho^\gamma} = \text{constant} \tag{321}$$

since flow across an expansion wave is adiabatic and reversible. From eq. 321, $p=p(\rho)$ only, so

$$\frac{\partial p}{\partial x} = \frac{dp}{d\rho} \frac{\partial \rho}{\partial x} \tag{322}$$

Also, one can show (e.g. ref 4) that for weak waves, $u = u(\rho)$ only, so

$$\frac{\partial \rho}{\partial t} = \frac{d\rho}{du}\frac{\partial u}{\partial t} \tag{323}$$

and

$$\frac{\partial \rho}{\partial x} = \frac{d\rho}{du}\frac{\partial u}{\partial x} \tag{324}$$

so that eq. 322 becomes

$$\frac{\partial p}{\partial x} = \frac{dp}{d\rho}\frac{d\rho}{du}\frac{\partial u}{\partial x} \tag{325}$$

Substitute eq. 325 into eq. 119.

$$\frac{\partial u}{\partial t} + u\frac{\partial u}{\partial x} = -\frac{1}{\rho}\frac{dp}{d\rho}\frac{d\rho}{du}\frac{\partial u}{\partial x} \tag{326}$$

Now expand eq. 113,

$$\frac{\partial \rho}{\partial t} + u\frac{\partial \rho}{\partial x} + \rho\frac{\partial u}{\partial x} = 0$$

and substitute eq. 323 and eq. 324.

$$\frac{d\rho}{du}\frac{\partial u}{\partial t} + u\frac{d\rho}{du}\frac{\partial u}{\partial x} + \rho\frac{\partial u}{\partial x} = 0$$

$$\frac{d\rho}{du}\left[\frac{\partial u}{\partial t} + u\frac{\partial u}{\partial x}\right] + \rho\frac{\partial u}{\partial x} = 0$$

Now substitute eq. 326.

$$\frac{d\rho}{du}\left[-\frac{1}{\rho}\frac{dp}{d\rho}\frac{d\rho}{du}\frac{\partial u}{\partial x}\right] + \rho\frac{\partial u}{\partial x} = 0$$

$$\frac{\partial u}{\partial x}\left\{\rho - \frac{1}{\rho}\frac{dp}{d\rho}\left[\frac{d\rho}{du}\right]^2\right\} = 0$$

But $\frac{\partial u}{dx} \neq 0$, so the quantity in curly brackets must be zero. That term is set equal to zero and rearranged, with the following result.

$$\frac{dp}{d\rho}\left[\frac{d\rho}{du}\right]^2 = \rho^2$$

Since flow across an expansion wave is isentropic, $\frac{dp}{d\rho} = c^2$, where c is the speed of sound (ref 4). Substituting this, taking the square root of each term and rearranging results in

$$du = \pm \frac{c}{\rho} d\rho \tag{327}$$

where the positive sign indicates the wave is moving in the positive direction (ie positive running wave), and the negative sign indicates the wave is moving in the negative direction (ie negative running wave).

Equation 327 must be integrated to find the conditions within the expansion wave. First, substitute for the speed of sound of a perfect gas,

$$c = \sqrt{\gamma p/\rho}$$

so that eq. 327 becomes

$$du = \pm \left[\frac{\gamma p}{\rho^3} \right]^{1/2} d\rho \tag{328}$$

From eq. 321,

$$\frac{p}{\rho^\gamma} = \text{constant} = \frac{p_1}{\rho_1^\gamma}$$

Where the known conditions ahead of the expansion wave (subscript 1 in the case of a positive running wave as shown in figure 2) have been used to evaluate the constant. Solving for p and substituting into eq. 328,

$$du = \pm \left\{ \frac{\gamma}{\rho^3} \left[\frac{p_1}{\rho_1^\gamma} \rho^\gamma \right] \right\}^{1/2} d\rho$$

Now integrate over the whole expansion wave in order to relate the conditions behind it (subscript 0) to those ahead (subscript 1).

$$\int_0^1 du = \pm \left[\frac{\gamma p_1}{\rho_1^\gamma} \right]^{1/2} \int_0^1 \rho^{(\gamma-3)/2} d\rho$$

$$u_1 - u_0 = \pm \frac{2}{\gamma-1} \left[\frac{\gamma p_1}{\rho_1^\gamma} \right]^{1/2} \left[\rho_1^{(\gamma-1)/2} - \rho_0^{(\gamma-1)/2} \right]$$

Rearrange this and substitute the isentropic gas law (eq. 321) in the following form:

$$\frac{\rho_0}{\rho_1} = \left[\frac{p_0}{p_1} \right]^{1/\gamma}$$

to obtain

$$u_1 - u_0 = \pm \frac{2}{\gamma - 1} \left[\frac{\gamma p_1}{\rho_1} \right]^{1/2} \left[1 - \left[\frac{p_1}{p_0} \right]^{(\gamma-1)/2\gamma} \right]$$

When the right hand side is multiplied by

$$\frac{(p_1 - p_0)}{(p_1 - p_0)}$$

and the terms rearranged, the equation reduces to the following simplified form,

$$\pm K(u_1 - u_0) - (p_1 - p_0) = 0 \tag{329}$$

where

$$K = \frac{\gamma - 1}{2\gamma} \sqrt{\gamma p_1 \rho_1} \left\{ \frac{1 - \left[p_0/p_1 \right]}{1 - \left[p_0/p_1 \right]^{(\gamma-1)/2\gamma}} \right\} \tag{330}$$

Again, the positive sign in eq. 329 is associated with the positive running wave and the negative sign is associated with the negative running wave. From figure 2, conditions ahead of the positive running wave are denoted by subscript 1, while conditions ahead of the negative running wave are denoted by replacing the subscript 1 in eqs. 329 and 330 with a subscript 4. The pressure and velocity behind either wave is denoted by subscript 0. Using the square bracket notation to represent conditions across the expansion wave, eq. 329 can be rewritten

$$\pm K[u] - [p] = 0 \tag{331}$$

Finally, let $a = -K$ and $b = +K$. This is done so that the equations are similar to the momentum equations for the shock wave, eqs. 312 and 313. This substitution will simplify the final computer program.

For the negative running expansion wave ($p_4 > p_0$),

$$a[u] + [p] = 0 \tag{332}$$

where

$$a = \frac{\gamma-1}{2\gamma}\sqrt{\gamma p_4 \rho_4}\ \frac{1-\left[p_0/p_4\right]}{1-\left[p_0/p_4\right]^{(\gamma-1)/2\gamma}} \tag{333}$$

and for the positive running expansion wave ($p_1 > p_0$),

$$b[u] - [p] = 0 \tag{334}$$

where

$$b = \frac{\gamma-1}{2\gamma}\sqrt{\gamma p_1 \rho_1}\ \frac{1-\left[p_0/p_1\right]}{1-\left[p_0/p_1\right]^{(\gamma-1)/2\gamma}} \tag{335}$$

Generalized Conditions Behind a Wave

Attention is now turned to the practical problem of using the equations derived above to solve the Riemann problem at a particular cell boundary. Notice that the momentum equation for the negative running expansion wave, eq. 332, is identical in form to that of the negative running compression wave, eq. 313. The only difference is in the equation used to evaluate the mass velocity a. Thus any numerical scheme used will have to test to see if p_4 is greater or less than p_0 and then use the appropriate equation to compute a. A similar arguement can be made for the positive running waves and the value of b. With these differences in mind, the different forms of the variables a and b are momentarily disregarded. Thus for the negative running wave, expansion or compression,

$$a[u] + [p] = 0$$

or

$$a(u_4-u_0) + (p_4-p_0) = 0 \tag{336}$$

and for the positive running wave, expansion or compression,

$$b[u] - [p] = 0$$

or

$$b(u_1-u_0) - (p_1-p_0) = 0 \tag{337}$$

Solve eq. 336 for p_0.

$$p_0 = au_4 + p_4 - au_0 \tag{338}$$

Solve eq. 337 for u_0.

$$u_0 = \frac{1}{b}(p_0 - p_1) + u_1 \tag{339}$$

Now substitute eq. 339 into eq. 338.

$$p_0 = au_4 + p_4 - \frac{a}{b}(p_0 - p_1) - au_1$$

After rearranging,

$$p_0 = \frac{bp_4 + ap_1 + ab(u_4 - u_1)}{a + b} \tag{340}$$

Now substitute eq. 340 into eq. 339 and rearrange to obtain the following.

$$u_0 = \frac{au_4 + bu_1 + (p_4 - p_1)}{a + b} \tag{341}$$

Equations 340 and 341, when combined with the equations for a and b, are highly nonlinear. They must be solved iteratively for p_0, a and b, after which u_0 is found easily. The iterative technique used in this work is discussed in detail in Appendix B.

In the case of weak (sonic) waves, approximate formulae may be used to compute p_0 and u_0. These approximate formulae eliminate the need for iteration and significantly reduce computer time. Experience has shown that the full nonlinear equations need only be used when the cell is in proximity to an actual shock wave in the flow field. A comparison of the magnitudes of pressure in the two adjacent cells suffices to determine the need for the nonlinear equations when computing the Riemann problem on any particular boundary.

Weak waves result from the resolution of the discontinuity at a cell boundary when the fluid conditions (velocity, density, pressure) in the left and right cells are nearly equal. In most cases the grid cell size can be chosen small enough that the average properties in any two adjacent cells are nearly equal. In this way, the approximate formulae may be used everywhere except in the neighborhood of a discontinuity in the actual flowfield. In this case large differences in properties will exist across boundaries of adjacent cells. Note that the distinction between expansion and compression waves is unimportant for weak waves.

The essence of the approximation lies in the assumption that weak waves will travel at the local speed of sound. Thus the velocity of the negative running wave is

$$w = \sqrt{\gamma p_4 / \rho_4}$$

In terms of the mass velocity a (eq. 309) this is

$$w = a/\rho_4$$

Equating the two forms yields

$$a = \sqrt{\gamma p_4 \rho_4} \tag{342}$$

for a sonic wave. The pressure and density in the negative-most cell can be written

$$p_4 = \frac{p_4 + p_1}{2} + \frac{p_4 - p_1}{2}$$

$$\rho_4 = \frac{\rho_4 + \rho_1}{2} + \frac{\rho_4 - \rho_1}{2}$$

For small differences in pressure and density, the second term in each expression is seen to be much smaller than the first, and may be neglected. Substituting the remaining expressions into eq. 342 gives the mass velocity of the negative running sonic wave.

$$a = \left\{ \gamma \left[\frac{p_4 + p_1}{2} \right] \left[\frac{\rho_4 + \rho_1}{2} \right] \right\}^{1/2} \tag{343}$$

For the positive running wave, the mass velocity is

$$b = \sqrt{\gamma p_1 \rho_1}$$

where the pressure and density in the positive-most cell may be written as

$$p_1 = \frac{p_1 + p_4}{2} + \frac{p_1 - p_4}{2}$$

$$\rho_1 = \frac{\rho_1 + \rho_4}{2} + \frac{\rho_1 - \rho_4}{2}$$

Again the second terms are neglected, and the remainders used in the expression for b.

$$b = \left\{ \gamma \left[\frac{p_4 + p_1}{2} \right] \left[\frac{\rho_4 + \rho_1}{2} \right] \right\}^{1/2} \tag{344}$$

So for small differences in the fluid properties in the two cells, the mass velocities of the two waves are considered equal. This is valid because the density and pressure are nearly equal in the two cells. Combining eq. 343 and eq. 344,

$$a = b = \left\{ \gamma \left[\frac{p_4 + p_1}{2} \right] \left[\frac{\rho_4 + \rho_1}{2} \right] \right\}^{1/2} \tag{345}$$

With a = b, the momentum equations for the negative and positive running weak waves are:

$$a[u] + [p] = 0 \qquad \text{(negative running wave)}$$

$$a[u] - [p] = 0 \qquad \text{(positive running wave)}$$

With the subscript notation of figure 2, these are written

$$a(u_4 - u_0) + (p_4 - p_0) = 0 \tag{346}$$

$$a(u_1 - u_0) - (p_1 - p_0) = 0 \tag{347}$$

Equation 347 is subtracted from eq. 346 and the result rearranged to obtain

$$p_0 = \frac{p_1 + p_4}{2} + a \frac{u_4 - u_1}{2} \tag{348}$$

Equation 347 is added to eq. 346 and the result rearranged to obtain

$$u_0 = \frac{u_1 + u_4}{2} + \frac{1}{a} \frac{p_4 - p_1}{2} \tag{349}$$

In summary, the linear approximations to the solution of the Riemann problem at a cell boundary are:

$$p_0 = \frac{p_1 + p_4}{2} + a \frac{u_4 - u_1}{2}$$

(348)

$$u_0 = \frac{u_1 + u_4}{2} + \frac{1}{a}\frac{p_4 - p_1}{2}$$

(349)

$$a = \left\{ \gamma \left[\frac{p_4 + p_1}{2} \right] \left[\frac{\rho_4 + \rho_1}{2} \right] \right\}^{1/2}$$

(345)

These equations apply to weak waves, whether they are expansion or compression, negative running or positive running. Unfortunately, the situation is slightly more complicated for determination of density. As seen in figure 2, the density behind the waves is different on each side of the contact discontinuity. The density behind the negative running wave (expansion or compression) is (see Appendix A)

$$\rho_3 = \left[\frac{(\gamma+1)p_0 + (\gamma-1)p_4}{(\gamma-1)p_0 + (\gamma+1)p_4} \right] \rho_4$$

(350)

and the density behind the positive running wave (expansion or compression) is (see Appendix A)

$$\rho_2 = \left[\frac{(\gamma+1)p_0 + (\gamma-1)p_1}{(\gamma-1)p_0 + (\gamma+1)p_1} \right] \rho_1$$

(351)

The Computational Scheme

A typical Riemann situation is shown in figure 8. The discontinuity at cell boundary m has resolved itself into two waves. The conditions ahead of the waves are known from the previous time step. The conditions at the cell boundary (denoted by uppercase letters) are sought, so that fluxes across this boundary may be determined. Four possible outcomes exist, depending on the direction of propagation of each wave. The fluid properties behind the wave are given in Table 2 for each case. In all cases, the energy is found from the equation of state. Using the subscript notation of figure 2, and a and b for the mass velocities, the absolute velocities of the waves are

$$w^+ = u_1 + \frac{b}{\rho_1} \qquad \text{(positive running wave)}$$

(352)

$$w^- = u_4 - \frac{a}{\rho_4} \qquad \text{(negative running wave)}$$

(353)

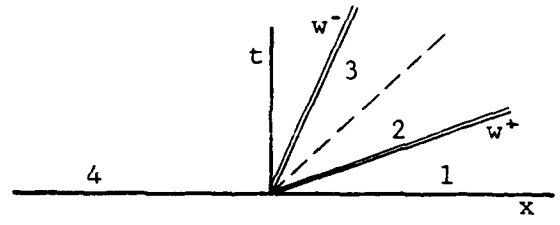

$U = u_4$

$R = \rho_4$

$P = p_4$

Case 1. w^+ and w^- are both positive.

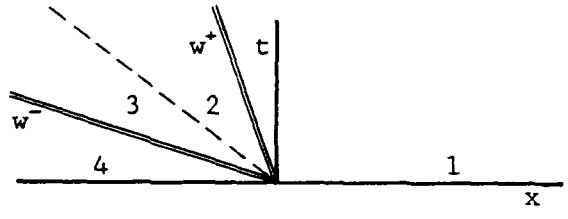

$U = u_1$

$R = \rho_1$

$P = p_1$

Case 2. w^+ and w^- are both negative.

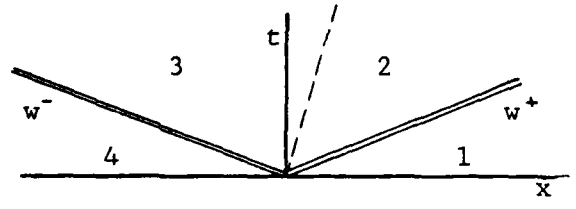

$U = u_0$

$R = \rho_3$

$P = p_0$

Case 3. w^+ and w^- have different signs; u_0 is positive.

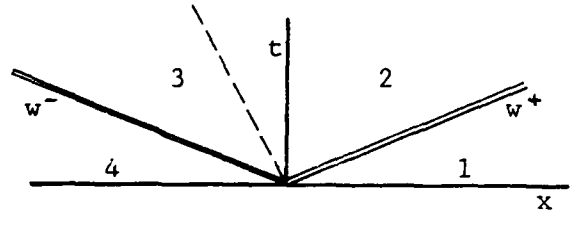

$U = u_0$

$R = \rho_2$

$P = p_0$

Case 4. w^+ and w^- have different signs; u_0 is negative.

Table 2. Fluid properties behind the waves emanating from the cell boundary for all four possible conditions.

Chapter 4

SAMPLE PROBLEM 1
Shock Wave Reflection from a Wall

Theoretical Study

The reflection problem may be stated as follows. Fluid flows steadily in a one dimensional pipe at a velocity of $u_1 = V$, as shown in figure 9a. At $x = 0$ and $t = 0$, an ideal valve is instantaneously closed, stopping the fluid motion at that point. The problem is to determine the resulting fluid motion (figure 9b).

Nature reconciles this seemingly impossible situation by creating a compressive wave in the incoming fluid. This wave travels into the incoming fluid, and is precisely of the proper strength required to leave the fluid behind itself motionless (the same velocity as the wall).

In deriving the equations describing this process, a positive sense is assumed for both the incoming fluid and the reflected wave, even though they must be of opposite sense in any real problem. As with all derivations, the proper technique is to assume positive for the derivation, and substitute positive or negative quantities (as the case may require) into the resulting equations. The benefit of this in the present case is to allow a single derivation for both reflection problems: the wall at the left (incoming fluid velocity is negative and reflected wave velocity is positive) and the wall at the right (incoming fluid velocity is positive and reflected wave velocity is negative).

The following notation applies to the flow field. The variables are shown schematically in figure 9b.

Subscript 1: conditions ahead of the wave
Subscript 0: conditions behind the wave

u: absolute velocity of the fluid
W: absolute velocity of the shock wave
v: velocity of the fluid relative to the wave

Equation 305, relating fluid velocity relative to the wave, will be required in the following forms.

$$v_0 = u_0 - W \tag{400}$$

$$v_1 = u_1 - W \tag{401}$$

From Appendix A, the conservation equations relating conditions across a shock wave are:

$$\rho_1 v_1 = \rho_0 v_0 \tag{501}$$

$$p_1 + \rho_1 v_1^2 = p_0 + \rho_0 v_0^2 \tag{502}$$

$$e_1 + \frac{p_1}{\rho_1} + \tfrac{1}{2} v_1^2 = e_0 + \frac{p_0}{\rho_0} + \tfrac{1}{2} v_0^2 \tag{503}$$

Also from Appendix A, the equation of state of a perfect gas is:

$$e = \frac{1}{\gamma - 1} \frac{p}{\rho} \tag{511}$$

From figure 9b, $u_1 = V$ and $u_0 = 0$, so the fluid velocities relative to the wave (eqs. 400 and 401) are as follows.

$$v_0 = -W \tag{402}$$

$$v_1 = V - W \tag{403}$$

The conservation equations (eqs. 501 through 503) can be reduced to a more useable form, as follows. Begin by substituting eqs. 402 and 403 into eq. 501 and rearranging.

$$\rho_0 = \rho_1 \left(1 - \frac{V}{W}\right) \tag{404}$$

Substitute eq. 402 and eq. 403 into eq. 502 and rearrange, then substitute eq. 404 to obtain the following.

$$p_0 = p_1 + \rho_1 V^2 \left(1 - \frac{W}{V}\right) \tag{405}$$

To modify the energy equation (eq. 503), substitute eqs. 402 and 403. The equation of state (eq. 511) is written twice (once for subscript 0 and once for subscript 1) and substituted into eq. 503. Next, eqs. 404 and 405 are substituted, with the following result.

$$\frac{2\gamma}{\gamma - 1} \left[\frac{p_1}{\rho_1} \left(\frac{V}{V - W} \right) \right] + \frac{2\gamma}{\gamma - 1} WV + V^2 - 2WV = 0$$

Finally, divide through by V, since $V \neq 0$ (trivial solution), multiply by (V-W), and rearrange to obtain the following quadratic equation in W.

$$W^2 - \left[\frac{3-\gamma}{2} V\right] W - \left[\gamma\frac{p_1}{\rho_1} + \frac{\gamma-1}{2} V^2\right] = 0$$

The solution of the quadratic equation is

$$W = \frac{3-\gamma}{4} V \pm \left[\left(\frac{3-\gamma}{4} V\right)^2 + \frac{\gamma-1}{2} V^2 + \gamma\frac{p_1}{\rho_1} \right]^{\frac{1}{2}} \tag{406}$$

For the present, wave reflection from a wall at the left is to be computed. For this case, the incoming velocity is negative, and we are looking for a positive wave velocity. For this example problem, the following values are given (ref 8):

$V = -428$ m/s (to the left)

$\rho_1 = 1.225$ kg/m^3

$p_1 = 101{,}300$ n/m^2

$\gamma = 1.4$

When these values are substituted into eq. 406, the wave velocity is either of the following.

$$W = \begin{cases} +255 \text{ m/s} \\ -590 \text{ m/s} \end{cases}$$

Consistent with the problem statement, the positive velocity is selected. This is substituted into eqs. 404 and 405 to obtain the remaining properties of the reflected wave.

$W = 255$ m/s

$\rho_0 = 3.280$ kg/m^3

$p_0 = 459{,}400$ n/m^2

Numerical Study

The reflection problem stated above was solved by the Godunov method in order to test its ability to predict shock wave reflection from a wall. This phenomenon plays an important part in the problem which ultimately will be solved; a hypervelocity jet travelling through a cylinder.

The one dimensional computational grid is shown in figure 10. It shows the left and right boundaries, and a typical cell boundary (m). Each fluid property in the domain (velocity, density, pressure, energy) is discretized by assigning some average value in each cell. These values are constant throughout the cell, and are denoted by lower case letters (u,ρ,p,e). As a

result of this discretization, a discontinuity exists at each cell boundary. The discontinuity is resolved by expansion or compression waves that emanate from the boundary. The constant fluid properties behind each set of waves (i.e. at the boundary) are denoted by upper case letters (U,R,P,E). Subscripts for average cell properties (u,ρ,p,e) are denoted by the letter i, while subscripts for boundary values (U,R,P,E) are denoted by the letter m.

Boundary conditions are provided by virtual cells (shown dashed in figure 10) at the wall and upstream. Reflection conditions at the wall (m = 0) are provided by assigning density, pressure, and energy in the virtual cell to be equal to those of the first cell, while the velocity in the virtual cell is set to the negative of the velocity in the first cell. This antisymmetric condition guarantees that the fluid velocity at the wall will be zero.

On the downstream boundary, free stream conditions are specified in the virtual cell for all time. This boundary condition may cause a disturbance to propagate into the computational domain. Consequently, the domain was made large enough to insure that the disturbances would not reach the computational region of interest for the length of time being computed.

The following initial values are provided to begin the computation. The energy was found from the equation of state, eq. 511.

u_i = -428 m/s

ρ_i = 1.225 kg/m^3

p_i = 101,300 n/m^2

The flow chart for the one dimensional code is shown in figure 11. A listing of the code is given in Appendix C (this is actually the code for sample problem 2, the shock tube, so the boundary conditions are different).

Results are presented graphically in figures 12 through 15. The code predictions are in excellent agreement with the theoretical determinations made above. Figure 12 shows the fluid velocity at three different times after reflection. At t = .001 s for example, the reflected wave is about 0.25 m from the wall. The fluid velocity ahead of the wave is 428 m/s (to the left), while the fluid velocity behind the wave is zero. The wave propagates to the right at a velocity of 256 m/s (the theoretical value was 255 m/s). The shock is spread over one cell (0.10 m); the fluid velocity is zero at x = 0.20 m and -428 m/s at x = 0.30 m. This typical result is the best possible resolution with this finite grid.

The density shock wave is seen in figure 13. The predicted density in the first cell is low by about 5%, but all other cells are within 1%. The problem in the first cell is discussed by Godunov in ref 2 (paragraph 6). He believes that the system "errs in entropy" in computing the unsteady portion of the reflection process. No attempt was made here to correct the problem, since it only affects the first cell. The pressure shock (figure 14) and the energy shock (figure 15) are also in excellent agreement with theory (within 1%), although the energy curve shows a slight distortion at the wall due to the density error there.

Chapter 5

SAMPLE PROBLEM 2
The Shock Tube

Experimental Results

An experiment was conducted in the BRL 2-inch (51 mm) shock tube to check the predictions of the one-dimensional code. Figure 16 is a photograph of the shock tube and the instrumentation used. The main components of the instrumentation shown in figure 16 are quartz pressure transducers and a four channel digitizing oscilloscope. Dimensions of the shock tube are given in figure 17. The ends of the shock tube were closed in order to reflect the waves.

Each test began with air at atmospheric pressure and temperature in each section of the shock tube. The two sections were separated by a 0.002 inch (0.05 mm) mylar diaphragm. Pressurized air at room temperature was introduced slowly into the driver secton until the diaphragm ruptured. Figure 18 shows a typical diaphragm after rupture. A total of five tests were done, but the results of the first were erratic so were disregarded. The data from the remaining four tests was averaged and this average was used to compare to the code prediction.

The table below gives the data that was manually recorded for each test, and the averge value used in the code verification.

Test	2	3	4	5	AVG
Driver Pressure, psig	61.5	59.1	60.1	58.6	59.8
Room Temperature, °C	25.3	26.4	27.1	27.7	26.6
Atmospheric Pressure, psia	14.83	14.83	14.83	14.83	14.83
Δt_{23}, μs	212.	215.	213.	216.	214.

The output from the pressure transducers was stored in the digitizing oscilloscope. Immediately following each test, the data was reduced by a microcomputer (shown in figure 19) and stored on tape for later plotting. These plots are given in figures 20 - 23, the pressure-time trace for each gage on each test. These data were also averaged, and plotted as the circles in the graphs at the end of this section.

The utilization of the data in figures 20 - 23 begins in time with the arrival of the first shock wave. This is of necessity t = 0, since the oscilloscope does not trigger when the diaphragm breaks, but rather writes continuously. Similarly, data after about 8 msec (station 1) or 9 msec (station 2) is not useful, as it is altered by a small shock wave that is reflected from the remains of the diaphragm (resulting from the main reflected wave which is by this time travelling back into the driver section after its reflection from the wall in the driven section). Data from station 3 was not used in this evaluation.

Experimental Chamber Pressure Correction

While the code assumes an ideal diaphragm rupture, in reality it never is. Some of the energy of the gas in the driver (chamber) is consumed in this non-ideal rupture. This pressure loss is well known to shock tube researchers, having been discussed in 1950 by C. W. Lampson (ref 9) of BRL. This loss can be corrected when predicting shock pressure by reducing the measured chamber pressure by some amount, and then assuming a perfect diaphragm rupture. To determine this "diaphragm opening coefficient", theoretical shock pressures must be computed. (Other factors contributing to inaccuracies are viscous effects, including the effect of the boundary layer on the gage reading, and the finite volume of gas in the driver section.)

To obtain an independent comparison, the following nonlinear equation for shock pressure is taken from Anderson (ref 4).

$$\frac{p_4}{p_1} = \frac{p_0}{p_1}\left\{1 - \frac{(\gamma-1)\left(\frac{a_1}{a_4}\right)\left(\frac{p_0}{p_1}-1\right)}{\left[2\gamma[2\gamma+(\gamma+1)\left(\frac{p_0}{p_1}-1\right)]\right]^{\frac{1}{2}}}\right\}^{-2\gamma/\gamma-1}$$

where p_4 = initial absolute chamber pressure

p_1 = initial absolute driven section pressure

p_0 = pressure behind the resultant shock wave

Since the gas in both sections of the shock tube is initially at the same temperature, the sonic velocities are equal: $a_1 = a_4$. For air ($\gamma = 1.4$) the equation reduces to

$$p_4 = p_0\left[1 - \frac{(p_0/p_1) - 1}{\sqrt{7[7+6((p_0/p_1)-1)]}}\right]^{-7}$$

For the problem at hand, p_1 is atmospheric pressure (.102 MPa during this experiment).

To determine a theoretical curve of shock pressure (p_0) vs chamber pressure (p_4), one needn't solve the above non-linear equation for p_0. Instead, values of p_0 are substituted and p_4 is computed. The results of this are plotted in figure 24. Also shown is experimental data supplied by G. Coulter of TBD, BRL. The difference is apparent. Close examination of the curves shows that the experimentally determined chamber pressure should be reduced by 5.5% (in the region $.480 \leq p \leq .540$ mpa) to account for losses in the non-ideal diaphragm rupture. That is, in an experimentally determined chamber pressure of p_4, 5.5% of it is consumed by the diaphragm rupture, leaving .945 p_4 to form the shock wave. Consequently the chamber pressure used in the code must be .945 p_4, where p_4 is the experimental chamber pressure, and .945 is the diaphragm opening coefficient.

Theoretical Study

Definition of Terms. The following schematics illustrate the subscript notation used. As can be seen, 4 denotes the driver (high pressure) side, and 1 the driven side.

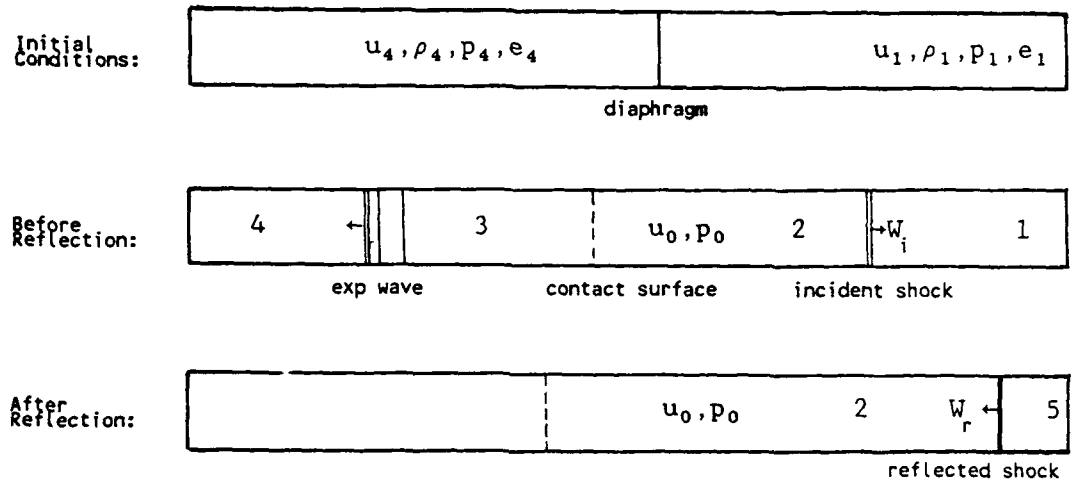

Data. The following measurements were taken during the experiment.

$T_4 = 26.6°C$ $T_1 = 26.6°C$

$p_4 = 74.6$ psia (.487 MPa) $p_1 = 14.8$ psia (.102 MPa)

In addition, the initial velocities in the two chambers are assumed to be zero.

$u_4 = 0$ $u_1 = 0$

Computed Conditions. The following values are required for the theoretical computations and as inputs to the computer code. A value of 287 J/kg•K was used for R, and of course $\gamma = 1.4$.

$$\rho_4 = \frac{p_4}{RT_4} = 5.66 \text{ kg/m}^3$$

$$\rho_1 = \frac{p_1}{RT_1} = 1.19 \text{ kg/m}^3$$

$$e_4 = \frac{1}{\gamma-1} RT_4 = 215{,}100 \text{ J/kg}$$

$$e_1 = \frac{1}{\gamma-1} RT_1 = 215{,}100 \text{ J/kg}$$

Theoretical Computations

In order to avoid any biasing of the theoretical predictions in favor of the code predictions, Anderson's equations (ref 4) will be used instead of the relations derived in this report for the one dimensional code.

A. Speed of Sound in the Undisturbed Gas, a_1 and a_4.

$$a_1 = \sqrt{\gamma R T_1} = 347 \text{ m/s}$$

$$a_4 = \sqrt{\gamma R T_4} = 347 \text{ m/s}$$

B. Pressure of gas behind the incident shock wave, p_0 (ref 4, eq. 7.94).

$$\frac{p_4}{p_1} = \frac{p_0}{p_1}\left\{ 1 - \frac{(\gamma-1)\left(\frac{a_1}{a_4}\right)\left(\frac{p_0}{p_1}-1\right)}{\left[2\gamma[2\gamma+(\gamma+1)\left(\frac{p_0}{p_1}-1\right)]\right]^{\frac{1}{2}}} \right\}^{-2\gamma/\gamma-1}$$

Substitute $\gamma = 1.4$ and $a_1 = a_4$ and rearrange:

$$p_0 = p_4\left\{ 1 - \frac{0.4(p_0-p_1)}{\sqrt{2.8p_1}\ \sqrt{2.4p_0+0.4p_1}} \right\}^7$$

After substituting p_1 and p_4, the above equation is solved by iteration with the result:

$p_0 = .213$ MPa

C. Velocity of incident shock, W_i (ref 4, eq 7.14).

$$W_i = \left[\frac{\gamma+1}{2\gamma}\left(\frac{p_0}{p_1}-1\right) + 1 \right]$$

$W_i = 482$ m/s

D. Velocity of gas behind the incident shock wave, u_0 (ref 4, eq. 7.16).

$$u_0 = \frac{a_1}{\gamma}\left(\frac{p_0}{p_1}-1\right)\left\{ \frac{\frac{2\gamma}{\gamma+1}}{\frac{p_0}{p_1} + \frac{\gamma-1}{\gamma+1}} \right\}^{\frac{1}{2}}$$

$u_0 = 194$ m/s

E. Density behind the incident shock wave (ρ_2) (ref 4, eq. 7.11).

$$\rho_2 = \rho_1 \left\{ \frac{1 + \frac{\gamma+1}{\gamma-1}\frac{p_0}{p_1}}{\frac{\gamma+1}{\gamma-1} + \frac{p_0}{p_1}} \right\}$$

$$\rho_2 = 1.991 \text{ kg/m}^3$$

F. Pressure behind the reflected shock wave (p_5). The velocity of the incoming fluid, $V = u_0$, is positive in the current problem. Equation 406 is now applied to a reflected wave travelling in the negative x direction (to the left), thus requiring that W_r be negative. Equations 404 and 405 are then used to compute the density and pressure behind the reflected wave. In the current notation, eq. 406 is written as follows.

$$W_r = \frac{3-\gamma}{4} V \pm \left[\left(\frac{3-\gamma}{4}V\right)^2 + \frac{\gamma-1}{2}V^2 + \gamma\frac{p_0}{\rho_2} \right]^{\frac{1}{2}}$$

$$W_r = -326.6 \text{ m/s} \quad \text{(to the left)}$$

$$p_5 = p_0 + \rho_2 V^2 \left(1 - \frac{W_r}{V}\right) \tag{405}$$

$$p_5 = .414 \text{ MPa}$$

G. Density behind reflected wave (ρ_5).

$$\rho_5 = \rho_2 \left(1 - \frac{V}{W_r}\right) \tag{404}$$

$$\rho_5 = 3.174 \text{ kg/m}^3$$

Numerical Study

The computational grid used for the shock tube problem is presented schematically in figure 25. A complete listing of the code used to solve this problem is given in Appendix C. The code results are presented graphically in figures 26 and 27, and numerically in the summary of the experimental evaluation that is given in Table 2 below.

Figures 26 and 27 show the pressure-time history at stations 1 and 2 respectively. The solid line shows the code prediction, while the circles indicate experimental data. The code prediction is based on the corrected chamber pressure in both figures. The circles represent averages of the

data from the four tests (figures 20 - 23). Since the instrumentation did not record the diaphragm rupture (i.e. t = 0), the experimental arrival time of the incident shock was made to coincide with that predicted by the code.

In figure 26, the incident shock wave is seen to arrive at station 1 at 1.2 msec after diaphragm rupture. The constant pressure behind the shock wave begins to drop at about 2.5 msec, as the expansion wave (reflected from the driver end of the shock tube) arrives. At 4.5 msec, the reflected shock (reflected from the closed end of the driven section) passes through the expansion wave at station 1, causing a jump in pressure. The expansion wave continues to reduce the pressure at station 1, when at 5.2 msec the head of the expansion wave returns (after reflection at the closed end of the driven section of the shock tube), causing a noticeably increased rate of pressure decrease. At about 8.5 msec the experimental traces showed a reflection of the reflected shock wave from the remains of the diaphragm, so no more experimental results are plotted. The code, however, shows the main driver end reflection of the reflected shock wave, which arrives at 9.3 msec.

In figure 27, the incident shock wave is seen to arrive at 2.4 msec, followed quickly by the reflected shock (2.9 msec), and the expansion wave (that was reflected from the driver end) at 3.6 msec.

Both figures show general agreement between the code and the experiment. The pressure behind the incident wave is predicted by the code to be a constant .213 MPa at both stations, while it actually was .215 MPa at station 1 and .212 MPa at station 2. The code predicts the pressure behind the reflected wave to be .413 MPa, while it actually was .407 MPa. Collision of waves is similarly well predicted, as can be seen in figures 26 and 27. Verification of this fact was a principal goal of this study.

Digital output from the code was used to compute the velocities of the incident (w_i) and reflected (w_r) shock waves between stations 1 and 2.

$$W_i = \frac{.1684m - 0.6096m}{00237s - .00122s} = 486 \text{ m/s}$$

$$W_r = \frac{.6906m - 1.1684m}{00446s - .00290s} = -358 \text{ m/s} \qquad \text{(to the left)}$$

The incident wave speed was experimentally determined by measuring with an electronic counter the wave's time of passage between stations 2 and 3.

$$W_i = \frac{.2700m - 1.1684m}{214\mu s} = 475 \text{ m/s}$$

No direct measurements were made for the reflected wave speed, but it can be obtained from the pressure-time traces in figures 20-23. The average velocity of the reflected wave is

$$W_r = \frac{0.6906m - 1.1684m}{.00122+.00332)s - (.00237+.00052)s} = -339 \text{ m/s}$$

The expansion wave properties were not predicted as well as the shock wave properties and the wave velocities. This is common in shock tube predictions (for example, see ref 10 and 11) and is believed to be the result of the interaction of the cold (expanded) gas from the driver section with the hot (compressed) gas in the driven section. Although the code does not consider this effect, the wave shapes in figures 26 and 27 are accurate, and the magnitudes of the pressure predictions are within 10%, and usually much less than that.

Note that a small error in arrival time of the reflected wave (at station 1 for example) causes a large error in the prediction of expansion wave pressures. In fact some of the error in the expansion wave predictions seen in figures 26 and 27 may be due to viscous effects in the boundary layer of the expansion wave. Any slowing of the wave would cause the experimental points in the expansion wave to be shifted to the right with respect to the code prediction.

The code predicts shock wave speeds to be slightly higher than the experimentally determined values with the wave travelling the farthest (the reflected wave) being most in error. Also, a drop in the experimental pressure behind the incident wave is noticed between stations 1 and 2. Both of these phenomena are attributed to viscous attenuation of the shock wave. If viscous effects were included in the code, the predictions of wave speed and pressure would be even better than those discussed above. However, viscous effects are rightfully negligible in the hypervelocity problem ultimately to be solved, so no attempt was made to modify the code. Some quantification is possible, however, and is useful to the overall evaluation of the code.

Emrich and Wheeler (ref 12) discuss shock attenuation due to wall effects (mainly a turbulent boundary layer) and propose the following empirical equation to predict the shock attenuation.

$$\left[\frac{p_0}{p_1} - 1 \right]_x = \left[\frac{p_0}{p_1} - 1 \right]_0 \exp\left(-A\frac{x}{D}\right)$$

where
- D = hydraulic diameter of the shock tube
- x = distance the shock has travelled
- A = an empirical constant
- p_0 = pressure behind the shock wave
- p_1 = pressure ahead of the shock wave

They give examples of the use of this equation for shock strengths (p_0/p_1) of 1 to 15. They also suggest a value of 0.0024 for A. The shock strength in the experiment under study here is about 5. To evaluate the constant A, measurements of p_0 for the incident wave made at stations 1 and 2 are used.

station	x/D	p_0	p_1
1	12	.215 MPa	.102 MPa
2	23	.212	.102

These values are substituted into the equation, using (23-12) = 11 diameters for the distance the shock has travelled. The result is that A = 0.00245. Thus the general relationship is

$$\left[\frac{p_o}{.102} - 1 \right]_x = \left[\frac{p_o}{.102} - 1 \right]_0 \exp(-.00245 \frac{x}{D})$$

This method reconciles the difference between the experimental reflected pressure at station 2 (.407 MPa) and the code prediction (.413 MPa), which was close to the theoretical prediction (.414 MPa). However, the experimental value for the pressure behind the incident shock at station 1 (.215 MPa) was actually higher than theoretical and code predictions (both were .213 MPa). This is contrary to the effects of viscous attenuation and must be attributed to experimental error (which includes the possibility of inputting erroneous initial conditions into the code).

Attenuation of the expansion wave and its reflections was not considered, due to uncertainty of the applicability of this method to the pressure distribution within the expansion wave.

The experimental verification of the one-dimensional code is summarized in table 2. The summary shows that the code predictions are in excellent agreement with both theory and experiment for all flow parameters studied.

The code predictions were also checked against the predictions of a Beam-Warming type of code used in the Terminal Ballistics Division of the BRL to study and predict shock tube behavior. The BRL uses shock tubes extensively in the study of explosive blast dynamics; how shock waves from explosions affect structures, for example.

For this comparison, code predictions for velocity, pressure and density as functions of position in the shock tube were plotted every millisecond from 0 to 12 milleseconds. These plots are shown in figues 28, 29 and 30, where the plot for t = 12 milleseconds is omitted due to space restrictions. Looking at the pressure plots (figure 30) for example, one can see the original shock wave travelling to the right, and the original expansion wave travelling to the left at t = 1 millesecond. The expansion wave has already begun its reflection from the left wall. At t = 3 milleseconds the shock wave has reflected from the right wall. The two reflected waves collide between 3 and 4 milleseconds, followed by reflection of the expansion wave from the right wall beginning just prior to t = 4 milleseconds. The reflected portion of the expansion wave interacts with the incident portion in the t = .005 millesecond frame, and begins to chase the reflected shock wave that is travelling toward the left wall. The two actually collide just prior to impact with the left wall. The remaining frames show a continuation of this process of reflection and collision.

One additional observation worthy of note is seen in the density plots (figure 29). The contact surface is clearly seen at t = 1 millesecond between the left running expansion wave and the right running shock wave. This contact surface moves to the right, and its interaction with the reflected shock wave is seen in the t = 4 millesecond and t = 5 millesecond

	Experimental	Code	Theoretical
Pressure behind incident Shock wave (p_0), MPa (station 1/station 2)	.215/.212	.213	.213
Pressure behind reflected Shock wave (p_5) MPa	.407	.413	.414
Speed of incident Shock wave (W_i) m/s	475	486	482
Speed of reflected shock wave (W_r) m/s	339	358	327
Velocity of gas behind the incident wave (u_0) m/s	-	193	194
Velocity of gas behind the reflected wave (u_5) m/s	-	<0.01	0
Density of gas behind the incident wave ρ_2 kg/m^3	-	1.99	1.99
Density of gas behind the reflected wave ρ_5 kg/m^3	-	3.16	3.17

Table 3. Summary of results showing a comparison between code predictions, theoretical predictions, and experimental data.

frames. Following the collision, the contact surface moves to the left. Notice that the code predicts a smearing out (or smearing) of this contact surface with time.

Figure 31 shows the comparison of the predictions of the two codes. Velocity, density and pressure are plotted as functions of position for times of 4, 8 and 12 milleseconds. These are the same as the plots just discussed. Predictions of the Godunov type code developed here are again shown as a solid line. Superimposed on these plots are the results of the Beam-Warming code, shown as circles. In every case the agreement between the two codes is excellent.

CONCLUSIONS AND RECOMMENDATIONS

This effort was the first phase of a project to write an axisymmetric fluid dynamics code and apply it to the hypervelocity problem of a shaped charge jet within a cylindrical tunnel. In this phase of the project, the necessary equations were derived and a one dimensional Godunov code was written for an inviscid, perfect gas.

Theoretical and experimental verifications were done which showed that the Godunov technique accurately predicted those flow phenomena critical to this study: shock and expansion wave formation, wave reflection, and wave/wave collisions. The details are summarized as follows:

1. Predictions of pressure were within 2% of the experimental values.
2. Predictions of velocities were within 6% of the experimental values.
3. Predictions of fluid densities were within 1% of theoretical values.

As a result of the techniques learned and verifications made, a decision was made to expand the present code to include axisymmetric and real gas considerations. This effort is reported on in ref 21.

FIGURES

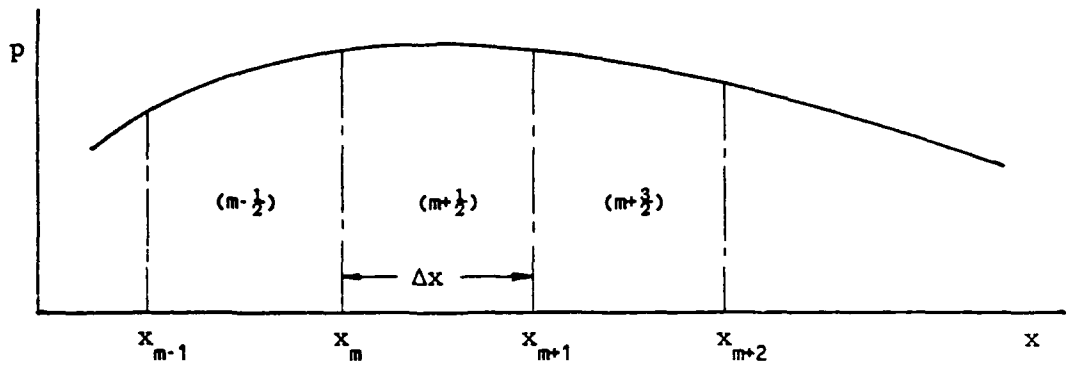

Figure 1a. Pressure in a One Dimensional Fluid.

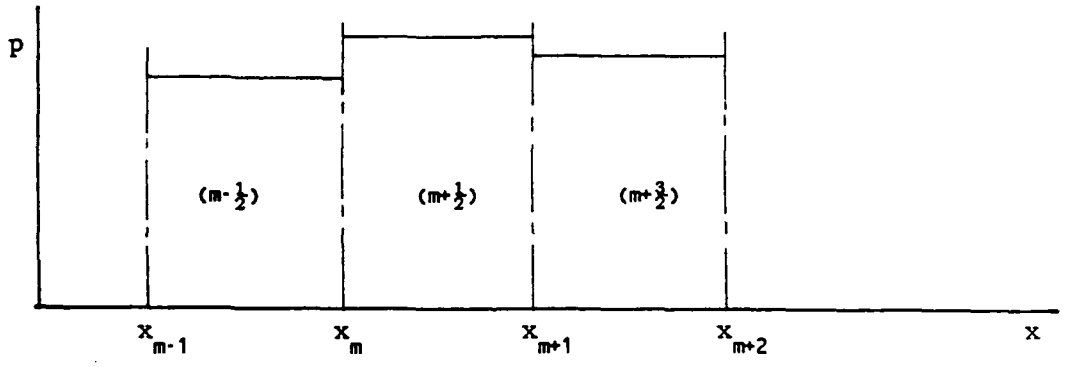

Figure 1b. Discretized Pressure in a One Dimensional Fluid.

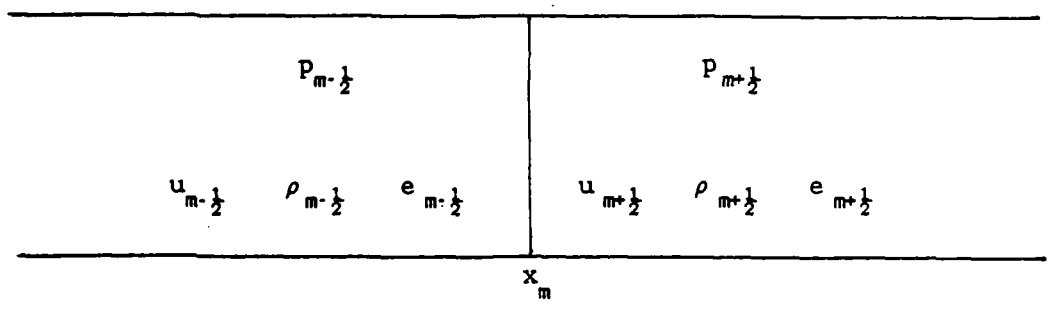

Figure 1c. The Classical Shock Tube Problem.

Figure 1. The Discretized Flowfield

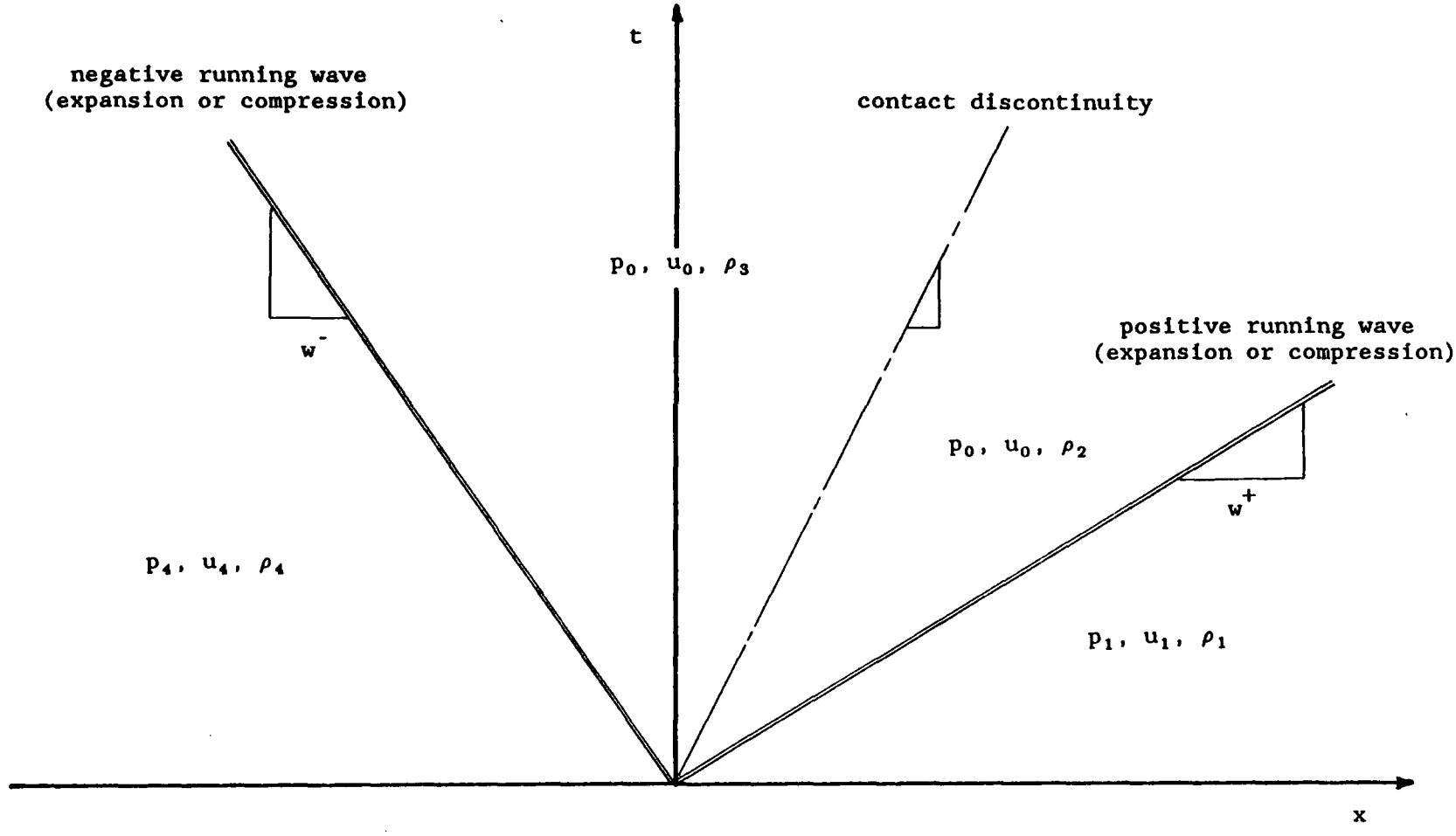

Figure 2. The x - t Diagram for the Riemann Problem

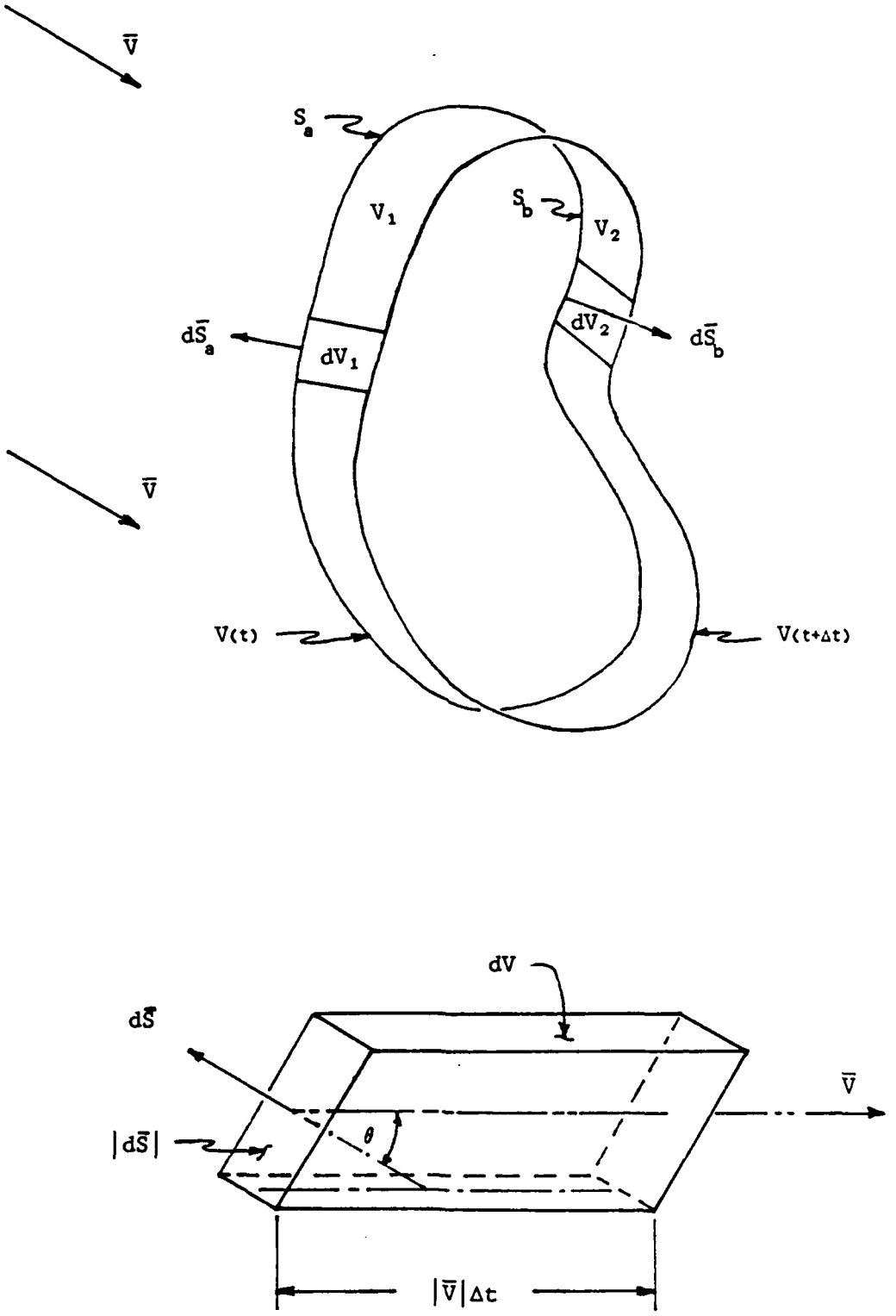

Figure 3. The Lagrangian Control Volume

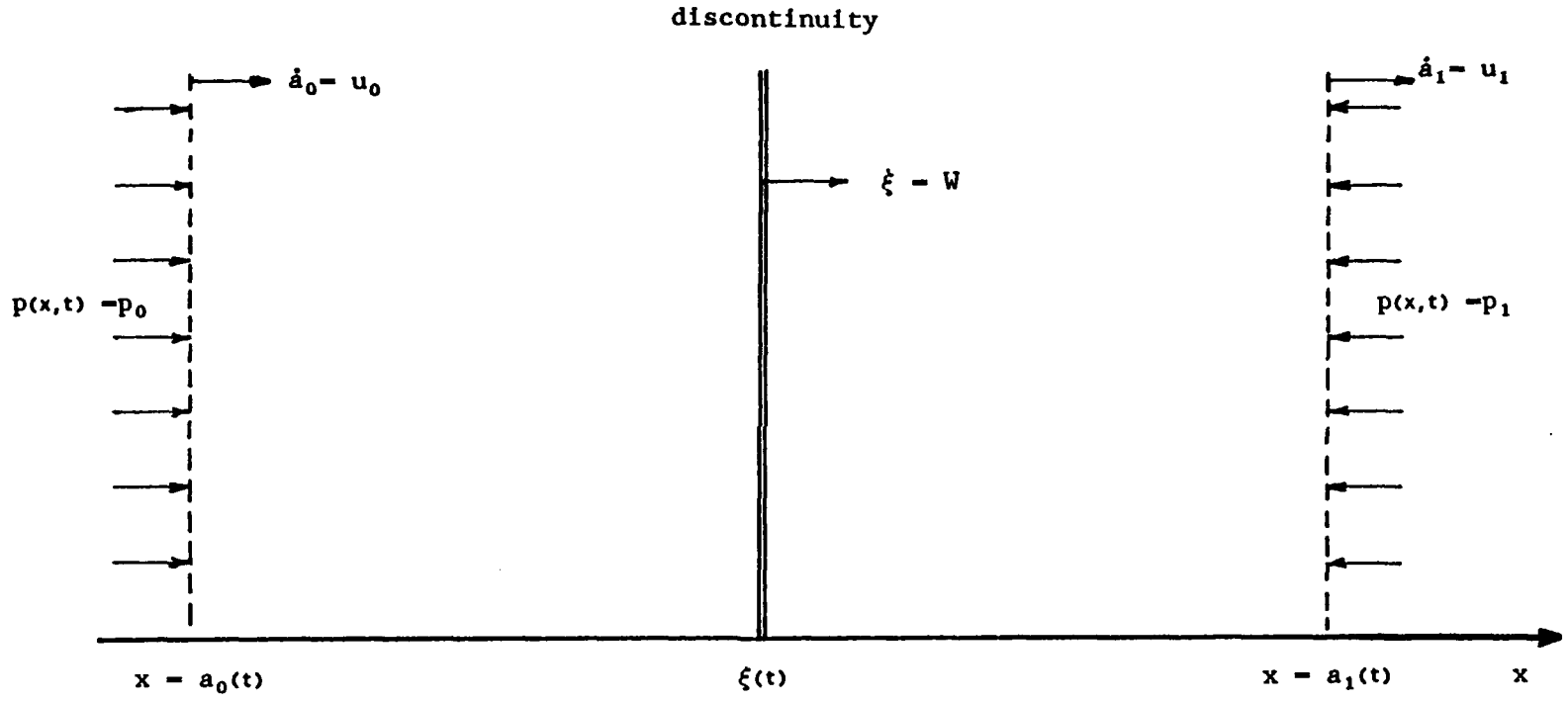

Figure 4. The Lagrangian Parameters

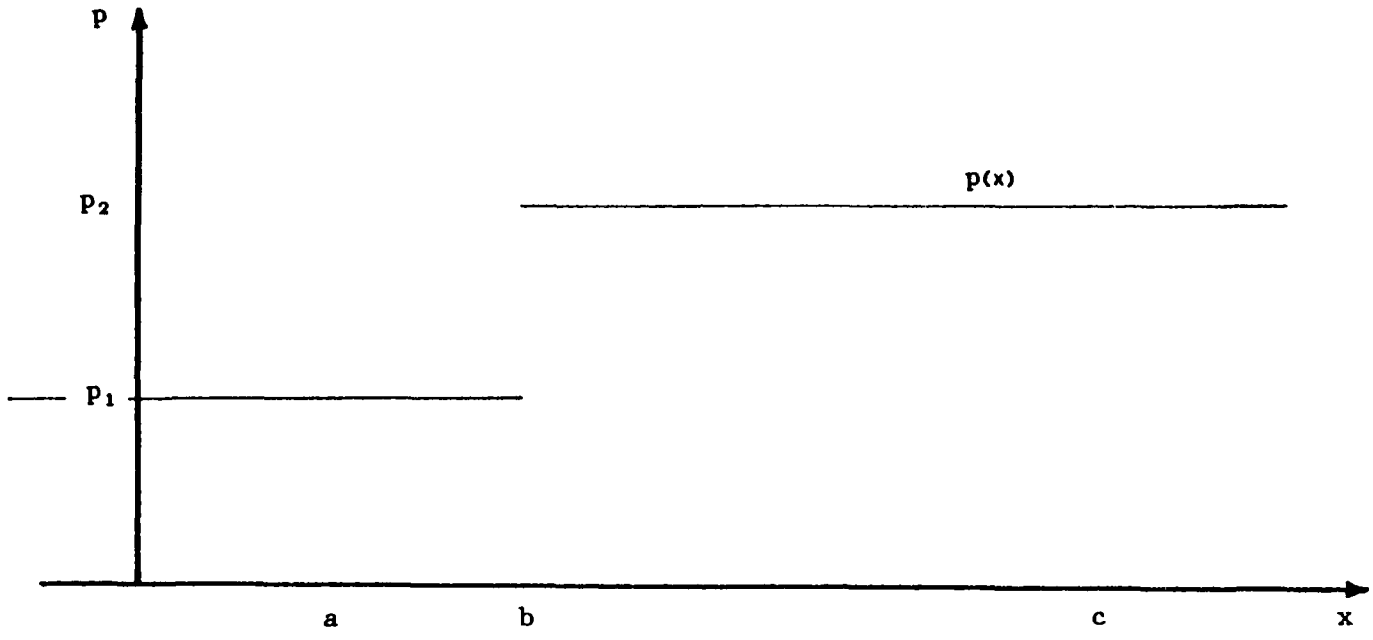

Figure 5. A Pressure Discontinuity in Space

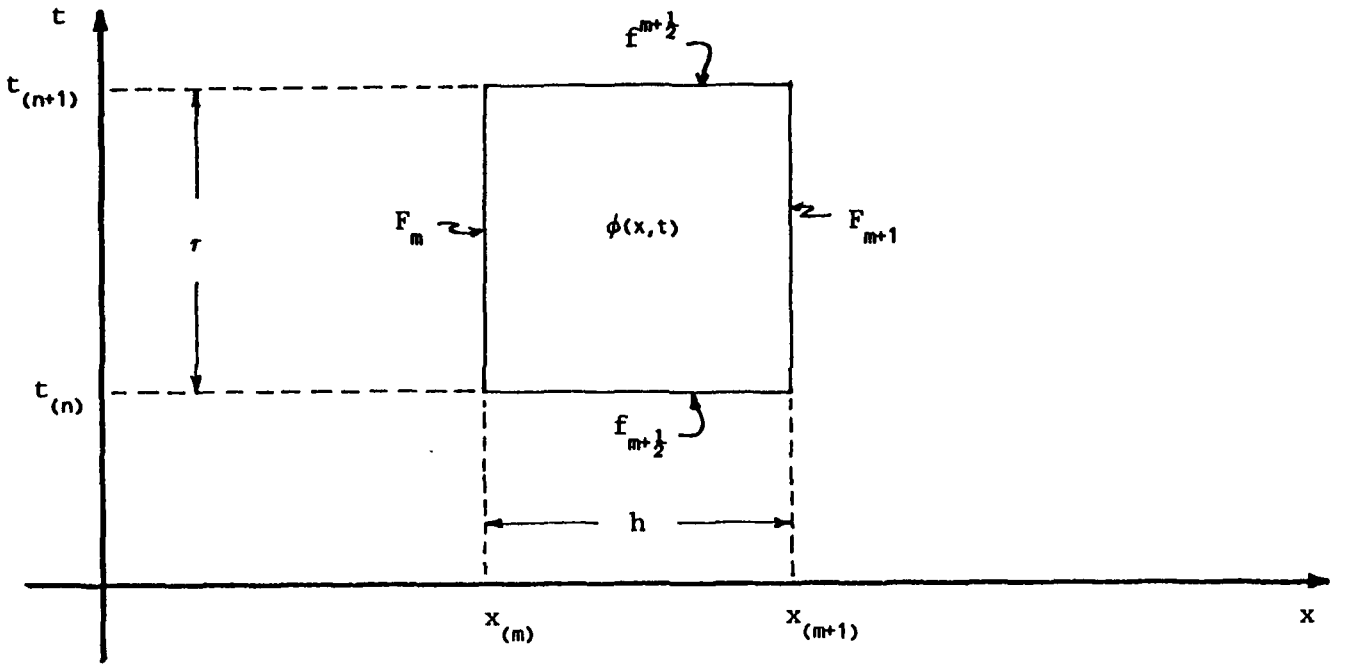

Figure 6. An Arbitrary Integration Area

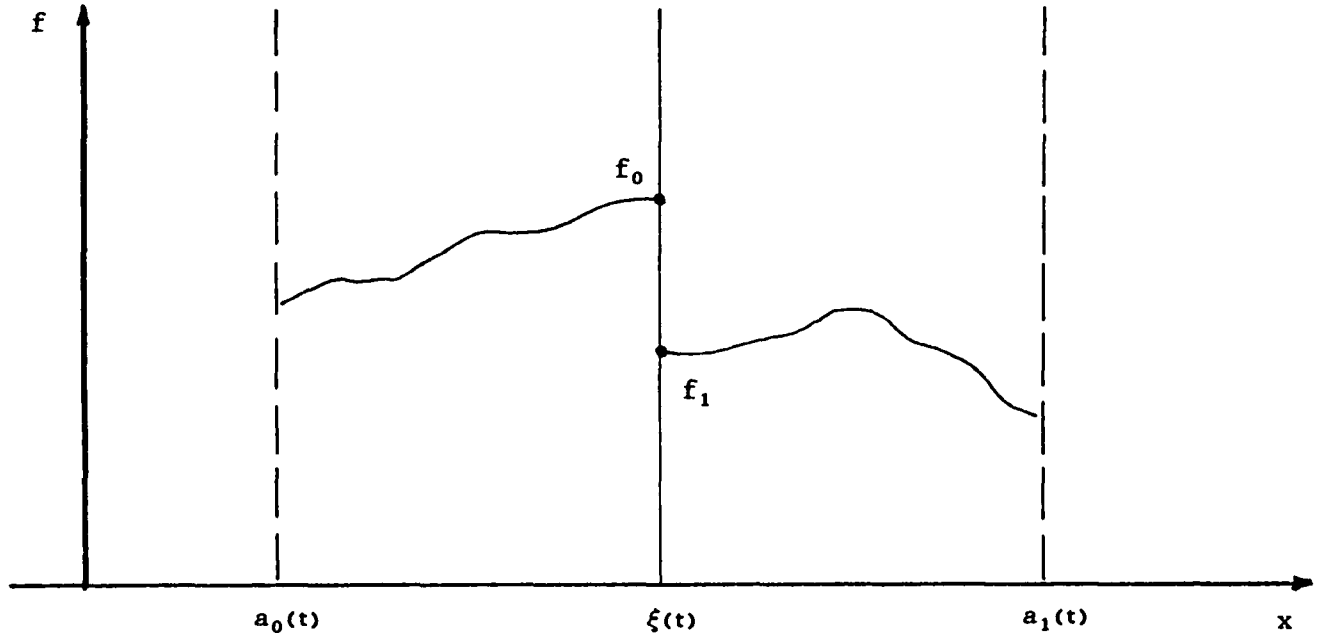

Figure 7. A Snapshot in Time of a Discontinuity

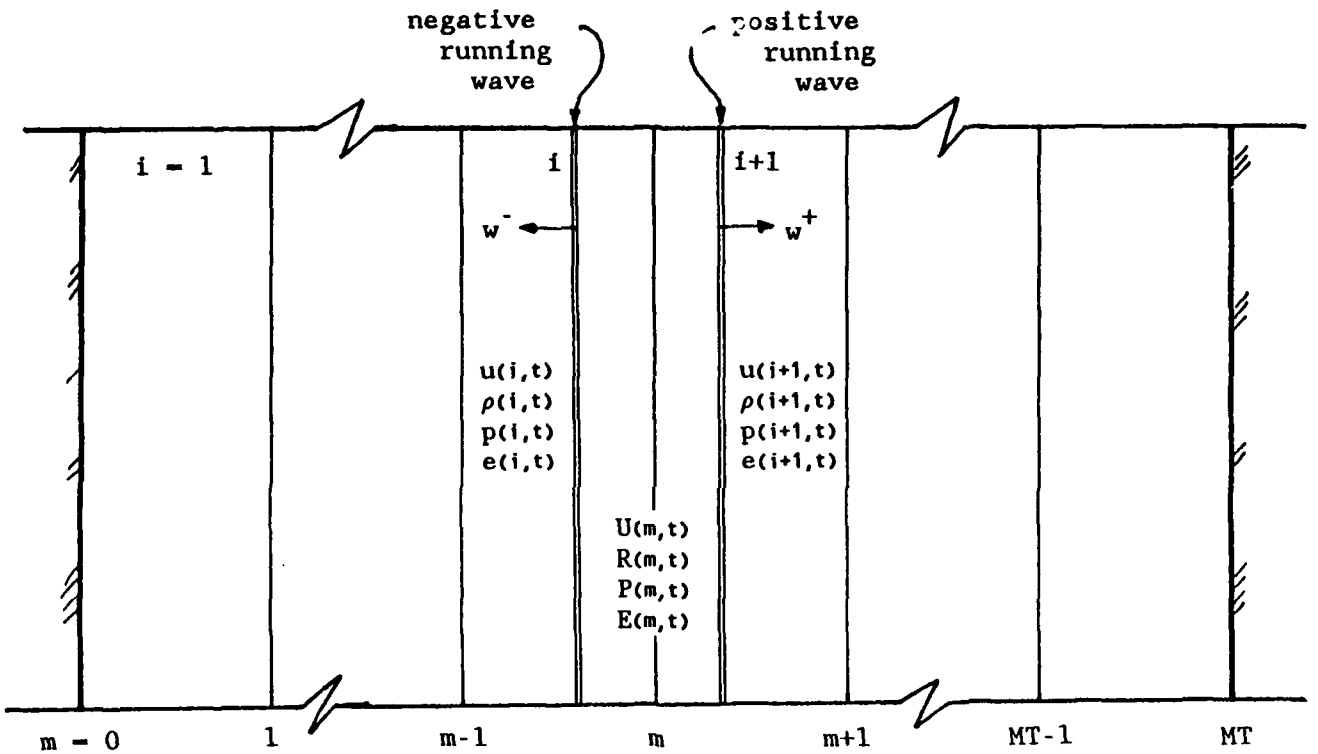

Figure 8. A Typical Computation Situation

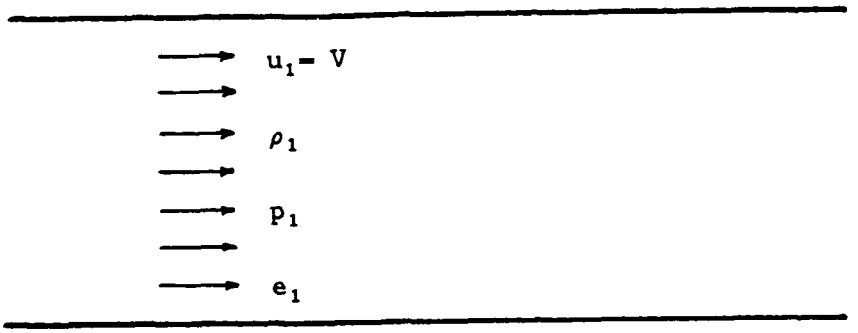

Figure 9a. Before reflection.

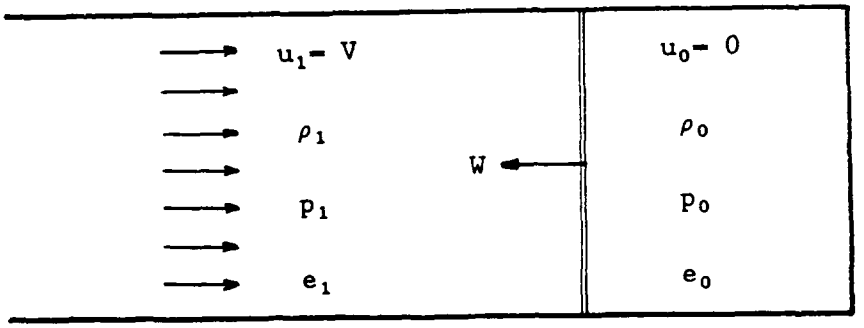

Figure 9b. After reflection.

Figure 9. The One Dimensional Reflection Problem

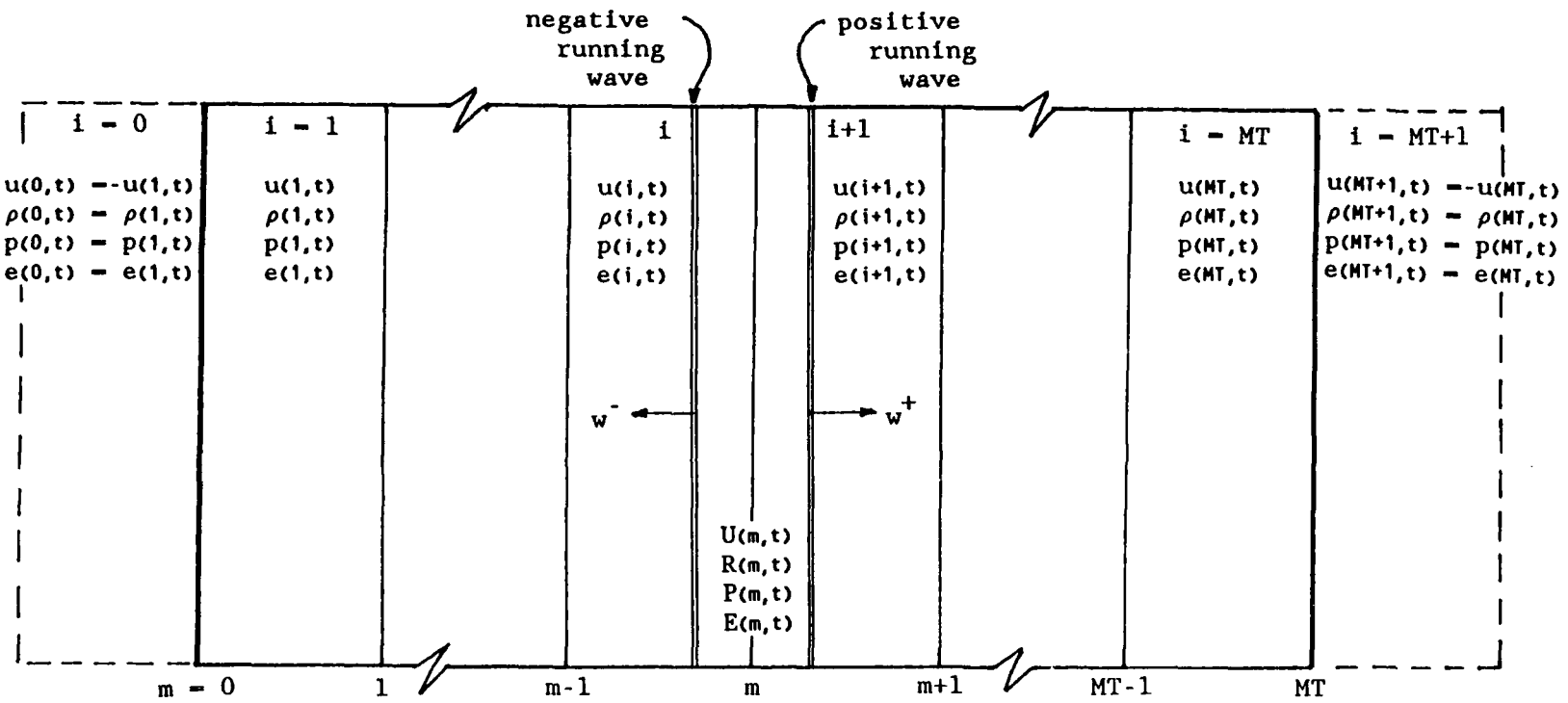

Figure 10. A One Dimensional Computational Grid

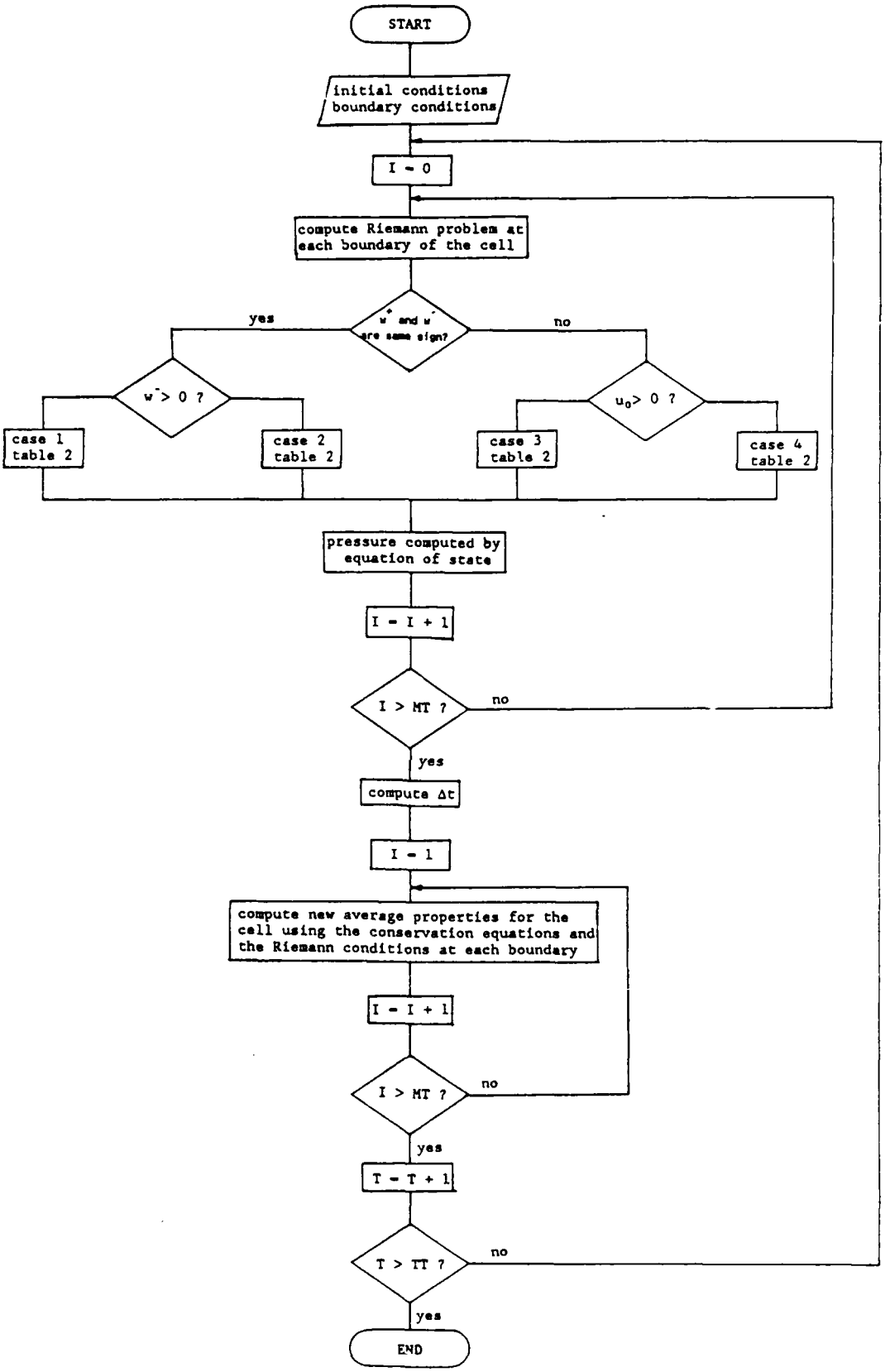

Figure 11. A Flow Chart of the Computer Program

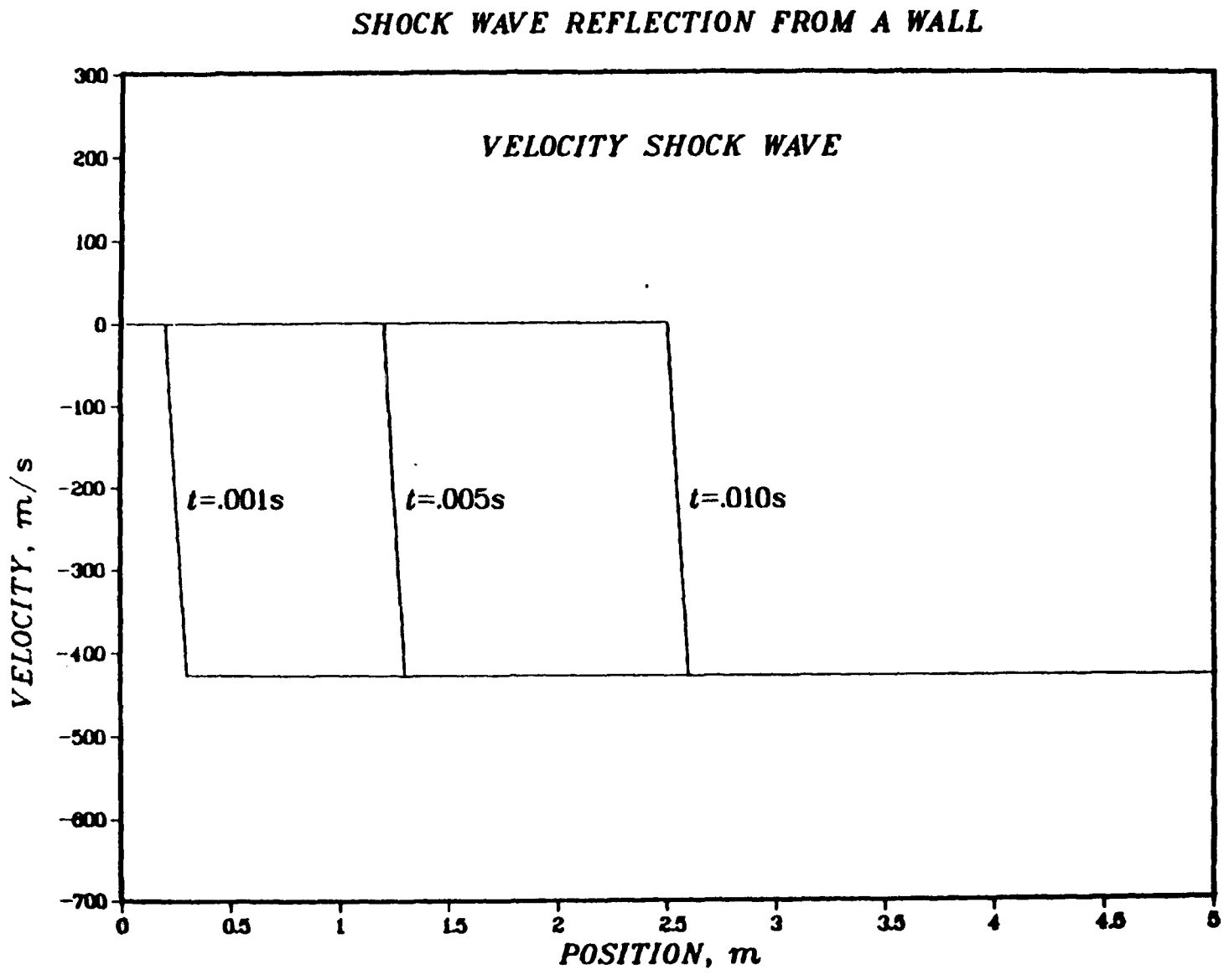

Figure 12. The Velocity Shock Wave

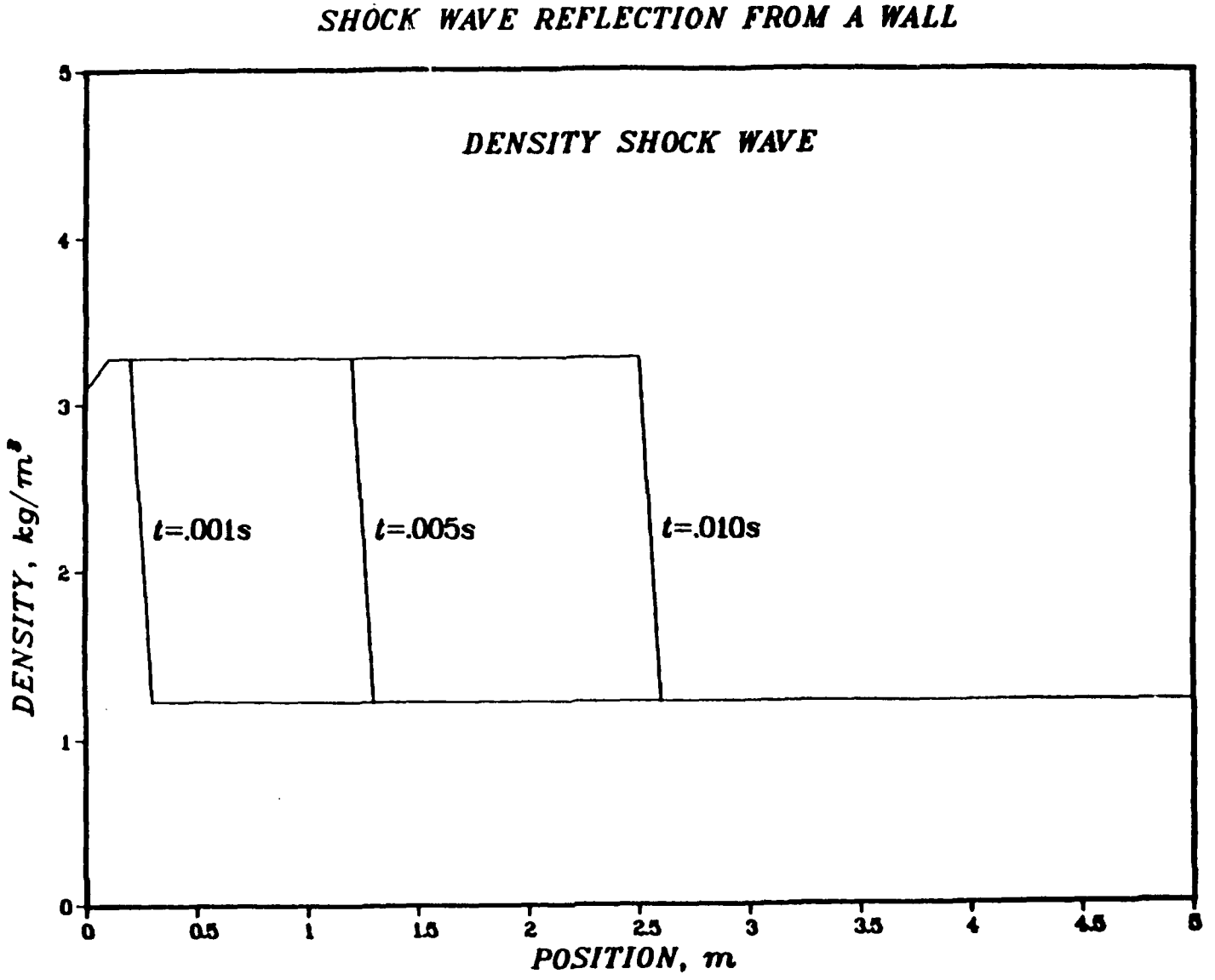

Figure 13. The Density Shock Wave

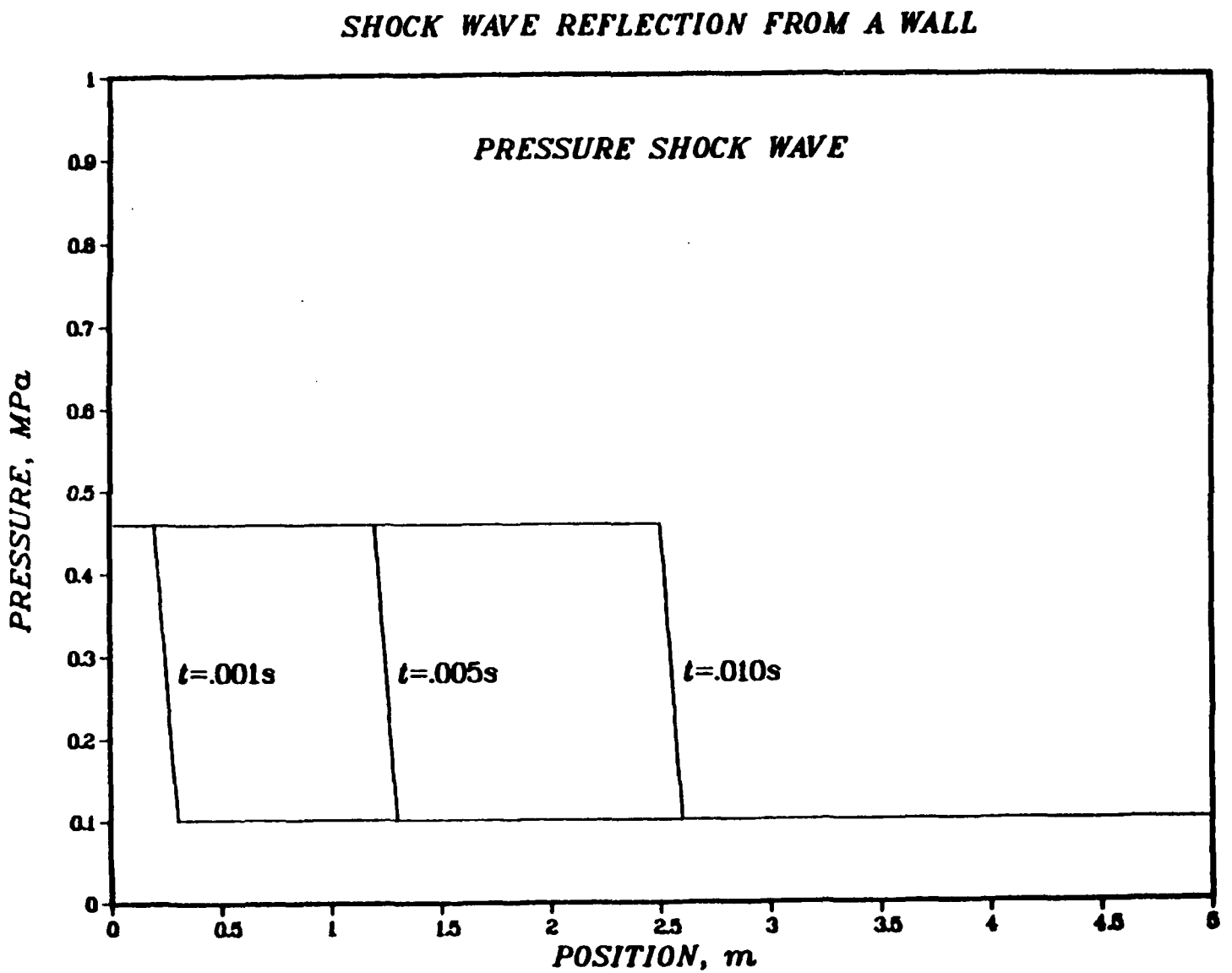

Figure 14. The Pressure Shock Wave

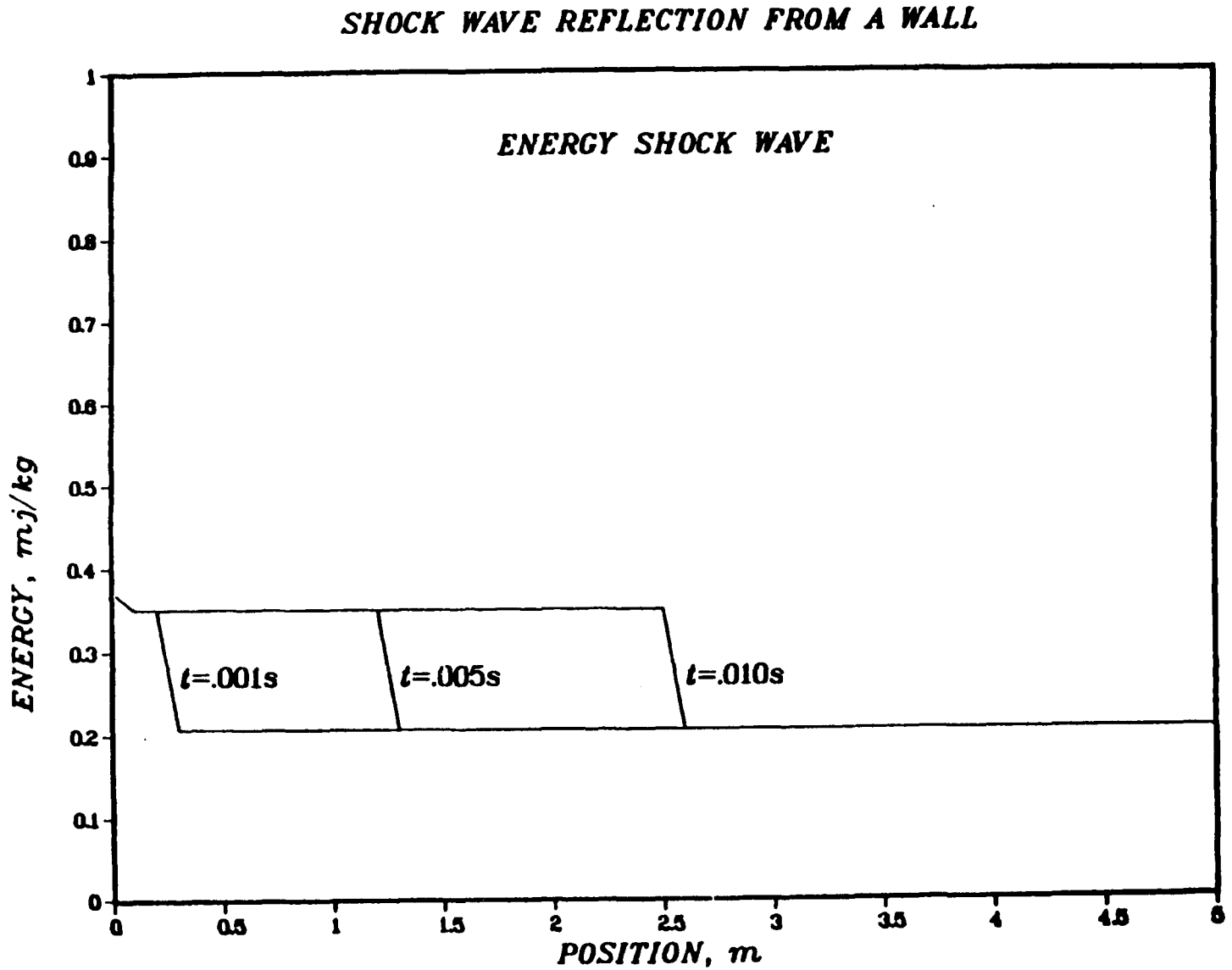

Figure 15. The Energy Shock Wave

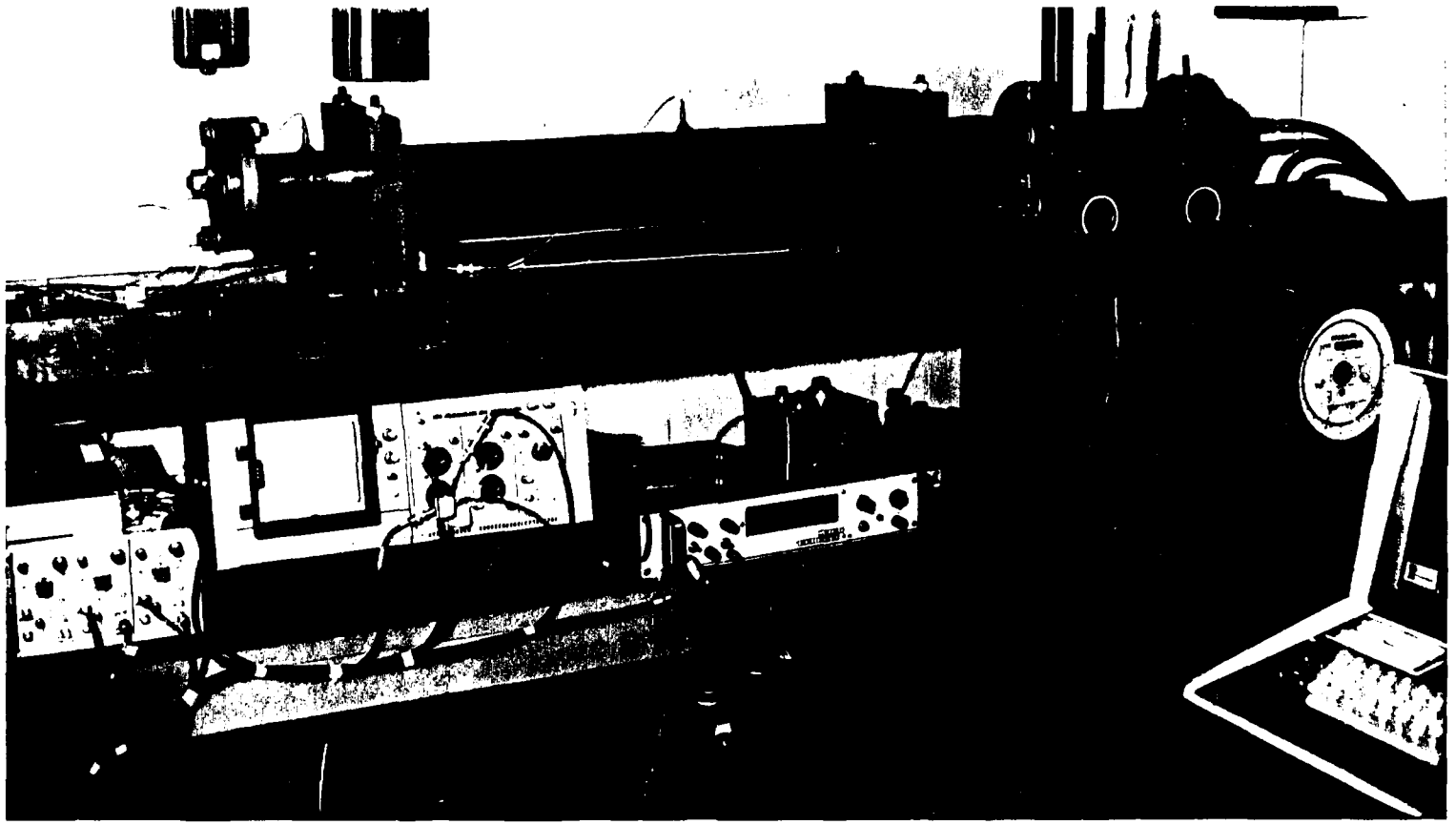

Figure 16. A Photograph of the Shock Tube

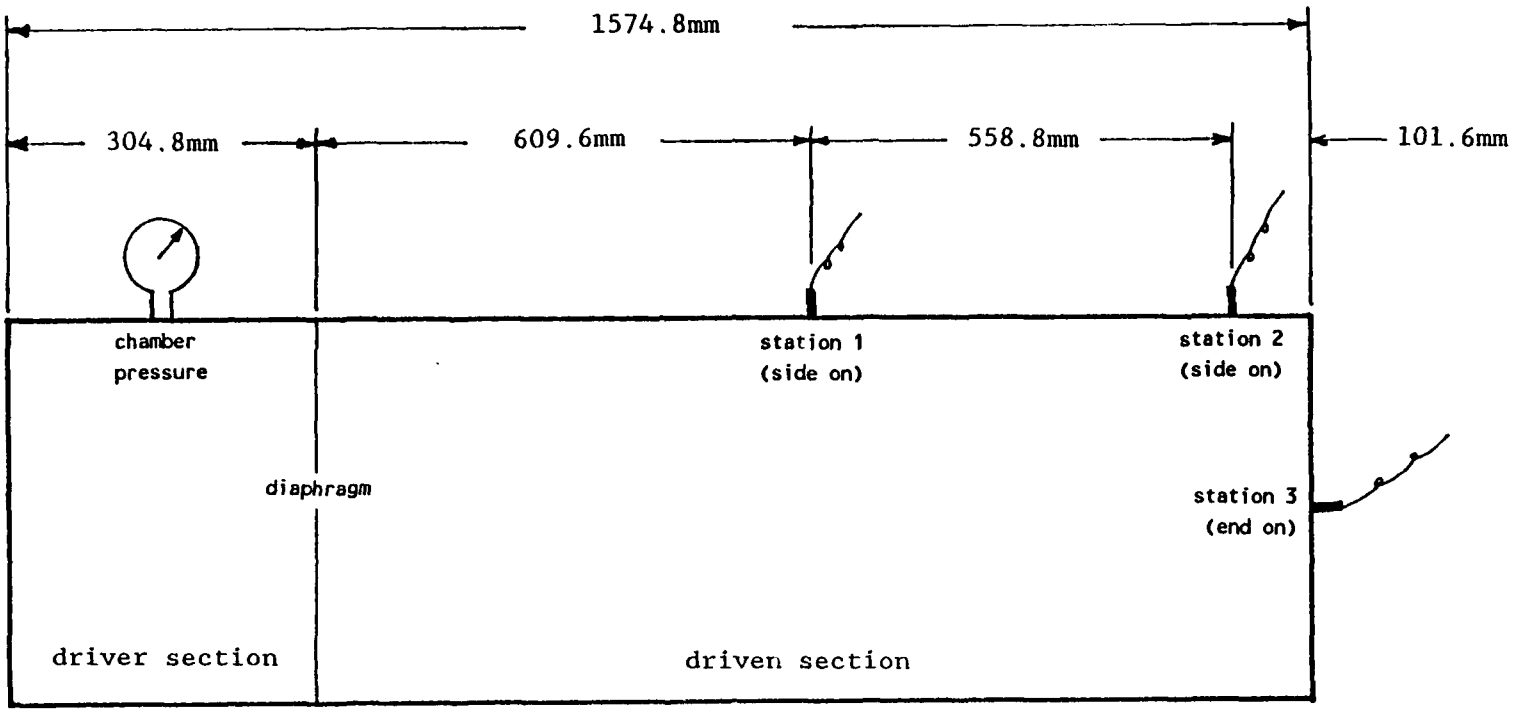

Figure 17. A Schematic of the Shock Tube

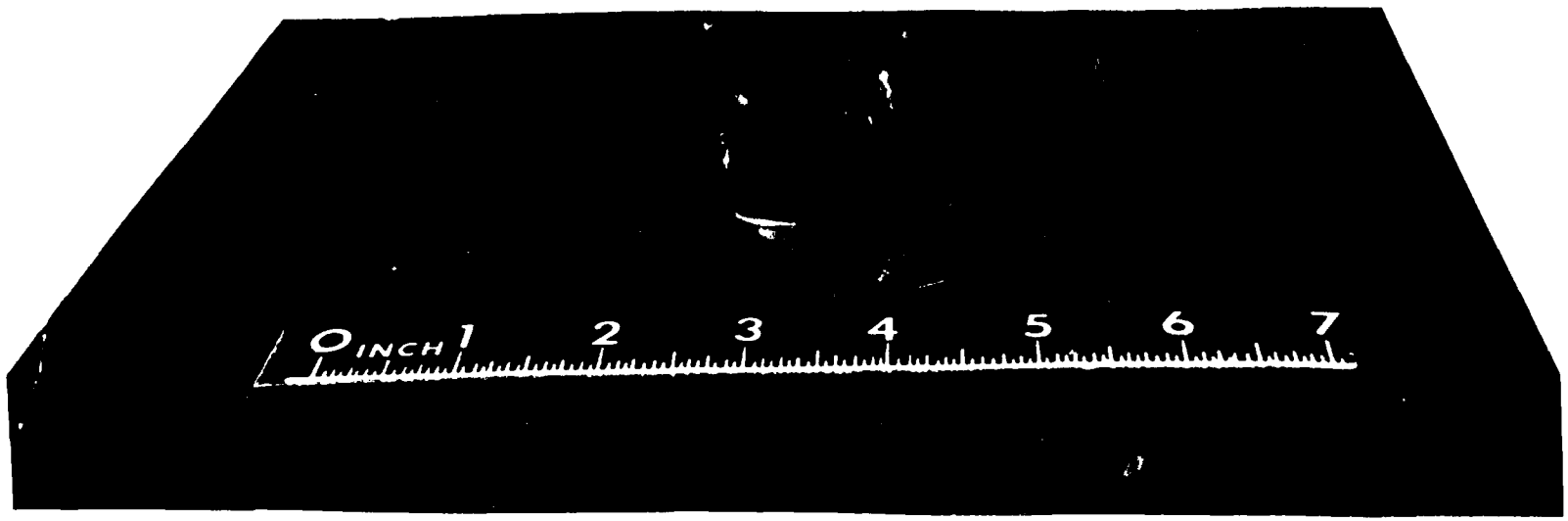

Figure 18. A Ruptured Diaphragm from the Shock Tube

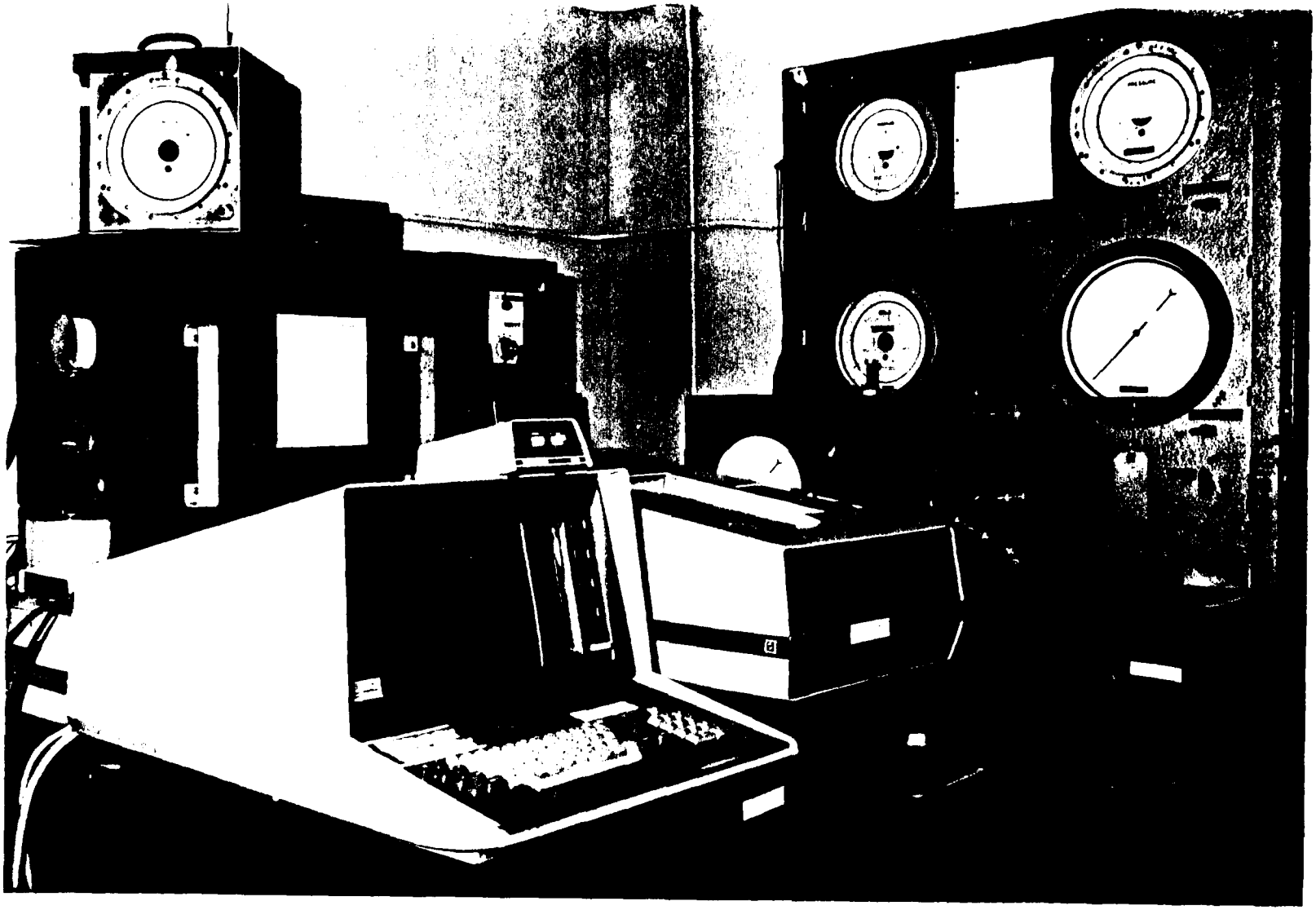

Figure 19. The Microcomputer for the Shock Tube Data

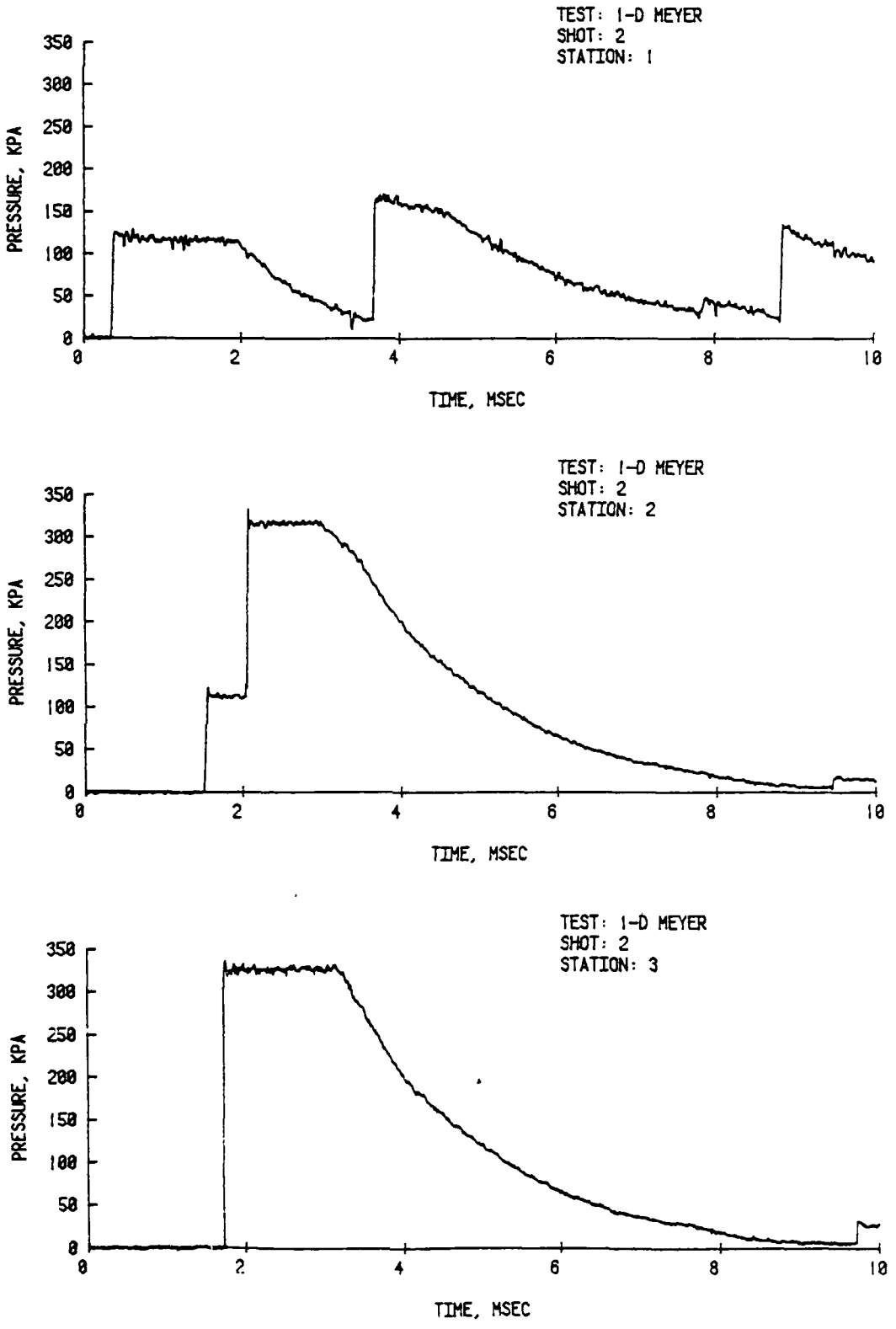

Figure 20. Shock Tube Pressure Data: Shot No. 2

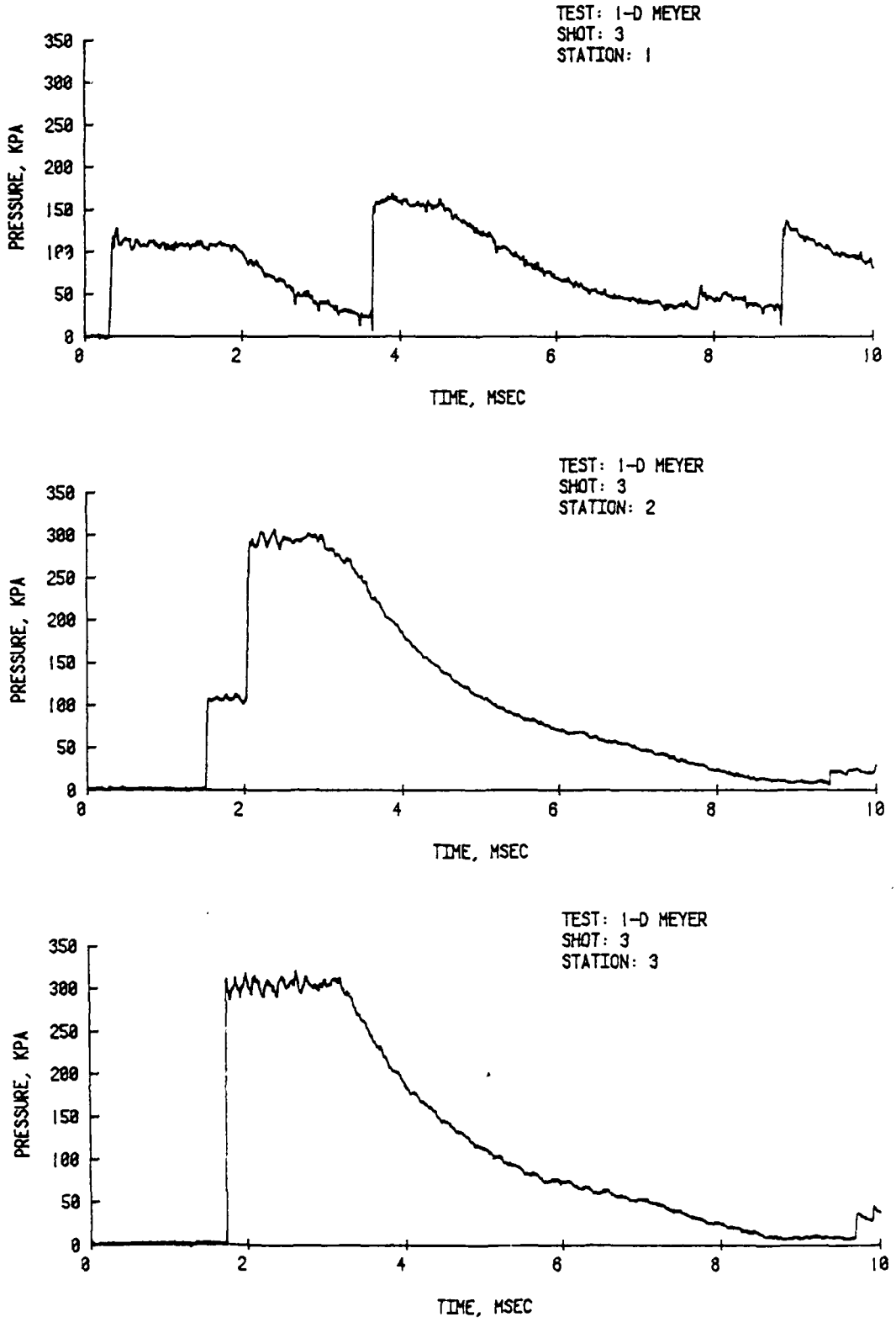

Figure 21. Shock Tube Pressure Data: Shot No. 3

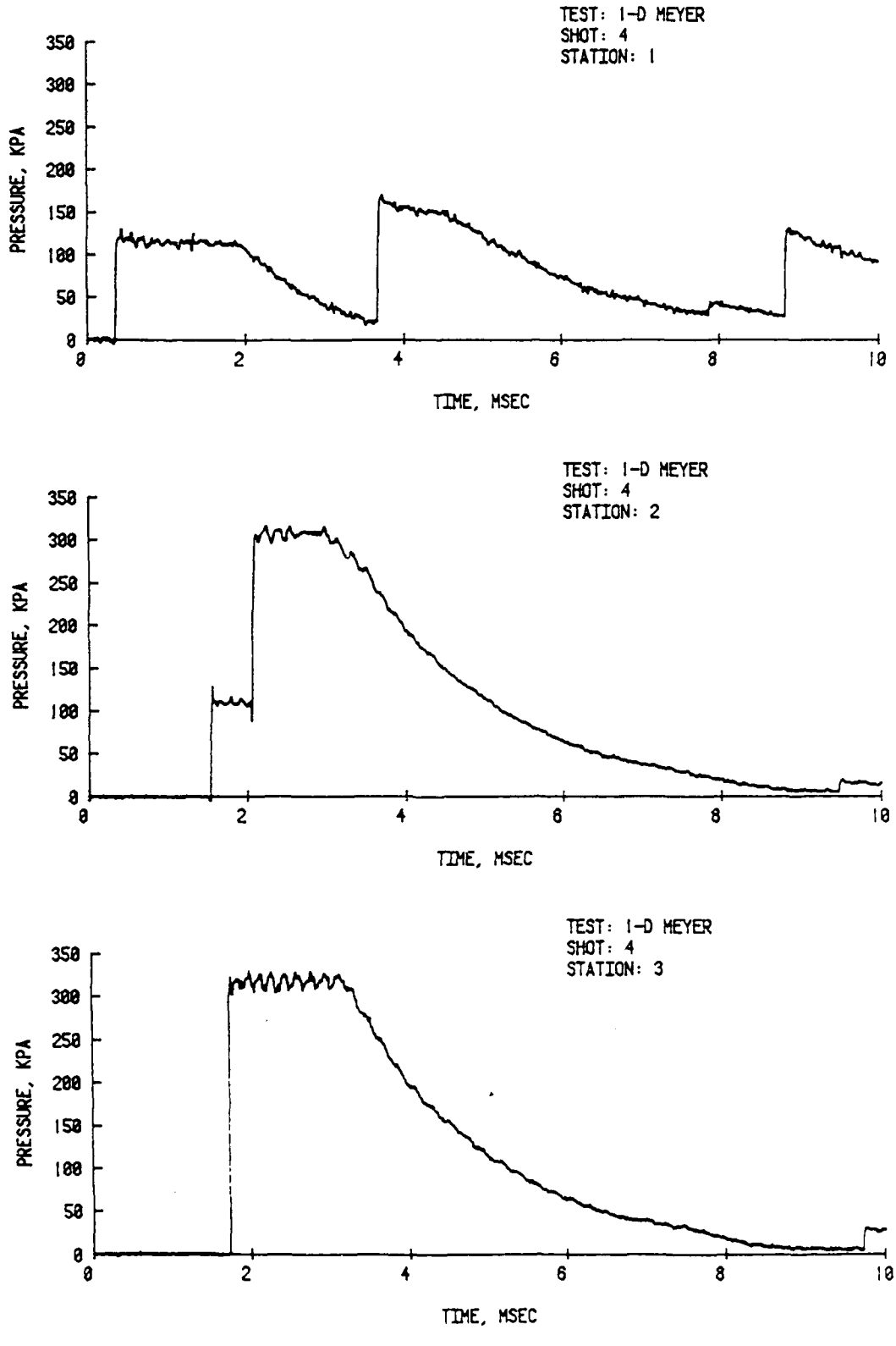

Figure 22. Shock Tube Pressure Data: Shot No. 4

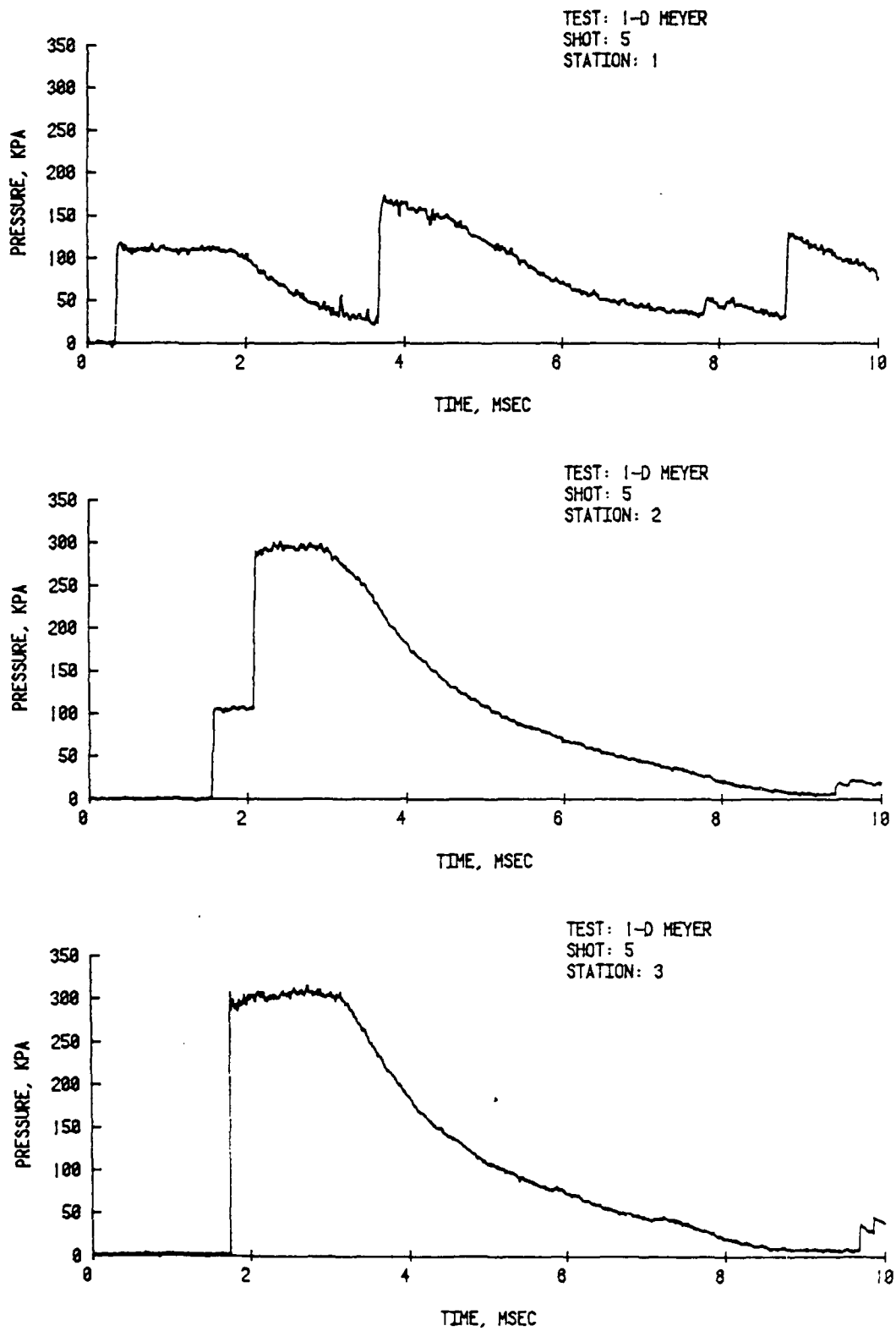

Figure 23. Shock Tube Pressure Data: Shot No. 5

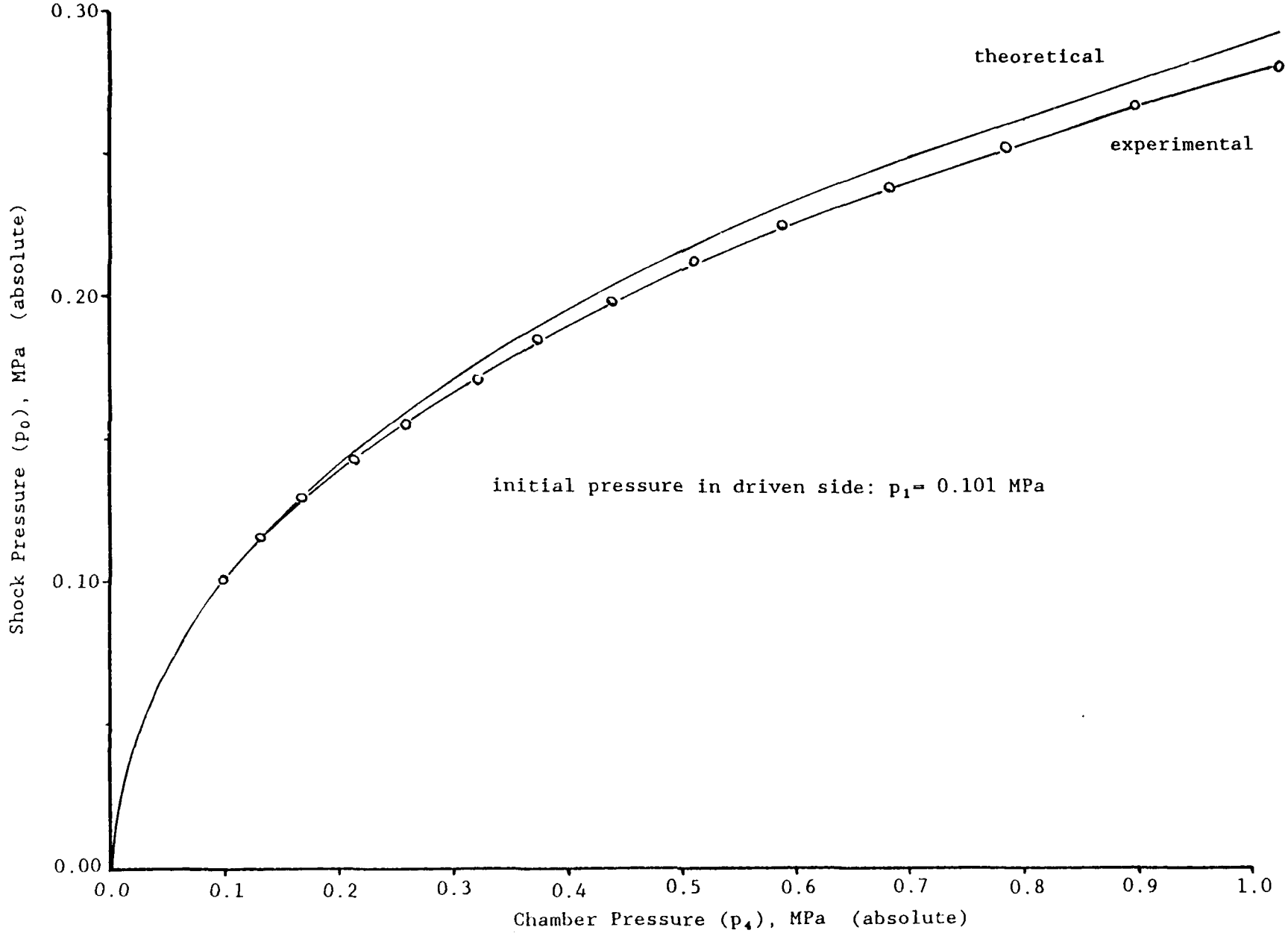

Figure 24. Pressure Behind the Shock Wave in a Shock Tube

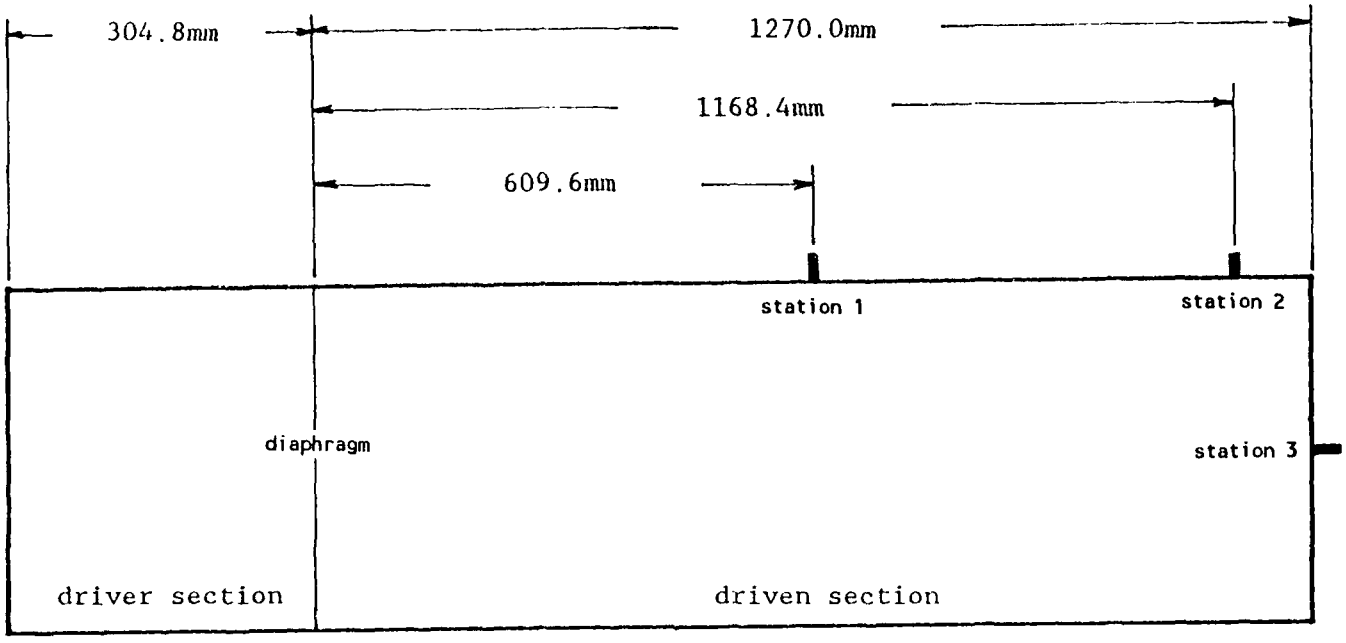

MD = (304.8)mm / 3 = 101.6mm → 102 cells

MR = (1270.0)mm / 3 = 423.3mm → 423 cells

MT = (1574.8)mm / 3 = 524.9mm → 525 cells

STA1 = (609.6 + 304.8)mm / 3 = 304.8mm → cell # 305

STA2 = (1168.4 + 304.8)mm / 3 = 491.1mm → cell # 491

Figure 25. Computational Domain for the Shock Tube

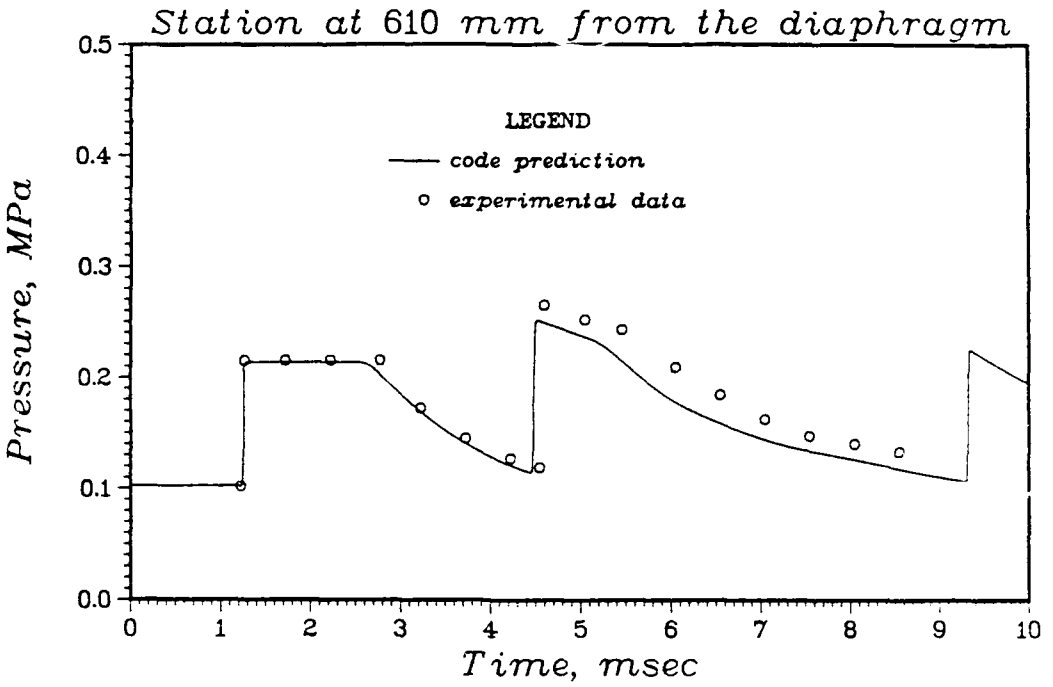

Figure 26. Pressure at Station 1

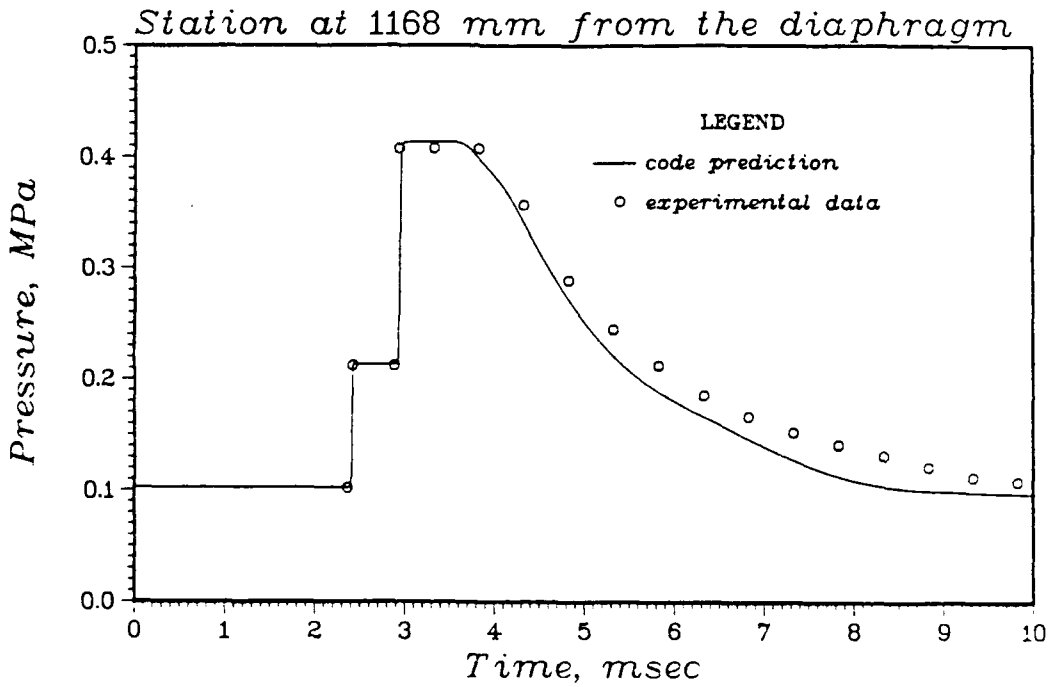

Figure 27. Pressure at Station 2

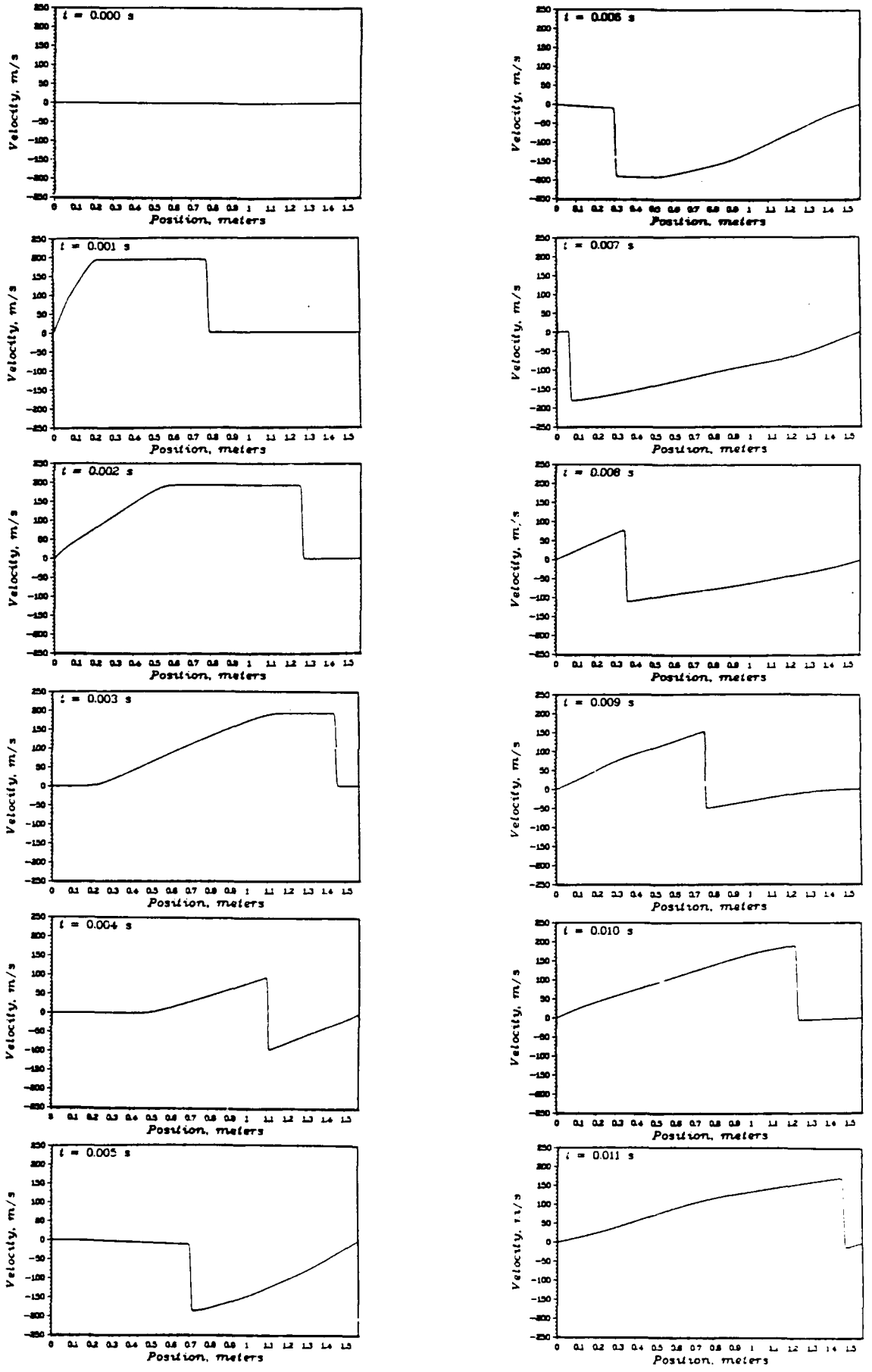

Figure 28. Predicted Fluid Velocity in the Shock Tube

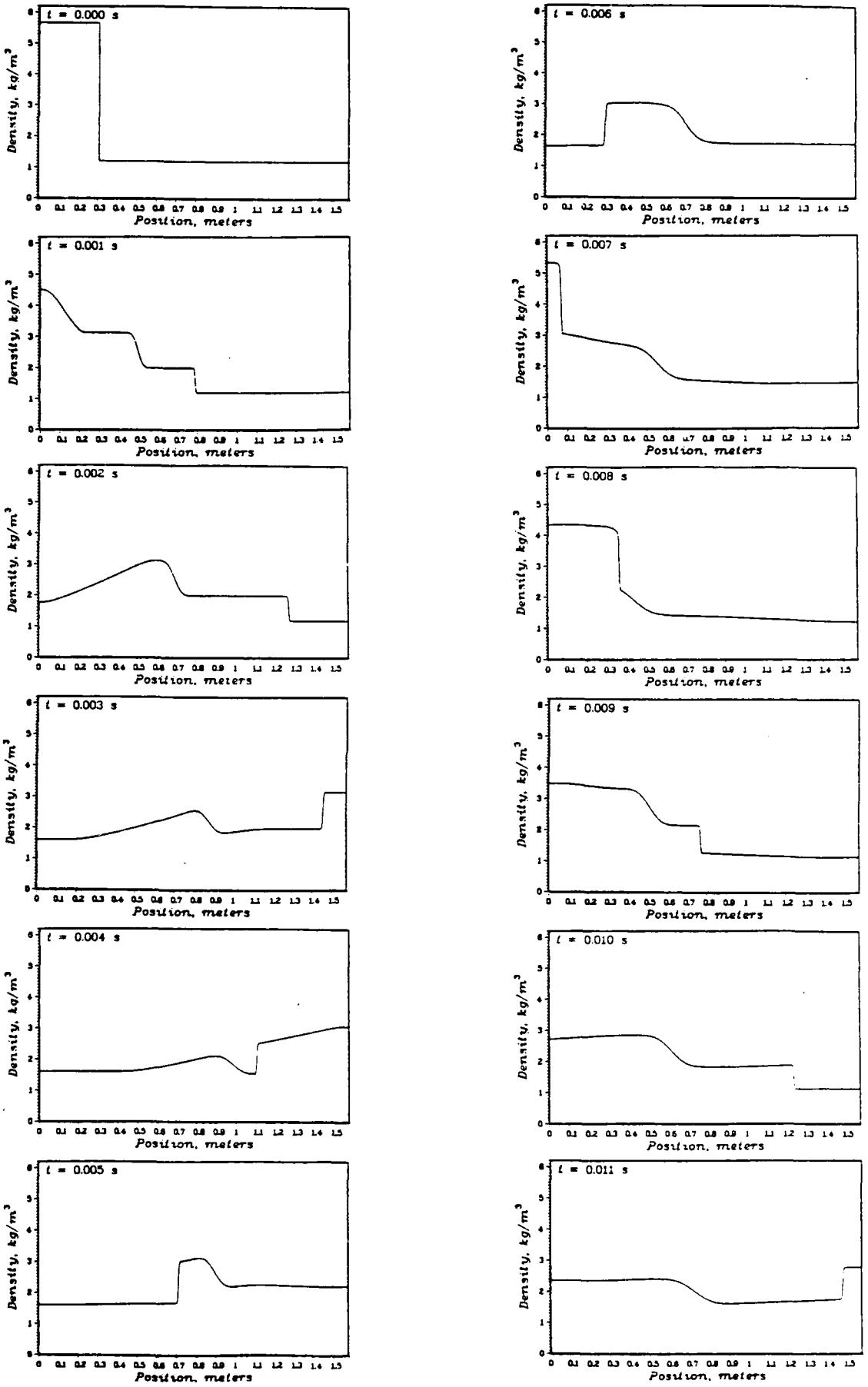

Figure 29. Predicted Fluid Density in the Shock Tube

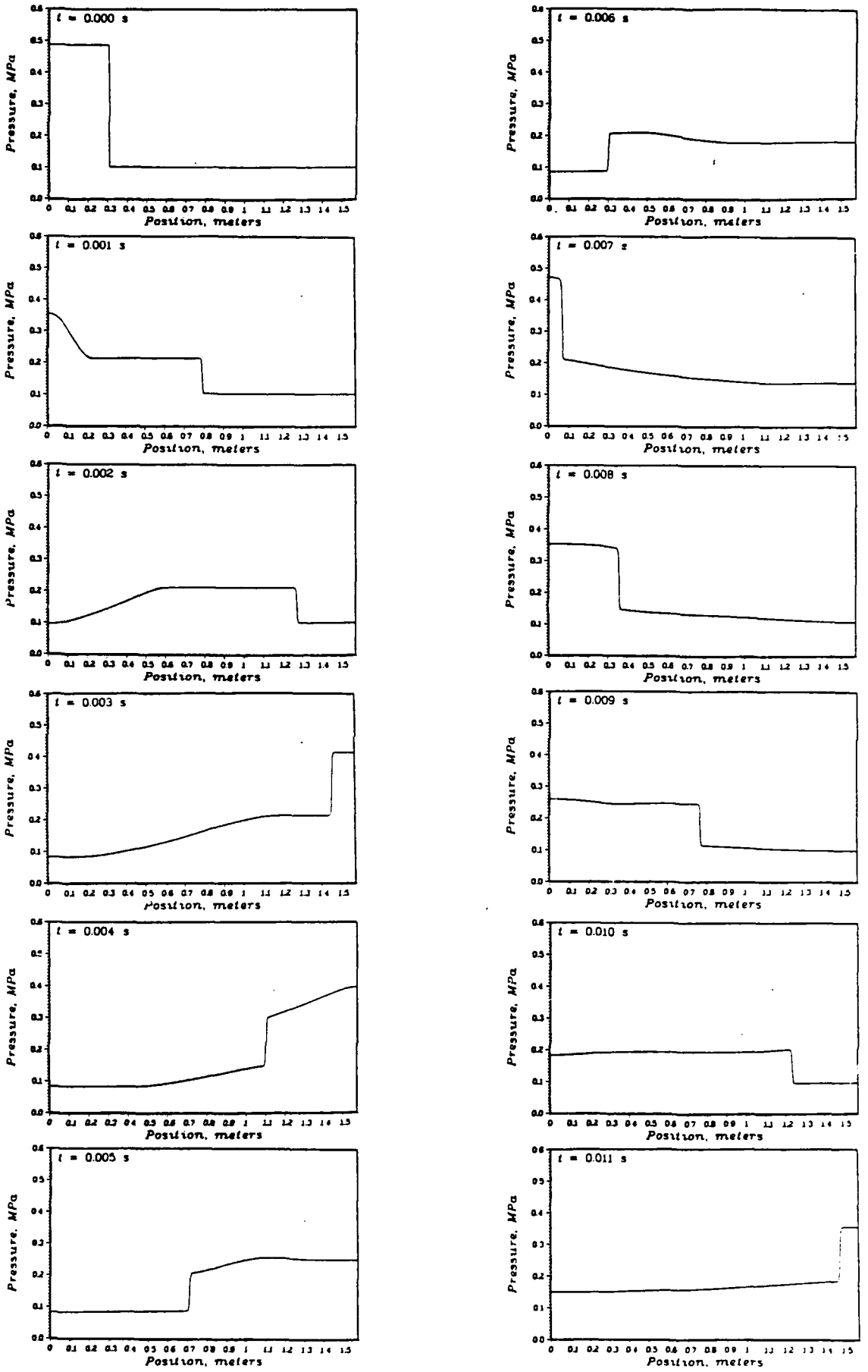

Figure 30. Predicted Fluid Pressure in the Shock Tube

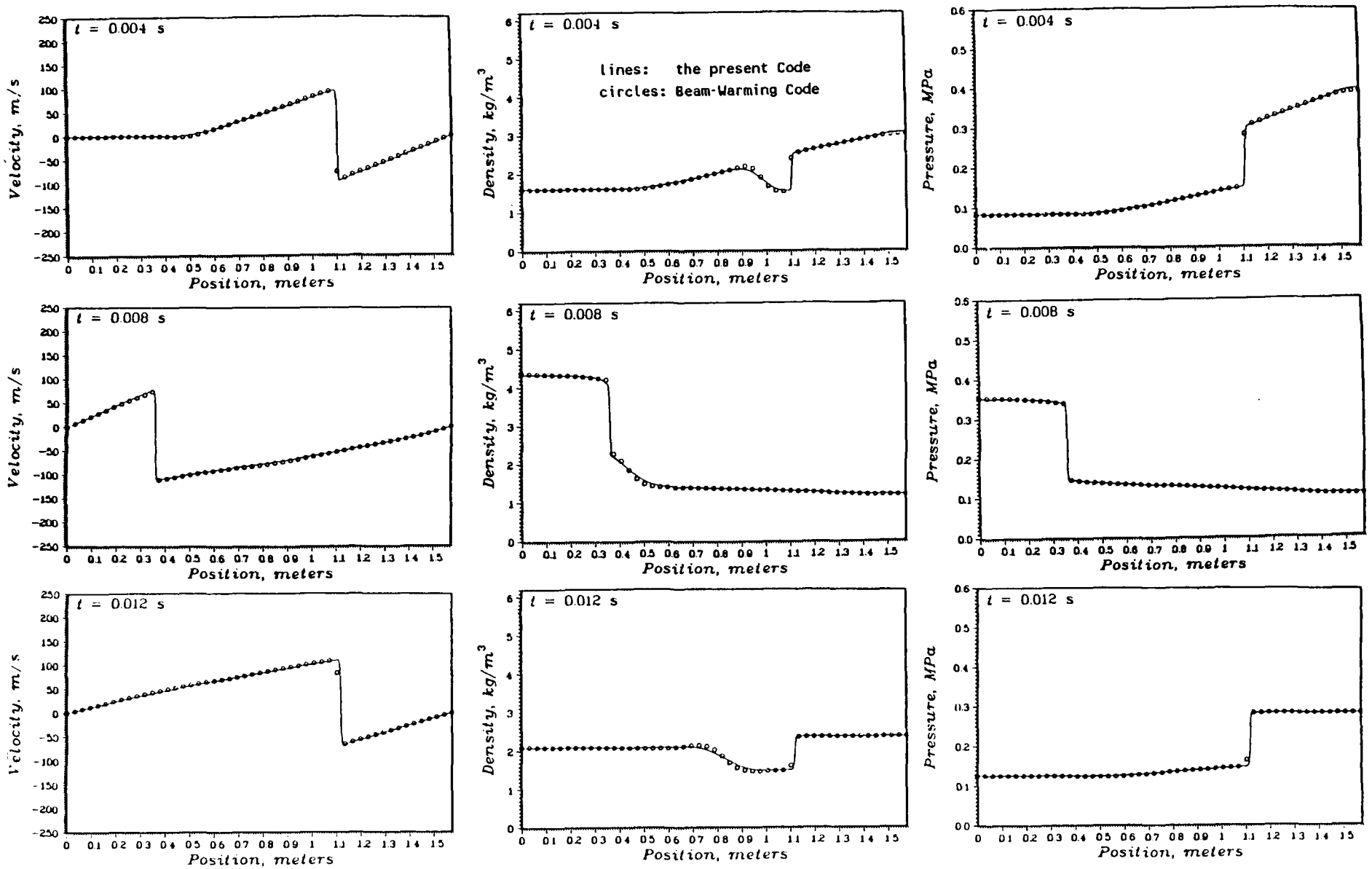

Figure 31. A Comparison of the Code with a Beam-Warming Code

REFERENCES

1. Godunov, S. K., et.al., "A Difference Scheme for Two Dimensional Unsteady Problems of Gas Dynamics and computation of Flow with a Detached Shock Wave". Moscow: Zh. Vychyslitelnoi Mat. i Mat. Fiziki, Vol I, No 6, pp1020, 1961. Also Cornell Aeronautical Lab Transl. by I. Bohachevsky.

2. Godunov, S. K., "Finite Difference Method for Numerical Computation of Discontinuous Solutions of the Equations of Fluid Dynamics". Moscow: Matematicheskii Sbornik, Vol 47, No 3, pp271, 1959. Also Cornell Aeronautical Lab transl. by I. Bohachevsky.

3. Greenberg, M. D., Foundations of Applied Mathematics. Englewood Cliffs, NJ: Prentice-Hall, Inc., 1978.

4. Anderson, J. D. Jr., Modern Compressible Flow. New York: McGraw-Hill Book Company, 1982.

5. Hayes, W. D., and Probstein, R. F., Hypersonic Flow Theory. New York: Academic Press, 1959.

6. Noh, W., "Numerical Methods in Hydrodynamic Calculations". University of California/Livermore: Lawrence Livermore Laboratory, 1976.

7. Richtmyer, R. D., and Morton, K. W., Difference Methods for Initial-Value Problems, 2nd ed. New York: John Wiley & Sons, 1967.

8. Holt, M., Numerical Methods in Fluid Dynamics, Berlin: Springer-Verlag, 1977.

9. Lampson, C. W., "Resume of the Theory of Plane Shock and Adiabatic Waves with Applications to the Theory of the Shock Tube". Aberdeen Proving Ground, MD: Ballistic Research Laboratory, Tech Note 139, 1950.

10. Glass, I. I., and Hall, J. G., "Handbook of Supersonic Aerodynamics: Section 18, Shock Tubes". Washington: Bureau of Naval Weapons Publication, NAVORD Report 1488 (vol 6), 1959.

11. Glass, I. I., et al., "A Theoretical and Experimental Study of the Shock Tube". University of Toronto: Institute of Aerophysics, 1953.

12. Emrich, R. J., and Wheeler, D. B. Jr., "Wall Effects in Shock Tube Flow". The Physics of Fluids, Vol 1, No 1, 1958.

13. Courant, R. and Friedrichs, K. O., Supersonic Flow and Shock Waves. New York: Interscience Publishers, Inc., 1948.

14. Van Leer, B., "Towards the Ultimate Conservation Difference Scheme. V. A Second-Order Sequel to Godunov's Method". Journal of Computational Physics 32, 101-136, 1979.

15. Peyret, R. and Taylor, T. D., Computational Methods for Fluid Flow. Berlin: Springer-Verlag, 1983.

16. Scarborough, J. B., Numerical Mathematical Analysis, 4th ed. Baltimore: Johns Hopkins Press, 1958.

17. Chorin, A. J., "Random Choice Solution of Hyperbolic Systems". Journal of Computational Physics 22, 517-533, 1976.

18. Sod, G. A., "A Survey of Several Finite Difference Methods for Systems of Nonlinear Hyperbolic Conservation Laws". Journal of Computational Physics 27, 1-31, 1978.

19. Pizer,S. M., Numerical Computing and Mathematical Analysis, Chicago: Science Research Associates, Inc.,1975.

20. Ostrowski, A. M., Solution of Equations and Systems of Equations, 2nd ed. New York: Academic Press, 1966.

21. Meyer, H. W. Jr., "Investigation of the Hypersonic Flowfield Surrounding a Shaped Charge Jet", Ballistic Research Laboratory Technical Report BRL-TR-2883, December 1987.

Appendix A

DENSITY RATIO ACROSS THE WAVE

In deriving the density ratio across a wave, the shock wave will be considered first. Following that derivation, some comments will be made regarding the applicability of using the same expression for computing the density ratio across an expansion wave.

The shock wave equations for a negative or a positive running wave were derived in Chapter 3 (eqs. 306, 311, and 314). Those equations relate the conditions across the shock wave, and do so in terms of absolute velocities of the fluid. The equations may be expressed in terms of fluid velocities relative to a moving shock wave, since the conditions are invariant with respect to shock wave translation (ref 13). This transformation is detailed in ref 4, and the result is given here. The following notation is required.

Subscript 1: conditions ahead of the wave
Subscript 0: conditions behind the wave

u: absolute velocity of the fluid
W: absolute velocity of the shock wave
w: velocity of the wave relative to the fluid ahead

When expressed in terms of the above notation, the shock wave equations become the following.

$$\rho_1 w = \rho_0 (W-u_0) \tag{501}$$

$$p_1 + \rho_1 w^2 = p_0 + \rho_0 (W-u_0)^2 \tag{502}$$

$$e_1 + \frac{p_1}{\rho_1} + \tfrac{1}{2} w^2 = e_0 + \frac{p_0}{\rho_0} + \tfrac{1}{2}(W-u_0)^2 \tag{503}$$

Equations 501 through 503 relate conditions behind a moving shock wave (negative or positive running) to conditions ahead of the shock wave, and do so in terms of fluid velocities relative to the moving wave. Notice that $(W-u_0)$ is the velocity of the shock wave relative to the fluid behind, or the negative of the velocity of the fluid behind the shock wave relative to the shock. Similarly, w is the negative of the velocity of the fluid ahead of the shock wave relative to the shock.

These equations are manipulated to obtain the density ratio across the shock as a function of the pressure across the shock. Equations 501 and 502 are used to obtain expressions for the velocities w and $(W-u_0)$, each in terms of the pressures and densities of the fluid ahead of and behind the shock wave. These expressions are then used to eliminate the velocities from the energy equation, eq 503, with the following result.

$$e_1 + \frac{p_1}{\rho_1} + \frac{1}{2}\frac{\rho_0}{\rho_1}\left[\frac{p_1 - p_0}{\rho_1 - \rho_0}\right] = e_0 + \frac{p_0}{\rho_0} + \frac{1}{2}\frac{\rho_1}{\rho_0}\left[\frac{p_1 - p_0}{\rho_1 - \rho_0}\right] \tag{508}$$

The last step is to express the fluid energy in terms of pressure and density, leaving only pressures and densities in the equation. For a calorically perfect gas,

$$p = \rho RT \tag{509}$$

$$e = c_v T \tag{510}$$

where T is the absolute temperature in Kelvins. Equations 509 and 510, together with the definitions

$$R = c_p - c_v$$

$$\gamma = c_p / c_v$$

can be combined to obtain the equation of state of a perfect gas.

$$e = \frac{1}{\gamma - 1}\frac{p}{\rho} \tag{511}$$

The equation of state is the closure equation for the system of equations eq. 501 through eq. 503 (three equations, four unknowns). Equation 511 is substituted into eq. 508, and after considerable rearranging, the desired result is obtained.

$$\rho_0 = \frac{(\gamma+1)p_0 + (\gamma-1)p_1}{(\gamma-1)p_0 + (\gamma+1)p_1}\rho_1 \tag{512}$$

Equation 512 relates the density behind the shock wave to the density ahead of the shock wave (presumeably a known quantity), in terms of the strength of the shock wave (indicated by the pressures on either side of the shock wave, p_1 and p_0).

Even though the shock wave equations were used in deriving eq. 512, no assumptions were necessary regarding the strength of the shock. Therefore, eq. 512 is appropriate for any strength shock wave.

Equation 512 is known as the shock adiabat (ref 1,14). The corresponding relation for an expansion wave is the Poisson adiabat (ref 1,14), or isentropic gas law, eq. 321. It can be written in a form similar to eq. 512:

$$\rho_0 = \left[\frac{p_0}{p_1}\right]^{1/\gamma}\rho_1 \tag{513}$$

In the accoustic approximation (i.e. for waves in which $p_0 \approx p_1$), the two expressions (eq. 512 and eq. 513) are approximately equal, since the density ratio tends to unity in each case (as should be expected). Further, since in the limit of an infinitely weak wave there is no distinction between expansion and compression waves, use of eq. 512 for both types of weak waves is appropriate. Godunov (ref 1) makes the assumption that eq. 512 can be used also for strong expansion waves, making it the only equation required to compute the density ratio across any wave. Experience here indicates that this is a valid approximation for a perfect gas. Also, Peyret and Taylor (ref 15) list an alternate expression for the density and state that its results are consistent with eq. 512.

Appendix B

ITERATIVE SOLUTION TO THE RIEMANN PROBLEM EQUATIONS

In most cases a basic iterative approach to the solution of the non-linear equation for the pressure behind the waves emanating from the cell boundaries is adequate. These equations are derived above, and are repeated here for convenience.

$$p_0 = \frac{bp_4 + ap_1 + ab(u_4 - u_1)}{a + b} \tag{340}$$

The mass velocities of the two waves that emanate from the boundary under study are a and b.

$$a = \frac{\gamma-1}{2\gamma}\sqrt{\gamma p_4 \rho_4}\ \frac{1-\left[p_0/p_4\right]}{1-\left[p_0/p_4\right]^{(\gamma-1)/2\gamma}} \qquad p_0 < p_4 \tag{333}$$

$$a = \sqrt{\gamma p_4 \rho_4}\left\{1 - \frac{\gamma+1}{2\gamma}\left[1 - \frac{p_0}{p_4}\right]\right\}^{1/2} \qquad p_0 \geq p_4 \tag{318}$$

$$b = \frac{\gamma-1}{2\gamma}\sqrt{\gamma p_1 \rho_1}\ \frac{1-\left[p_0/p_1\right]}{1-\left[p_0/p_1\right]^{(\gamma-1)/2\gamma}} \qquad p_0 < p_1 \tag{335}$$

$$b = \sqrt{\gamma p_1 \rho_1}\left\{1 - \frac{\gamma+1}{2\gamma}\left[1 - \frac{p_0}{p_1}\right]\right\}^{1/2} \qquad p_0 \geq p_1 \tag{320}$$

For such nonlinear algebraic equations, of the form

$$p_0 = f(p_0) \tag{601}$$

convergence of the iterations is not always guaranteed. Godunov (Ref 2) indicates the equation may not converge for a strong rarefaction wave, but presents no supporting data. Considering the complexity of the equation, his statement may have been based on actual numerical examples. In view of this, an investigation of the conditions for convergence of eq. 601 is

enlightening, and will lead to a modification to eq. 601 which will guarantee convergence in all cases, and in general will speed up the rate of convergence. A summary of the method used is given below, followed by a detailed derivation of the method.

Summary of the Method

The condition for convergence of the iterations of the nonlinear algebraic equation, eq. 601, is expressed mathematically by

$$|f'(\zeta)| < 1 \tag{610}$$

where ζ is the solution of eq. 601. Computing the derivative of eq. 340 is a horrendous task. Fortunately, modifications can be made to eq. 601 which will guarantee convergence of any function, for any finite value of f', and without any knowledge of the analytic form of f'. In one approach, Chorin (ref 17) and Sod (ref 18) use the following iterating function in place of (eq. 601).

$$p_0 = [1-c]p_0 + cf(p_0) \tag{614}$$

Notice that the p_0 on the right hand side represents the current value of the iterate, while the p_0 on the left hand side represents the new value. Chorin and Sod assign arbitrary values to the constant c (but $c \leq 1$) until convergence is achieved. However, convergence of eq. 614 is guaranteed if c satisfies the following equation.

$$c = \frac{1}{1-f'(\zeta)} \tag{617}$$

Substituting eq. 617 into eq. 614 results in the following iterating function.

$$p_0 = \frac{f(p_0)-f'(\zeta)p_0}{1 - f'(\zeta)} \tag{618}$$

With superscripts to denote sequential iterates, the derivative is approximated in the following manner.

$$f'(\zeta) \approx \frac{f(p_0^{i}) - f(p_0^{i-1})}{p_0^{i} - p_0^{i-1}} \tag{621}$$

This is consistent with the accuracy of the finite difference method that is being used to numerically solve the fluid equations of motion. Now eq. 618 is rewritten with iterative superscripts and eq. 621 is substituted, and the following iteration function results.

$$p_0^{i+1} = \frac{f(p_0^i)\Delta p_0^i - p_0^i \Delta f^i}{\Delta p_0^i - \Delta f^i} \tag{623}$$

where

$$\Delta p_0^i = p_0^i - p_0^{i-1} \tag{624}$$

$$\Delta f^i = f(p_0^i) - f(p_0^{i-1}) \tag{625}$$

Equation 623 is the recommended iterating function. To begin the computations, p_0^0 and p_0^1 are required. These may be computed with

$$p_0^0 = \frac{p_1 + p_4}{2} \tag{626}$$

$$p_0^1 = f(p_0^0) \tag{627}$$

Details of the Derivation

Derivation of the conditions for convergence of eq. 601 can be found in most texts on numerical analysis (e.g. ref 16), and is summarized in the following way.

The solution of eq. 601 is denoted by ζ. Then in eq. 601,

$$\zeta = f(\zeta) \tag{602}$$

In what will be referred to below as the standard iteration technique, the iterations are begun with an initial guess, p_0^0 . The first revised value is the result of substituting p_0^0 into eq. 601, and is written

$$p_0^1 = f(p_0^0) \tag{603}$$

The revised value is then substituted into eq. 601 for a new revised value, written p_0^2 and so on. With the help of the mean value theorem, one can show that the error in the nth iteration is a function of the derivative of eq. 601, f', as follows.

$$[\zeta - p_0^n] = [\zeta - p_0^0] \prod_0^n f'(\zeta_n) \tag{609}$$

Here ζ_n represents some value between the true root (ζ) and the initial guess (p_0^0). Thus if the derivative of f in eq. 601 is less than one in the neighborhood of the root ζ, the right hand side of eq. 609 will include the product of a series of n numbers, each of which is less than one. Thus the error in the nth iteration,

$$[\zeta - p_0^n]$$

will be less than the error in the initial guess,

$$[\zeta - p_0^0]$$

and this error can be made as small as desired by increasing n. Notice that the initial guess must be within the region near the root ζ in which the derivative is less than one. Also notice that the smaller (i.e. closer to zero) that f' is, the faster will be the convergence.

The condition for convergence of the iterations of the nonlinear algebraic equation, eq. 601, is expressed mathematically by

$$|f'(\zeta)| < 1 \tag{610}$$

Computing the derivative of eq. 340 is a horrendous task. As mentioned above, Godunov states that the iterations of eq. 340 may not converge for strong rarefaction waves. Five numerical examples of strong rarefaction waves were computed as part of this study, and in all cases standard iteration of eq. 340 resulted in convergence in fifteen or fewer iterations. Other investigators (ref 14,17,18) indicated they had encountered convergence problems. Modifications can be made to eq. 601 which will guarantee convergence of any function, for any finite value of f', and without any knowledge of the analytic form of f'. Godunov (ref 2) proposes such a modification, but without any supporting rationale. The origin of his scheme is obscure. Although it apparently works, several authors (ref 14,17,18) have used alternate methods. The method presented here is similar to Godunov's, and is an extension of the method used by Chorin (ref 17) and Sod (ref 18). It is apparently similar to one proposed by Bedijn, as referred to in appendix A of ref 14, but no paper by Bedijn on the subject could be found.

The first step in deriving the modified iterating function is to rewrite eq. 601.

$$\psi(p_o) = p_o - f(p_o) \tag{611}$$

The solution to eq. 611 is $p_o = \zeta$, for which $\zeta = f(\zeta)$ (eq. 602 above), and

$$\psi(\zeta) = 0 \tag{612}$$

Solve eq. 611 for $f(p_o)$ and take the derivative:

$$f' = \frac{df(p_o)}{dp_o} = 1 - \psi'$$

Substitute this into eq. 610

$$|1 - \psi'(p_o)| < 1$$

$$0 < \psi' < 2 \tag{613}$$

This is the condition for convergence of the iterating function, eq. 611. It is the same as the condition (eq. 610) for the iterating function eq. 601, in that the function f in eq. 611 is still subject to eq. 610 in order that eq. 613 will be satisfied. However, ψ in eq. 611 can be multiplied by some non-zero constant c without changing the root ζ in eq. 612. If c is properly chosen, eq. 613 can be satisfied regardless of the value of f'. A new iterating function is written.

$$F(p_o) = p_o - c\psi(p_o)$$

$$= p_o - c[p_o - f(p_o)]$$

Notice that at the root ζ, the quantity in brackets is zero and $F(\zeta)$ converges to the root ζ. Rearranging,

$$F(p_o) = [1-c]p_o + cf(p_o) \tag{614}$$

This is the iterating function used by Chorin (ref 17) and Sod (ref 18). More will be said about their application later.

To study the conditions for convergence of the iterating function F, eq. 614 is differentiated and substituted into eq. 610.

$$F' = [1-c] + cf'$$

$$f' = \frac{1}{c}\,[F'-1+c]$$

and in eq. 610:

$$\left|\frac{1}{c}\,[F'-1+c]\right| < 1$$

$$|F'| < 1 \tag{615}$$

Not surprisingly, the requirement for convergence is the same as that of $f(p_0)$. The improvement results from the arbitrary constant c, whose value can be chosen such that eq. 615 is satisfied regardless of the value of f'. An arbitrary requirement is now imposed to define the arbitrary constant c, that in the neighborhood of the root ζ,

$$F'(\zeta) = 0 \tag{616}$$

Surely this will satisfy the convergence criterion eq. 615. It will in fact provide the quickest convergence of the iterations. differentiate eq. 614,

$$F'(p_0) = [1-c] + cf'(p_0)$$

$$F'(\zeta) = [1-c] + cf'(\zeta) = 0$$

$$c = \frac{1}{1-f'(\zeta)} \tag{617}$$

Selection of c in accordance with eq. 617 will guarantee convergence of F in eq. 614. By inspection of eq. 617, two restrictions on $f'(\zeta)$ are apparent, but both are easy to accept without limiting the procedure. First, since $c \neq 0$, $f'(\zeta)$ must be finite. Second, since c must be finite, $f'(\zeta) \neq 1$. There is negligible chance of this occurring numerically (i.e. $f' = 1.000000$ etc. or even close to it) in a function as complex as eq. 340. A special algorithm for computing c can be invoked if f' is computed to be too close to 1 for reliable computation of c. This was not a problem in the present work. In any case the value of c can be controlled (limited to some maximum value, for example) since there is some latitude in the choice of the magnitude of F': it need only be less than one, not necessarily equal to zero.

The following cases are possible for eq. 617.

1. $f'(\zeta) < 0 \quad \rightarrow \rightarrow \quad 0 < c < 1$

   Underrelaxation: eq. 614 produces a new value between p_0^i and $f(p_0^i)$.

2. $f'(\zeta) = 0 \quad \rightarrow \rightarrow \quad c = 1$

   Equation 614 reduces to the original function, which converges unaided.

3. $0 < f'(\zeta) < 1 \quad \rightarrow \rightarrow \quad c > 1$

   Overrelaxation: new value from eq. 614 is outside interval p_0^i to $f(p_0^i)$.

4. $f'(\zeta) = 1 \quad \rightarrow \rightarrow \quad c \rightarrow \infty$

   Problem area: see above discussion.

5. $f'(\zeta) > 1 \quad \rightarrow \rightarrow \quad c < 0$

   Alternating convergence : sign of $(p_0^{i+1} - p_0^i)$ is opposite that of $(p_0^i - p_0^{i-1})$.

Equation 617 can be substituted into eq. 614 to obtain a single expression for the iterating function.

$$p_0 = F(p_0) = \frac{f(p_0) - f'(\zeta) p_0}{1 - f'(\zeta)} \tag{618}$$

Note that combining eq. 611 with eq. 618 leads to the Newton-Raphson method (see, for example, ref 19). For clarity, let

$$\alpha = f'(\zeta) \tag{619}$$

so that

$$p_0 = F(p_0) = \frac{f(p_0) - \alpha p_0}{1 - \alpha} \tag{620}$$

This is the iterating function to be used in place of eq. 601. To verify that the solution of eq. 601 is also a solution of eq. 620, substitute $p_0 = f(p_0) = \zeta$ into eq. 620.

$$\zeta = \frac{\zeta - \alpha\zeta}{1 - \alpha} = \frac{1 - \alpha}{1 - \alpha} \zeta = \zeta$$

For a final check, differentiate eq. 620, where $\alpha = f'(\zeta)$ is not a function of the variable p_0.

$$F'(p_0) = \frac{f'(p_0) - \alpha}{1 - \alpha}$$

and at the root $p_0 = \zeta$:

$$F'(\zeta) = \frac{f'(\zeta) - \alpha}{1 - \alpha} = \frac{\alpha - \alpha}{1 - \alpha} = 0$$

Thus the iterating function $F(p_0)$ will converge rapidly.

Godunov (ref 2) proposes an iterating function similar to eq. 620, but with α replaced by $-\alpha$. The equation he gives for α bears little analytical resemblance to $-f'(\zeta)$, and no numerical resemblance. The derivation of his scheme must differ from the above derivation in some way (perhaps many ways), but since he makes no comments about the origin of his scheme, and since the origin is by no means obvious, it must remain unknown for the present. Thus a comparison of the method presented here with Godunov's method is not possible. A discussion of the present technique for improving convergence of the iteration may be found in ref 20.

Chorin (ref 17) proposed a method based on eq. 614. Sod (ref 18) also used the method. In Chorin's method, eq. 614 is the iterating function, and c is initially assigned a value of 1. Since this reduces eq. 614 to the original iterating function (eq. 601), Chorin starts all iterations with the original function. If this function fails to converge after twenty iterations, he resets c to 1/2 and continues to iterate. If convergence still does not occur in another twenty steps, he resets c to 1/4, and so on. In practice, he states he never had to go beyond 1/4. Thus he is manually imposing values for c that correspond to $f'(\zeta) \leq 0$ (cases 1 and 2 above, for eq. 617). Theoretical justification of this approach is not discussed in his paper, and is not easily obtained (if at all) from 340. Numerically, however, the method apparently worked well for him as well as for Sod.

The difficulty with the method proposed above, and that which is avoided in Chorin's method, is that the value of $\alpha = f'(\zeta)$ is unknown, due to the complexity of $f(p_0)$ (eq. 340) and to the fact that the solution (ζ) is not known a priori. But since the iterations are simply a series of approximations to the root ζ, using a valid approximation to the derivative $f'(\zeta)$ is quite consistent. Thus eq. 619 is written

$$\alpha = f'(\zeta) = \left.\frac{df}{dp_0}\right|_{p_0=\zeta} \approx \left.\frac{\Delta f}{\Delta p_0}\right|_{p_0\approx\zeta}$$

$$\alpha^i = \frac{\Delta f^i}{\Delta p_0^i} = \frac{f(p_0^i) - f(p_0^{i-1})}{p_0^i - p_0^{i-1}} \qquad (621)$$

Now rewrite eq. 620 with iterative superscripts:

$$p_0^{i+1} = \frac{f(p_0^i) - \alpha^i (p_0^i)}{1 - \alpha^i} \tag{622}$$

Substitute eq. 621 into eq. 622 to obtain

$$p_0^{i+1} = \frac{f(p_0^i)\Delta p_0^i - p_0^i \Delta f^i}{\Delta p_0^i - \Delta f^i} \tag{623}$$

where

$$\Delta p_0^i = p_0^i - p_0^{i-1} \tag{624}$$

$$\Delta f^i = f(p_0^i) - f(p_0^{i-1}) \tag{625}$$

Equation 623 is the recommended iterating function. To begin the computations, p_0^0 and p_0^1 are required. These may be computed with

$$p_0^0 = \frac{p_1 + p_4}{2} \tag{626}$$

$$p_0^1 = f(p_0^0) \tag{627}$$

Equation 626 is suggested by several authors as a good initial estimate. p_1 and p_4 are the pressures in the right and left cells prior to resolution of the discontinuity at their common boundary. Equation 627 is simply the first revised estimate based on the standard (unmodified) iterating technique (eq. 601). Thus the first two iterates are the same as those of both the standard method (eq. 601) and Chorin's method (eq. 614).

Van Leer (ref 14) notes that during the iteration large negative values of $[u_4-u_1]$ (i.e. $u_1 >> u_4$) may lead to a negative value for p_0. Hence he suggests a minimum allowable (positive) value for p_0^{i+1}, say ϵ, which is the minimum meaningful pressure for the flowfield under study. If the next iteration also results in a negative pressure, he suggests stopping the iteration and setting $p_0 = \epsilon$.

Chorin makes another numerical suggestion. He notes that erroneous convergence occurs immediately if $p_1 = p_4$ in eq. 626. Therefore he suggests that his iteration scheme be carried out for at least two steps. This requirement is guaranteed in the method presented here, since the first iteration computed by equation eq. 623 is p_0^2. This is the first iterate to

be compared to its previous iterate to determine if the desired level of convergence has been achieved.

Several numerical examples were studied using the four methods discussed above: Unmodified iteration, Godunov's method, Chorin's method, and the present method. The results in all cases substantiated the conclusions drawn here regarding the actual convergence of the various methods for different situations, as well as the rates of convergence. In all cases, the present method converged, and did so the fastest. The other methods did not converge in every case.

Two of the numerical examples are worth noting. The first was simply an algebraic equation in which f' was clearly greater than one. This example demonstrated non-convergence of both the standard technique (eq. 601) and Chorin's method (eq. 614), and rapid convergence for the method presented here (eq. 623). The second numerical example studied a strong rarefaction, and all four methods (including Godunov's) converged. The method presented here converged fastest.

Appendix C

LISTING OF THE COMPUTER PROGRAM

```
      PROGRAM DIAFRAM
C
C ***************************************************************************
C
C                          10 APR 1985
C           EXPERIMENTAL VERIFICATION OF ONE-D CODE
C                      HUBERT W. MEYER JR.
C
C ***************************************************************************
C
      LOGICAL L
      INTEGER T,TT,STA1,STA2
      PARAMETER (MD=102,MR=423,MT=525,TT=2800,STA1=305,STA2=491)
      DIMENSION CU(0:MT,0:1),CR(0:MT,0:1),CP(0:MT,0:1),CE(0:MT,0:1)
      DIMENSION U(0:MT+1,0:1),R(0:MT+1,0:1),P(0:MT+1,0:1),E(0:MT+1,0:1)
      DIMENSION TIME(0:TT)
      DIMENSION PCD (0:50),FPCD (0:50)
      REAL MOM1,MOM2,MOM3,NRG1,NRG2,NRG3
C
      T=0
      TIME(0)=0.
      H=.003
      PMIN=1.
      G=1.4
      G1=(G-1)/(2.*G)
      G2=(G+1)/(2.*G)
C
C GENERAL NOTES:
C      1.  IN THE DIMENSIONED VARIABLES U(I,T), ETC, THE CURRENT
C TIME STEP IS DENOTED BY T=0 AND THE NEW (NEXT) TIME STEP BY T=1.  THUS
C U(17,0) IS THE CURRENT (KNOWN) VALUE AND U(17,1) IS THE NEW VALUE
C BEING COMPUTED.  THIS NOTATION APPLIES TO EACH TIME STEP IN TURN AS
C THE SOLUTION IS MARCHED OUT.
C      2.  IN THE PROGRAM, I ALWAYS DENOTES CELL NUMBER, WHILE M ALWAYS
C DENOTES A CELL BOUNDARY NUMBER.  SIMILARLY, U,R,P,E DENOTE AVERAGE
C CONDITIONS IN A CELL, WHILE CU,CR,CP,CE DENOTE CONDITIONS AT A CELL
C BOUNDARY, BEHIND THE WAVES RESULTING FROM THE DISCONTINUITY THERE.
C
C ***************************************************************************
C
C INITIAL AND BOUNDARY CONDITIONS
C
C ***************************************************************************
C
C INITIAL CELL PROPERTIES
C
C    DRIVER SECTION PROPERTIES
      DATA (U(I,0),I=1,MD)/MD*0./
      DATA (R(I,0),I=1,MD)/MD*5.66/
```

```
      DATA (P(I,0),I=1,MD)/MD*.487E6/
      DATA (E(I,0),I=1,MD)/MD*.2151065E6/
C
C     DRIVEN SECTION PROPERTIES
      DATA (U(I,0),I=MD+1,MT)/MR*0./
      DATA (R(I,0),I=MD+1,MT)/MR*1.19/
      DATA (P(I,0),I=MD+1,MT)/MR*.102E6/
      DATA (E(I,0),I=MD+1,MT)/MR*.2151065E6/
C
      NUM=0
      L=.FALSE.
   10 CONTINUE
      I=0
      WMAX=0.
      IF (L) NUM=NUM+1
      L=.FALSE.
      RNUM=NUM
      Z=RNUM/1000.
      IF (TIME(T).GE.Z) L=.TRUE.
C
C CONDITIONS AT THE LEFT BOUNDARY (WALL) ARE REFLECTION CONDITIONS.
C
      U(0,0)=-U(1,0)
      R(0,0)=R(1,0)
      P(0,0)=P(1,0)
      E(0,0)=E(1,0)
C
C CONDITIONS AT THE RIGHT BOUNDARY (WALL) ARE REFLECTION CONDITIONS.
C
      U(MT+1,0)=-U(MT,0)
      R(MT+1,0)=R(MT,0)
      P(MT+1,0)=P(MT,0)
      E(MT+1,0)=E(MT,0)
C
      IF ((MOD(T,50).EQ.0).OR.(T.LE.5)) THEN
      WRITE (5,100) TIME(T)
      WRITE (6,100) TIME(T)
CC    WRITE (6,103) T,CU(0,0),T,CR(0,0),T,CP(0,0),T,CE(0,0)
        WRITE (5,102) I,T,U(I,0),I,T,R(I,0),I,T,P(I,0),I,T,E(I,0)
      END IF
C
C
C
C ***************************************************************************
C
C COMPUTE THE GENERAL CONDITIONS BEHIND THE WAVES.
C
C ***************************************************************************
C
C GENERAL NOTE:  DUE TO THE APPROXIMATION OF A FINITE NUMBER OF CELLS
C WITH CONSTANT PROPERTIES IN EACH, DISCONTINUITIES EXIST IN THE
C PROPERTIES AT THE CELL BOUNDARIES.  THE DISCONTINUITIES ARE RESOLVED
C BY WAVES (COMPRESSION OR EXPANSION) THAT ORIGINATE AT THE BOUNDARIES.
C
```

```
C THE CONDITIONS BEHIND THESE WAVES ARE THE PRESSURE (P0) AND VELOCITY
C (U0) ON THE CONTACT DISCONTINUITY, AND THE DENSITY ON EITHER SIDE OF
C THE CONTACT DISCONTINUITY (R2 AND R3).
C
C
C COMPUTE P0 AND U0 BY APPROXIMATE FORMULAE FOR WEAK WAVES.
C
    1 IF (ABS(P(I+1,0)-P(I,0)).GT.(P(I+1,0)/100.)) GO TO 2
      IF (ABS(U(I+1,0)-U(I,0)).GT.ABS(U(I+1,0)/100.)) GO TO 2
      A=SQRT(0.25*G*(P(I,0)+P(I+1,0))*(R(I,0)+R(I+1,0)))
      B=A
      P0=0.5*(P(I,0)+P(I+1,0))+0.5*A*(U(I,0)-U(I+1,0))
      U0=0.5*(U(I,0)+U(I+1,0))+0.5*(P(I,0)-P(I+1,0))/A
      GO TO 6
C
C
C COMPUTE P0 AND U0 BY ITERATION OF FULL EQUATIONS FOR STRONG WAVES.
C
    2 PCD(0)=(P(I,0)+P(I+1,0))/2.
      N=0
    8 IF (N.GT.50) THEN
      PRINT*, 'ITERATIONS FAILED TO CONVERGE IN 50 TRIALS'
      PRINT*, '     N=',N,'  I=',I,'  T=',T
      PRINT*, ' '
      P0=PCD(N)
      GO TO 9
      END IF
      S=SQRT(G*P(I,0)*R(I,0))
      S1=SQRT(G*P(I+1,0)*R(I+1,0))
      PI=PCD(N)/P(I,0)
      PI1=PCD(N)/P(I+1,0)
        IF ((PCD(N)+1.).GE.P(I,0)) THEN
          A=S*SQRT(1.-G2*(1.-PI))
        ELSE
          A=G1*S*(1.-PI)/(1.-(PI**G1))
        END IF
        IF ((PCD(N)+1.).GE.P(I+1,0)) THEN
          B=S1*SQRT(1.-G2*(1.-PI1))
        ELSE
          B=G1*S1*(1.-PI1)/(1.-(PI1**G1))
        END IF
      F=(B*P(I,0)+A*P(I+1,0)+A*B*(U(I,0)-U(I+1,0)))/(A+B)
      FPCD(N)=MAX(PMIN,F)
      IF (N.EQ.0) THEN
      PCD(N+1)=FPCD(N)
      N=N+1
      GO TO 8
      END IF
      IF ((FPCD(N-1).EQ.PMIN).AND.(FPCD(N).EQ.PMIN)) THEN
      P0=PMIN
      PRINT*, 'NEGATIVE PRESSURE IN ITERATION WAS RESET TO PMIN.'
      PRINT*, '     N=',N,'  I=',I,'  T=',T
      PRINT*, ' '
      GO TO 9
```

```
      END IF
      DPCD=PCD(N)-PCD(N-1)
      DFPCD=FPCD(N)-FPCD(N-1)
      IF (ABS(DPCD).LT.ABS(PCD(N)/1000.)) THEN
      P0=PCD(N)
      ELSE
      PCD(N+1)=(FPCD(N)*DPCD-PCD(N)*DFPCD)/(DPCD-DFPCD)
      N=N+1
      GO TO 8
      END IF
    9 U0=(A*U(I,0)+B*U(I+1,0)+P(I,0)-P(I+1,0))/(A+B)
C
C
C COMPUTE DENSITY ON EACH SIDE OF THE CONTACT DISCONTINUITY.
C
    6 R2=((G+1.)*P0+(G-1.)*P(I+1,0))*R(I+1,0)/((G-1.)*P0+(G+1.)*P(I+1,0)
     +)
      R3=((G+1.)*P0+(G-1.)*P(I,0))*R(I,0)/((G-1.)*P0+(G+1.)*P(I,0))
C
C
C
C ***************************************************************************
C
C COMPUTE CONDITIONS BEHIND WAVES AT THE LOCATION OF THE CELL BOUNDARY
C
C ***************************************************************************
C
      M=I
      WL=U(I,0)-(A/R(I,0))
      WR=U(I+1,0)+(B/R(I+1,0))
      WMAX=MAX(WMAX,ABS(WL),ABS(WR))
      IF(((WL.GT.0.).AND.(WR.GT.0.)).OR.((WL.LT.0.).AND.(WR.LT.0.)))THEN
        IF (WL.GT.0.) THEN
          CU(M,0)=U(I,0)
          CR(M,0)=R(I,0)
          CP(M,0)=P(I,0)
        ELSE
          CU(M,0)=U(I+1,0)
          CR(M,0)=R(I+1,0)
          CP(M,0)=P(I+1,0)
        END IF
      ELSE
        IF (U0.GT.0.) THEN
          CU(M,0)=U0
          CR(M,0)=R3
          CP(M,0)=P0
        ELSE
          CU(M,0)=U0
          CR(M,0)=R2
          CP(M,0)=P0
        END IF
      END IF
      CE(M,0)=CP(M,0)/((G-1.)*CR(M,0))
      IF (((MOD(T,50).EQ.0).OR.(T.LE.5).OR.(T.EQ.399)).AND.((MOD(M,10).E
```

```
     +Q.0).OR.(M.LT.10))) THEN
        WRITE (6,101) M,T,CU(M,0),M,T,CR(M,0),M,T,CP(M,0),M,T,CE(M,0)
       END IF
       I=I+1
       IF (I.LE.MT) GO TO 1
C
C
C
C ***************************************************************************
C
C COMPUTE LENGTH OF CURRENT TIME STEP.
C
C ***************************************************************************
C
       IF(WMAX.EQ.0.) PRINT*, 'WMAX=0.'
       TAU=.9*H/WMAX
       TIME(T+1)=TIME(T)+TAU
       WRITE (8,105) T,TAU,TIME(T)
C
C
C
C ***************************************************************************
C
C UPDATE CELL PROPERTIES USING CONSERVATION EQUATIONS.
C
C ***************************************************************************
C
C GENERAL NOTE:  THE FLUX OF PROPERTIES INTO EACH CELL IS DETERMINED
C BY CONDITIONS AT THE CELL BOUNDARIES DURING THE TIME STEP, COMPUTED
C PREVIOUSLY.
C
       I=1
     3 M=I
       R(I,1)=R(I,0)-(TAU/H)*(CR(M,0)*CU(M,0)-CR(M-1,0)*CU(M-1,0))
       MOM1=R(I,0)*U(I,0)
       MOM2=CP(M,0)+CR(M,0)*(CU(M,0)**2.)
       MOM3=CP(M-1,0)+CR(M-1,0)*(CU(M-1,0)**2.)
       U(I,1)=(MOM1-(TAU/H)*(MOM2-MOM3))/R(I,1)
       NRG1=R(M,0)*(E(M,0)+(U(M,0)**2.)/2.)
       NRG2=CR(M,0)*CU(M,0)*(CE(M,0)+(CU(M,0)**2.)/2.+CP(M,0)/CR(M,0))
       NRG3=CR(M-1,0)*CU(M-1,0)*((CE(M-1,0)+(CU(M-1,0)**2.)/2.)+CP(M-1,0)
     +/CR(M-1,0))
       E(I,1)=((NRG1-(TAU/H)*(NRG2-NRG3))/R(I,1))-(U(I,1)**2.)/2.
       P(I,1)=(G-1.)*E(I,1)*R(I,1)
       IF (((MOD(T,50).EQ.0).OR.(T.LE.5)).AND.((MOD(I,10).EQ.0).OR.(I.LT.
     +10))) THEN
        WRITE (5,102) I,T,U(I,0),I,T,R(I,0),I,T,P(I,0),I,T,E(I,0)
       END IF
       Y=I
       IF (I.EQ.STA1) THEN
       WRITE (17,104) Y,U(I,0),R(I,0),P(I,0),E(I,0),TIME(T)
       END IF
       Y=I
       IF (I.EQ.STA2) THEN
```

```
      WRITE (27,104) Y,U(I,0),R(I,0),P(I,0),E(I,0),TIME(T)
      END IF
C     IF ((MOD(T,75).EQ.0).AND.((MOD(I,10).EQ.0).OR.(I.EQ.1))) THEN
C     IF((T.EQ.0).OR.(T.EQ.55).OR.(T.EQ.109).OR.(T.EQ.164).OR.(T.EQ.218)
C    +.OR.(T.EQ.273).OR.(T.EQ.328).OR.(T.EQ.382).OR.(T.EQ.437)
C    +.OR.(T.EQ.492).OR.(T.EQ.546).OR.(T.EQ.598).OR.(T.EQ.648)) THEN
      IF (L) THEN
      IF (I.EQ.1) WRITE (7,106) TIME(T)
        RI=I
        X=RI/100.
        WRITE (7,104) X,U(I,0),R(I,0),P(I,0),E(I,0),TIME(T)
      END IF
      I=I+1
      IF (I.LE.MT) GO TO 3
C
C
C
C **************************************************************************
C
C UPDATE CELL PROPERTIES AND PROCEED TO NEXT TIME STEP.
C
C **************************************************************************
C
      DO 7, I=1,MT
      U(I,0)=U(I,1)
      R(I,0)=R(I,1)
      P(I,0)=P(I,1)
      E(I,0)=E(I,1)
    7 CONTINUE
      T=T+1
      IF (T.LE.TT) GO TO 10
C
C
C
C **************************************************************************
C
C FORMAT STATEMENTS
C
C **************************************************************************
C
  100 FORMAT (1H1,'TIME=',F8.6/)
  101 FORMAT(5X,'CU(',I3,',',I3,')=',E16.9,6X,'CR(',I3,',',I3,')=',E16.9
     +,6X,'CP(',I3,',',I3,')=',E16.9,6X,'CE(',I3,',',I3,')=',E16.9)
  102 FORMAT(5X,'U(',I3,',',I3,')=',F16.9,7X,'R(',I3,',',I3,')=',E16.9,
     +7X,'P(',I3,',',I3,')=',E16.9,7X,'E(',I3,',',I3,')=',E16.9)
  103 FORMAT (5X,'CU(  0,',I3,')=',E16.9,6X,'CR(  0,',I3,')=',E16.9,
     +6X,'CP(  0,',I3,')=',E16.9,6X,'CE(  0,',I3,')=',E16.9)
  104 FORMAT (1X,6(E14.7))
  105 FORMAT (1X,I10,2F16.10)
  106 FORMAT (1X,E14.7)
      END
```

DISTRIBUTION LIST

No of Copies	Organization
12	Administrator Defense Technical Info Center ATTN: DTIC-DDA Cameron Station Alexandria, VA 22304-6145
1	HQDA (SARD-TR) Washington, DC 20310-0001
1	Commander US Army Materiel Command ATTN: AMCDRA-ST 5001 Eisenhower Avenue Alexandria, VA 22333-0001
1	Commander US Army Laboratory Command ATTN: AMSLC-DL Adelphi, MD 20783-1145
2	Commander Armament RD&E Center US Army AMCCOM ATTN: SMCAR-MSI Picatinny Arsenal, NJ 07806-5000
2	Commander Armament RD&E Center US Army AMCCOM ATTN: SMCAR-TDC Picatinny Arsenal, NJ 07806-5000
1	Director Benet Weapons Laboratory Armament RD&E Center US Army AMCCOM ATTN: SMCAR-LCB-TL Watervliet, NY 12189-4050
1	Commander US Army Armament, Munitions and Chemical Command ATTN: SMCAR-ESP-L Rock Island, IL 61299-5000
1	Commander US Army Aviation Systems Command ATTN: AMSAV-DACL 4300 Goodfellow Blvd. St. Louis, MO 63120-1798
1	Director US Army Aviation Research and Technology Activity Ames Research Center Moffett Field, CA 94035-1099

No of Copies	Organization
1	Commander US Army Communications - Electronics Command ATTN: AMSEL-ED Fort Monmouth, NJ 07703-5022
1	Commander US Army Missil· Command ATTN: AMSMI-RD Redstone Arsenal, AL 35898-5000
1	Commander US Army Missile Command ATTN: AMSMI-AS Redstone Arsenal, AL 35898-5000
1	Commander US Army Tank Automotive Command ATTN: AMSTA-TSL Warren, MI 48397-5000
1	Director US Army TRADOC Analysis Command ATTN: ATAA-SL White Sands Missile Range, NM 88002-5502
1	Commandant US Army Infantry School ATTN: ATSH-CD-CSO-OR Fort Benning, GA 31905-5660
1	AFWL/SUL Kirtland AFB, NM 87117-5800
1	Air Force Armament Laboratory ATTN: AFATL/DLODL Eglin AFB, FL 32542-5000
	Aberdeen Proving Ground Dir, USAMSAA ATTN: AMXSY-D AMXSY-MP, H. Cohen Cdr, USATECOM ATTN: AMSTE-TO-F Cdr, CRDEC, AMCCOM ATTN: SMCCR-RSP-A SMCCR-MU SMCCR-SPS-IL

USER EVALUATION SHEET/CHANGE OF ADDRESS

This laboratory undertakes a continuing effort to improve the quality of the reports it publishes. Your comments/answers below will aid us in our efforts.

1. Does this report satisfy a need? (Comment on purpose, related project, or other area of interest for which the report will be used.) _____

2. How, specifically, is the report being used? (Information source, design data, procedure, source of ideas, etc.) _____

3. Has the information in this report led to any quantitative savings as far as man-hours or dollars saved, operating costs avoided, or efficiencies achieved, etc? If so, please elaborate. _____

4. General Comments. What do you think should be changed to improve future reports? (Indicate changes to organization, technical content, format, etc.) _____

BRL Report Number _____ Division Symbol _____

Check here if desire to be removed from distribution list. ____

Check here for address change. ____

Current address: Organization _____
Address _____

----------FOLD AND TAPE CLOSED----------

Director
U.S. Army Ballistic Research Laboratory
ATTN: SLCBR-DD-T(NEI)
Aberdeen Proving Ground, MD 21005-5066

OFFICIAL BUSINESS
PENALTY FOR PRIVATE USE $300

NO POSTAGE NECESSARY IF MAILED IN THE UNITED STATES

BUSINESS REPLY LABEL
FIRST CLASS PERMIT NO 12062 WASHINGTON D.C.
POSTAGE WILL BE PAID BY DEPARTMENT OF THE ARMY

Director
U.S. Army Ballistic Research Laboratory
ATTN: SLCBR-DD-T(NEI)
Aberdeen Proving Ground, MD 21005-9989